UNIVERSITÀ DEGLI STUDI DI TRIESTE

UNIVERSITÀ DEGLI STUDI DI TRIESTE

XXXV CICLO DEL DOTTORATO DI RICERCA

IN NEUROSCIENZE E SCIENZE COGNITIVE

Effects of electrical stimulation on the physiology of the skeletal muscle cells

Settore scientifico-disciplinare: BIO/09

DOTTORANDO:
Gabriele Massaria

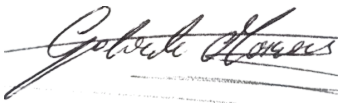

SUPERVISORE DI TESI
prof.ssa Paola Lorenzon

COORDINATORE

prof. Andrea Carnaghi

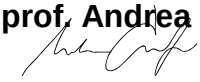

CO-SUPERVISORE DI TESI

prof.ssa Marina Sciancalepore

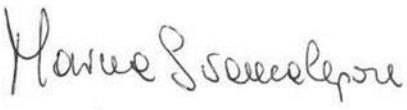

ANNO ACCADEMICO 2021/2022

Abstract

Functional innervation of skeletal muscle cells is required to guarantee muscle development and maintenance of trophic homeostasis of muscle mass. Impairments in nerve-muscle communication due to disuse, ageing or injuries affect skeletal muscles at metabolic, biochemical and structural levels producing alterations in biophysical membrane properties, nAChRs distribution, EC coupling mechanism, muscle fiber phenotype and release of myokines.

Electrical pulse stimulation (EPS) mimics nerve activity in inducing muscle cell contraction and it has been proposed as a tool to counteract muscle atrophy and to enhance muscle strength. Variations in activity of the fiber and in extent of the contraction are induced by modifying the parameters of EPS such as intensity, stimulation time intervals, pulse duration. Depending on the entity, the muscle contraction leads to a dynamic modulation of cellular activity in terms of intracellular Ca^{2+} changes, subcellular structures reorganization, gene transcription and myokine release.

In rodent skeletal myotubes, tetanic EPS induces two separate Ca^{2+} signals: a fast one, related to contraction and a slow signal related to transcriptional events. In the skeletal muscles, changes in the intracellular Ca^{2+} concentration via Ca^{2+} release from intercellular stores are achieved through the activation of ryanodine receptors (RyR) and Inositol-1,4,5-triphosphate receptor (IP_3R) channels. The localization of IP_3R1s close to the endplate zone, nearby the nicotinic acetylcholine receptors (nAChRs) and in the subsynaptic areas of neuromuscular junction (NMJ), suggests a role of EPS-mediated IP_3R1-induced Ca^{2+} release not only in gene expression regulation, but also in the mechanism stabilizing the NMJ apparatus. By using FDB denervated cultures as a cell model to reproduce *in vitro* the denervation effects at the endplate level, we observed a direct proportionality between the subsynaptic IP_3R1-stained volume and the endplate size. Moreover, we demonstrated a significant reduction of the IP_3R1-stained volume associated with the endplate fragmentation after *in vitro* denervation.

The role of electrical activity *vs* neural trophic factors, such as agrin, in controlling the subsynaptic IP_3R1-sensitive compartment was also investigated. The addition of agrin does not affect the reduction of denervation-induced subsynaptic IP_3R1 volumes,

whereas a positive electrical activity-dependent regulation of the endplate IP_3R1 distribution was observed.

Since the expression and distribution of some scaffold proteins are dependent on nerve and muscle activity, we also investigated the role of the scaffold protein Homer 2 in the stabilization of the NMJ using a transgenic Homer $2^{-/-}$ mice model. In skeletal muscle cells, Homer proteins colocalize with IP_3Rs, therefore a IP_3R-Homer interaction could be responsible for generating local IP_3-sensitive Ca^{2+} signals. Reduced size of NMJ was observed in single Homer $2^{-/-}$ FDB skeletal muscle fibers. Genes involved in controlling ubiquitination and ensuing proteolysis, such as *MuRF1* and *Atrogin-1*, appeared upregulated in Homer $2^{-/-}$ rat SOL, as occurs in conditions of atrophy, suggesting a role for Homer 2 as co-regulator of the skeletal muscle normo-trophic *status.* Further experiments are needed to better characterize the function of Homer 2 in the NMJ stability and in controlling the skeletal muscle trophism via putative nAChR-regulated intracellular signaling pathways.

The endocrine role of the skeletal muscle was also examined focusing on IL-6 release, a myokine known to be released upon contraction and to increase at the systemic level during exercise. Investigating the role of mechanosensitive Piezo 1 channels in the myokine release, we demonstrated that the specific Piezo1 agonist Yoda 1 to mimicked the EPS-induced myokine release suggesting that the chemical activation of the mechanosensitive channels might represent a pharmacological tool to promote myokine release in a pathophysiological scenario.

In conclusion, the findings of our research confirm that the EPS is a powerful tool to modulate different important aspects of the skeletal muscle physiology and that the knowledge of its effects at molecular level could help to improve the benefits of the therapeutic electrostimulation in clinics.

TABLE OF CONTENTS

1. INTRODUCTION

The high birth rate of the first half of the twentieth century and the increase of life expectancy in developed countries are responsible for an increase in the number of elderly people estimating that, by 2050, most of the world population will have an age over 65[1]. However, "living longer" is not always associated with the need to "live better". Indeed, a sedentary lifestyle represents one of the main problems of modern society and it is responsible for the dramatic growth of overweight and obesity and, in turn, of powerful risk factors for serious chronic diseases. According to data from the World Health Organization, physical inactivity is the fourth risk factor for mortality globally and about 3.2 million people die every year because they are not “active” enough. Lots of studies support that a constant physical exercise offers incredible benefits, which improve nearly every aspect of our physical and mental health.

Skeletal muscle converts chemical energy into mechanical energy to produce power, maintain posture, allowing respiratory movements, locomotion, and many other precise and non-precise body movements. In humans, the skeletal muscles comprise approximately 40% of total body weight and contains 50-75% of all body proteins[2]. Recent studies demonstrate their role as the principal reservoirs for amino acids, to maintain blood glucose levels during conditions of starvation and to maintain protein synthesis in vital tissues and organs, such as brain, skin and heart[3]. The roles of the skeletal muscles include the production of heat for the maintenance of core temperature and the consumption of the majority of oxygen used during physical activity. Moreover, exercise ameliorates brain functions, protects memory and thinking skills, promotes changes in brain structure[4], reduces feelings of anxiety and depression[5], and increases brain sensitivity to some neurotransmitters, such as serotonin and norepinephrine[6].

The adult skeletal muscle are very stable tissues with a low rate of turnover. However, they show an enormous plasticity and malleability in response to different physiological and pathological conditions. Innervation is fundamental for structural support and functional integrity of the skeletal muscles. Damage to nerves or spinal cord, neurodegenerative diseases and aging processes lead to denervation of muscle fibers. Denervation causes first the atrophy of the muscle, where a loss of function precedes loss of structure. With the atrophy becoming more and more severe, sarcomeric

organization is lost, and finally, there is a progressive replacement of myofibers with adipose and connective tissue.

The knowledge of the molecular mechanisms involved in the physiopathology of skeletal muscle cells is fundamental for the discovery of new therapeutic approaches for designing personalized preventive and rehabilitative intervention programs to attenuate muscle-related diseases and the age-related progressive impairment in motor function. In specific circumstances (muscle diseases, surgery, etc.), the real problem is not so much the time to dedicate to the physical exercise but the capability of the patient to perform the physical exercise. Because contractility is an essential feature of the muscle cells, patients unable to perform physical exercise develop progressive and sever defects in skeletal-muscle strength (weakness) and mass (wasting), worsening their conditions from a physical and a psychological point of view. To counteract the effects of disuse, the electrical stimulation of the muscle has been introduced and it is used for rehabilitation purposes. The electrical stimulation has been shown to be effective in treating impaired muscles[7] preserving muscle-protein synthesis and preventing muscle atrophy during prolonged periods of immobilization[8].

1.1 The skeletal muscle

The skeletal muscle system is made up of muscles of the locomotor system and some organs of the digestive and respiratory systems.

From a structural point of view, the skeletal muscle is a highly organized tissue containing several bundles of multinucleated and post-mitotic muscle cells (even a few hundreds), called myofibers or muscle fibers. Externally, each muscle fiber has a thin layer of connective tissue, named endomysium; more fibers together form a muscle bundle (fascicle), surrounded by a layer of connective tissue, called perimysium; finally, the whole muscle is covered by a dense external connective lamina, called epimysium (Fig. 1).

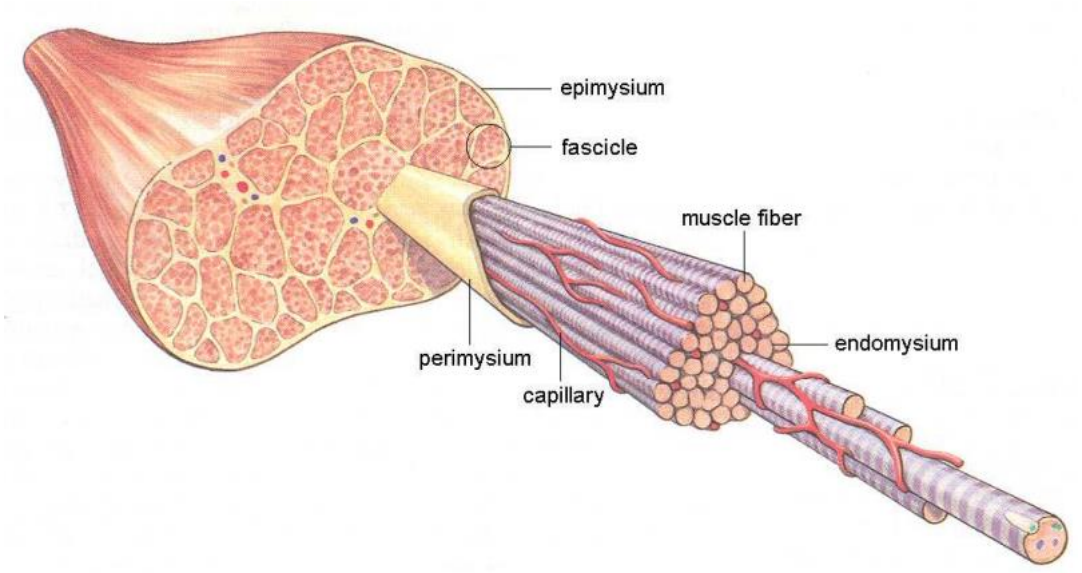

Fig. 1. The skeletal muscle structure. *The entire muscle is surrounded by the epimysium, which continues as perimysium covering the fascicles, and finally as endomysium which surrounds each individual muscle fibers (from Gray and Carter, 1995).*

At the intracellular level, each muscle fiber presents thousands of myofibrils, which in turn contains billions of myofilaments, all oriented according to the longitudinal axis of the fiber and organized in a characteristic pattern named sarcomere, which represents the basic cellular unit of the muscle fiber[9]. Each sarcomere is about 2 µm long, and formed by thick and thin myofilaments. They are arranged distinctively in a striated

pattern to form the dark A and the light I bands (Fig. 2). Their arrangement is symmetric: thick myofilaments of myosin are located and attached on both sides of a central M line, in the center of the sarcomere (dark A band) while thin myofilaments of actin are anchored at the poles of the sarcomere at the Z line level. The thick filaments are formed mainly by myosin proteins which have a diameter of 10 nm; the thin filaments are composed mainly of actin proteins and have a diameter of 6 nm. The sarcomeric myofilaments are the most abundant of the total protein content in a single muscle fiber, being approximately 70–80%[2] of the total.

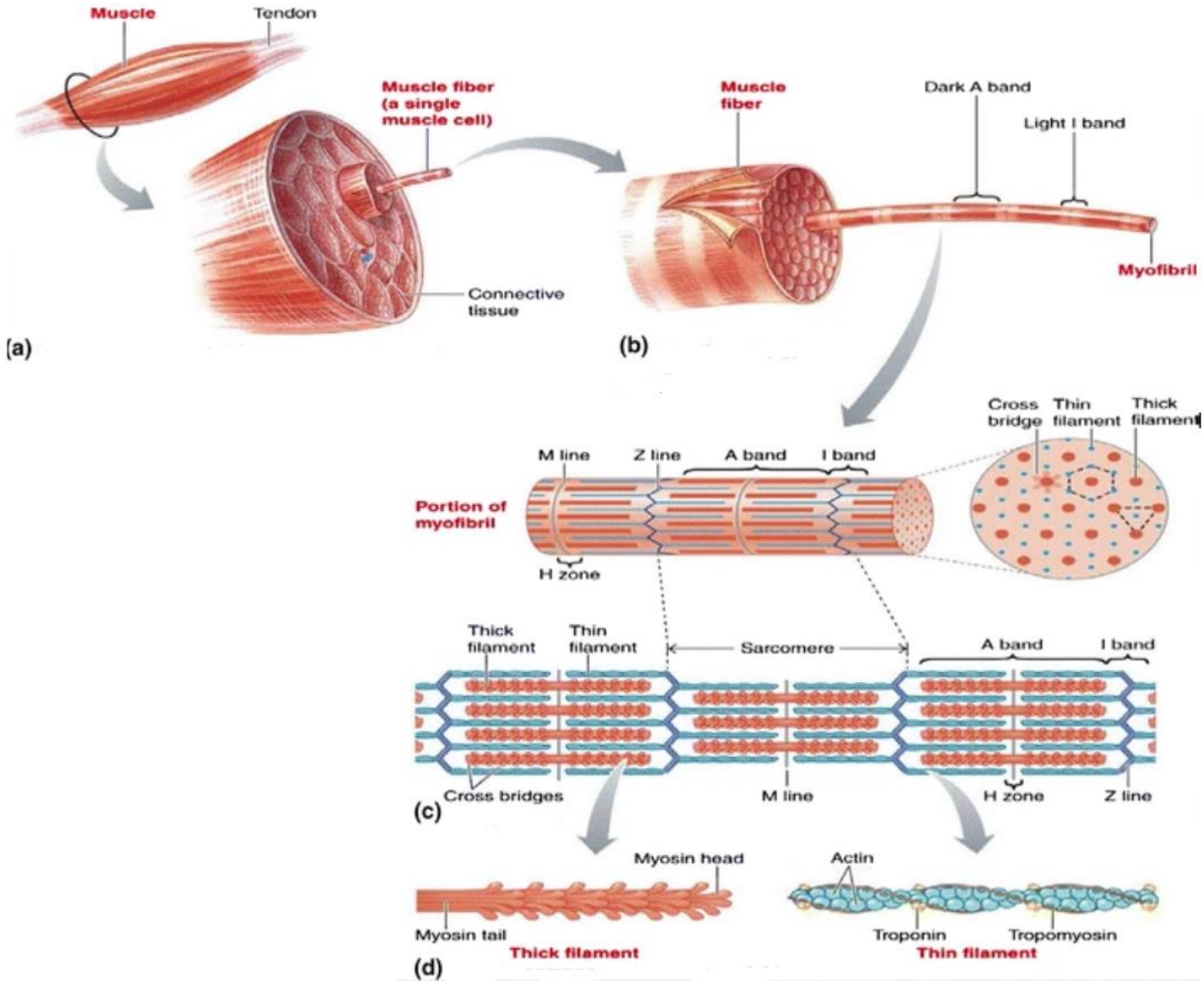

Fig. 2. *Structure of the skeletal muscle fiber. (a) The whole skeletal muscle vs the single skeletal muscle fiber. (b) A single skeletal muscle fiber and a myofibril. (c) Cytoskeletal components of a myofibril form sarcomeres. (d) Thick (myosin) and thin (actin) filaments (modified from 2).*

1.1a EC coupling

To induce skeletal muscle contraction, the action potentials generated by the motor neurons are transmitted to the skeletal muscle fibers. The excitation-contraction (EC) coupling machinery mediates the transduction of the nerve action potential into muscle action potential leading to an intracellular Ca^{2+} concentration ($[Ca^{2+}]_i$) increase triggering muscle contraction.

The skeletal muscle fibers contain a large intracellular Ca^{2+} store called sarcoplasmic reticulum (SR), which quickly releases and retrieves Ca^{2+} from the cytoplasm. To ensure a simultaneous Ca^{2+} release throughout the whole skeletal muscle fiber, the SR is distributed all over the cell and is under the control of the action potential generated by the skeletal muscle fiber. The transverse tubule (T-tubule) system is a network of tubular invaginations of the sarcolemma, which maintains the SR under strict control of the membrane depolarization via the opening of voltage-gated Ca^{2+} channels CaV1.1 (dihydropyridine receptors, DHPRs).

The SR is closely associate with T-tubules, in regions called terminal cisternae. Two terminal cisternae are associated to one T-tubule forming a triad. For skeletal muscle contraction, the main source of Ca^{2+} is represented by the Ca^{2+} released from the SR through the opening of the ryanodine receptor (RyR) channels, mainly located at the level of the terminal cisternae. There is a mechanical coupling between DHPRs located on T-tubule membranes and RyR type 1 (RyR1) localized on the junctional face of the terminal cisternae (Fig. 3). Conformational changes in DHPRs, induced by depolarization of the T-tubular membrane, are transmitted to RyR1, triggering its opening. Each single RyR1 interacts with four DHPRs[10].

The strength of muscle contraction is controlled by the amount of Ca^{2+} released from SR, which in turn, is modulated by the Ca^{2+} content in the SR lumen via Ca^{2+} uptake activity by the sarco-endoplasmic reticulum Ca^{2+}-ATPase (SERCA). Calsequestrin (CASQ), which binds up to 80 Ca^{2+} ions (mol/mol), is the high-capacity Ca^{2+} storage protein localized in the lumen of SR.

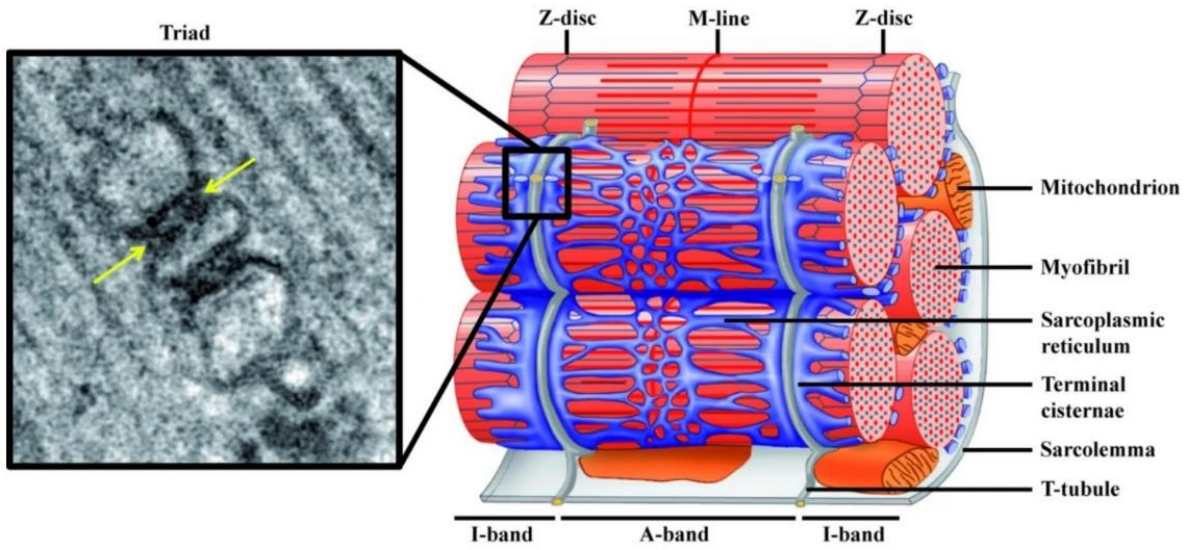

Fig. 3. *Triad organization in the skeletal muscle fiber. Left: Electron micrograph of a triad junction. A central T-tubule is flanked on both sides by two terminal cisternae elements of the SR. Arrows indicate electron-dense junctional feet corresponding to the DHPR-RYR1 receptor complex. Right: Schematic representation of a mammalian muscle sarcomere and surrounding membranes. T-tubules shown in gray are specialized invaginations of the sarcolemma. The elaborated sarcoplasmic reticulum network is shown in blue. Note the close proximity between the terminal cisternae of the SR and the T-tubules (from 10).*

1.1b Satellite cells and muscle regeneration

From birth to childhood, the number of skeletal muscle fibers composing a muscle remains constant. However, each fiber can undergo hypertrophy, a process through which cells grow in size due to the fusion of specific muscle stem cells, also known as satellite cells (SCs). Since their discovery by Mauro[11] (1961), SCs have been identified as the main source of new myonuclei in the postnatal skeletal muscle tissue[12,13]. Anatomically, these cells are located between the sarcolemma and the basal lamina of the skeletal muscle fibers (Fig. 4) and contribute to muscle growth, repair, and regeneration[14]. Upon appropriate stimuli, SCs switch from a typically quiescent state to an active one undergoing proliferation and/or differentiation.

In the quiescent state, SCs are characterized by a large nuclear-to-cytoplasmic ratio, small nucleus, few organelles and condensed chromatin, the classic morphological characteristics of quiescent cells[15]. Stem cells and muscle fiber progenitors can be also

identified and discriminated by fluorescence microscopy thanks to specific biomarkers (Fig. 4). Transcription factor Barx2, cell adhesion protein M-cadherin, tyrosine receptor kinase Met c-Met are markers for SCs located at the plasma membrane such as receptor α7-integrin, clusters of differentiation protein CD34, and many others[16]. In the adult skeletal muscle, all SCs express the paired box transcription factor Pax7, essential for SCs function, while subsets also express Pax3 and Myf5, defying a large heterogeneity in SCs population.

SCs undergo self-renewal through both symmetric and asymmetric division to keep muscle stem cell pool, largely depending on cell position in relation to fiber[16]. When activated, a group of SCs express Pax7 and upregulate MyoD leaving the quiescent state, while the remaining stem cells downregulate MyoD and contrast the further myogenetic process maintaining a mitotically inactive state. Megeney et al.[17] demonstrated in transgenic $MyoD^{-/-}$ mice a reduced regenerative capacity after injury, confirming that MyoD is crucial for promoting the progression of myoblast to terminal differentiation[17]. Myogenesis continues with the expression of MyoD, Myf5, Myogenin and MRF4 and it is considered completed with the activation of muscle specific proteins (myosin heavy chains, MHC) and the fusion of myoblasts into myotubes.

SCs not only are responsible for muscle hypertrophy, but they also make muscle regeneration possible. Regeneration is one of the hallmarks of the mature skeletal muscle tissue and it is a highly orchestrated process, which involves the interaction between SCs and their microenvironment. Under unstressed conditions, SCs stay in the quiescent state, but when required, in response to external signals, such as injury, SCs start to proliferate and express myogenic markers.

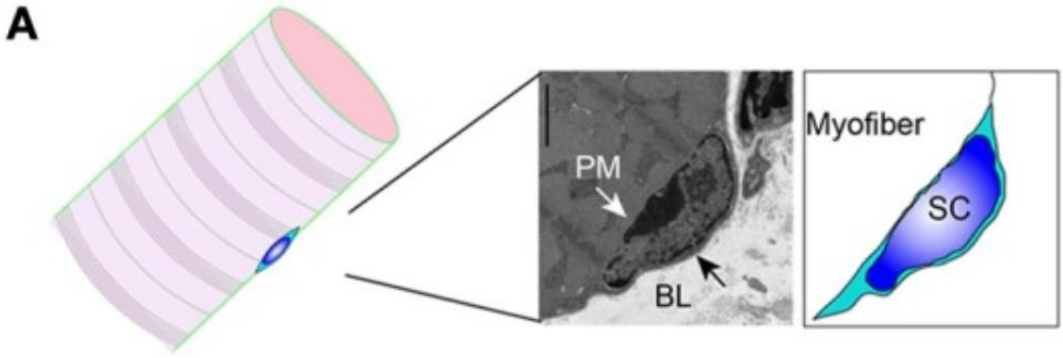

Fig. 4. *Localization of a SC in a skeletal muscle fiber. PM, plasma membrane; BL, basal lamina; SC, satellite cell (modified from 17).*

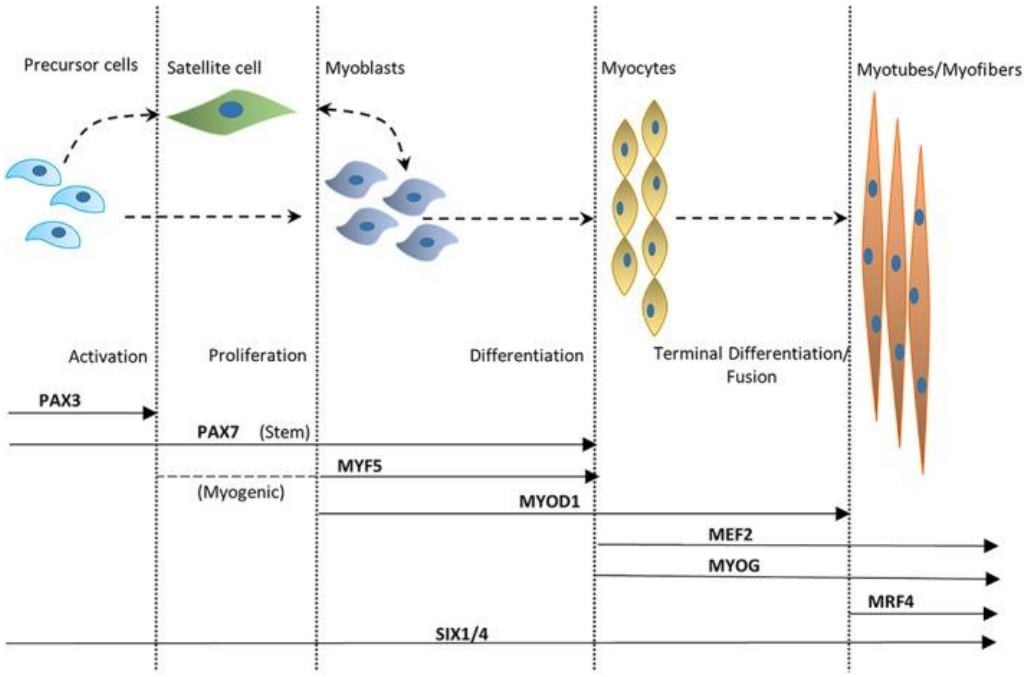

Fig. 5. *Temporal and hierarchical sequence of transcription factors activation during the various stages of adult myogenesis (from 9).*

1.1c Fiber types

From a physiological point of view, the characteristics defining the skeletal muscle fiber "type" are movement rates, response to neural inputs, and metabolic styles[18,19]. Skeletal muscle fiber diversity involves all functional cell compartments, including membrane excitation, EC coupling, contractile machinery, cytoskeleton scaffold, and energy supply systems. Nowadays, different techniques are available to analyze skeletal muscle fiber types, such as tissue homogenate analysis, histological analysis of tissue sections and the electrophoretic analysis of MHC isoform expression[20]. The skeletal muscle fibers are divided into "slow-twitch" (type I) and "fast-twitch" (type II; Table 1[21]). Fast-twitch fibers are also subclassified into the three major subtypes IIA, IIX, and IIB. The co-expression of various MHC isoforms in different fibers of a muscle group leads to the distinction of more subtypes (I/IIA, IIA/IIX, IIX/IIB), resulting in different ATP usage and muscle contraction speeds, from the slowest (type I) to the fastest (type IIB)[18].

In humans, type I fibers, also called red fibers due to the high content of myoglobin (chromoprotein with a high capacity to accumulate oxygens), are characterized by numerous mitochondria and a dense network of capillaries. The high level of oxidative enzymes, such as succinate dehydrogenases, justify the oxidative metabolism used by this type of fibers. Type I fibers are also named "slow-twitch" and thanks to the high number of mitochondria and the low speed of ATP usage, they are remarkably resistant to fatigue, but develop low forces (1-10% compared to type II fibers).

Type IIB fast-twitch fibers, also defined as white fibers due to the lack of myoglobin, have larger diameter and develop powerful contractions generating very high forces. However, because of the high consumption of ATP and the presence of few mitochondria, they take advantage of anaerobic glycolysis. As a results, the fatigue of these fibers occurs quickly because of the limited glycogen reserves.

Type IIA fast-twitch fibers (resistant to fatigue) possess intermediate structural and biochemical characteristics compared to the two previous fibers' types. Like fibers type I, they are enriched in mitochondria and capillaries but have glycolytic and oxidative enzymes, thus they show greater resistance to fatigue than IIB fibers. Moreover, their contraction speed is moderately fast and develop a contraction force doubled than IIB fibers.

Type IIX fibers are characterized by a glycolytic metabolism and they have intermediate characteristics between type IIA and type IIB fibers. Having a high activation threshold, they are activated by high efforts.

Reduced muscle use has been shown to cause atrophy of all muscle fiber types but particularly of type I, accompanied by a fiber-type shift from type I and IIA fibers to type IIX[22–25]. However, Ditor et al.[26] observed a pronounced atrophy of type IIA fibers in spinal cord injured subjects.

	Type I fibers (red)	Type II a fibers (red)	Type II x fibers	Type II b fibers (white)
Contraction time	Slow	Moderately Fast	Fast	Very fast
Size of motor neuron	Small	Medium	Large	Very large
Resistance to fatigue	High	Fairly high	Intermediate	Low
Activity Used for	Aerobic	Long-term anaerobic	Short-term anaerobic	Short-term anaerobic
Maximum duration of use	Hours	<30 minutes	<5 minutes	<1 minute
Power produced	Low	Medium	High	Very high
Mitochondrial density	Very High	High	Medium	Low
Capillary density	High	Intermediate	Low	Low
Oxidative capacity	High	High	Intermediate	Low
Glycolytic capacity	Low	High	High	High
Major storage fuel	Triglycerides	Creatine phosphate, glycogen	ATP, Creatine phosphate, glycogen (little)	ATP, Creatine phosphate
Note	Consume lactic acid	Produce lactic acid and Creatine phosphate	Consume Creatine phosphate	Consume Creatine phosphate
Myosin heavy chain,human genes	MYH7	MYH2	MYH1	MYH4

Table 1. *Human skeletal muscle fiber type classification and properties (from 21).*

1.1d Motor units

In the adults, each muscle fiber is innervated by a single motor neuron, but a single motor neuron innervates more muscle fibers. A motor neuron and its associated muscle fibers form the “motor unit”, which represents the smallest functional unit of the skeletal muscle. The number of fibers innervated by a single motor neuron (innervation ratio) determines the capability of the muscle to develop fine or gross movements. Small motor units are required for fine movements (i.e. finger movements), while large motor units prevail in the muscles characterized by large powerful movements.
Each muscle contains, in various proportions, different types of motor units, which are subdivided according to the metabolic characteristics of the innervated fibers (oxidative or glycolytic). Generally, they are subdivided in:

- Slow motor units: slow speed of contraction, very resistant to fatigue;
- Fast fatiguing motor units: high force, poorly resistant to fatigue;
- Fast fatigue-resistant motor units: with intermediate characteristics.

It is important to mentioned that, according to the “principle of size”, i.e. the smallest is the cell body of the motor neuron the lowest is its activation threshold, the motor units whose motor neurons have the smallest cell body are recruited first. This explains why we are able to graduate the strength of the muscles and the extent of the movements in relation to the needs.

1.1e Muscle plasticity/adaptation

The skeletal muscle has the ability to change fiber type composition and mass in response to its activity (physical exercise *vs* disuse), type of loading (resistance exercise *vs* microgravity) and other environmental factors (hypoxia and thermal stress).

The extraordinary ability of the skeletal muscle to adapt involves the modification of both intra- (mitochondria, myofibrils, etc.) and extra- (capillaries, nerve endings, connective tissue) muscular compartments. Intramuscular structural and functional adaptations are the result of a rapid change in the expression of key genes that are activated or silenced depending on their function. As an example, endurance training induces an increase in oxidative capacity with the transition from fast-twitch to slow-twitch muscle fiber, whereas strength training results in slow-twitch to fast-twitch muscle fiber transition with muscle hypertrophies.

Genetic diseases are associated to muscle adaptation and differences in composition. There are many inherited myopathies and other acquired muscle-related disorders that preferentially affect specific skeletal muscle fiber types and it remains still unclear why certain muscle diseases preferentially affect particular fiber types[27] (Table 2).

Disorder	Fiber-type effects
Duchenne muscular dystrophy	Type 2X fibers first to degenerate.
Facioscapulohumeral muscular dystrophy	Maximum force-generating capacity reduced in type 2 fibers. Increased proportion of type 1 fibers.
Myotonic dystrophy Type 1 (DM1)	Type 1 fiber atrophy and high frequency of type 1 fibers with central nuclei. Force generation reduced more in type 1 fibers.
Myotonic dystrophy Type 2 (DM2)	Type 2 fiber atrophy, type 2 fiber hypertrophy, and high frequency of type 2 fibers with central nuclei.
Congenital fiber type disproportion	Predominant proportions of type 1 fibers that are consistently much smaller than type 2 fibers.
Myosinopathies	*MYH7* mutations can cause smaller diameter type 1 fibers. *MYH2* mutations lead to loss of type 2A fibers.
Pompe disease	In mouse model, type 2 fibers smaller with massive autophagic build-up.
Obesity and type 2 diabetes	Reduced proportions of type 1 fibers and increased proportions of type 2X fibers.
Muscle inactivity (spinal cord injury, bed rest)	Type 1 fiber atrophy. Fiber-type shift from type 1 and 2A to 2X.
Aging/sarcopenia	Type 2 fiber loss and atrophy. Smaller diameter type 2 fibers.
Heart failure, chronic obstructive pulmonary disease	Fiber-type shift from type 1 to type 2 (limb muscles). Fiber-type shift from type 2 to type 1 (diaphragm).

Table 2. *Examples of muscle disorders with effects on specific skeletal muscle fiber types (from 27).*

1.1f The NMJ

The neuromuscular junction (NMJ) is the highly specialized synapse through which the nerve ending of a motor neuron communicates with a single skeletal muscle fiber by the release of the neurotransmitter acetylcholine (ACh). At the presynaptic level, the nerve ending includes small synaptic vesicles containing ACh, which is released at the active zones when the neuronal action potential propagates to the nerve ending. Slow muscles are activated at a frequency of 10-20 Hz, whereas fast muscles are activated at a frequency up to 100 Hz[28]. The ACh release is triggered by an increase in the $[Ca^{2+}]_i$ resulting from the opening of voltage-gated Ca^{2+} channels induced by the motor neuron action potential. Each vesicle contain about 5.000-10.000 ACh molecules[29,30].

The synaptic cleft (50-100 nm wide) separates the presynaptic terminal from the motor-end plate. Within the synaptic cleft and surrounding the nerve and muscle fiber, there is the basal lamina, a single layer of condensed extracellular matrix. At synaptic level, the basal lamina is enriched of proteins which are not present in the extra synaptic regions, such as acetylcholinesterase (AChEs), which control the transmission between the motor neuron and the skeletal muscle fiber.

The area of the sarcolemma that interacts with the neuron is the motor endplate. The motor endplate is characterized by strong invaginations called junctional folds[31]. The crests of these folds contain about 10.000 nicotinic acetylcholine receptors (nAChRs) per square micron. To examine the morphological properties of the motor-end plate, light confocal microscopy and fluorescent labeling techniques are generally used to generate three-dimensional image reconstructions.

The nAChRs are densely clustered in winding, band-like arrays on the post-synaptic membrane, giving rise to the so called “pretzel”-like structure shape[32] (Fig 6).

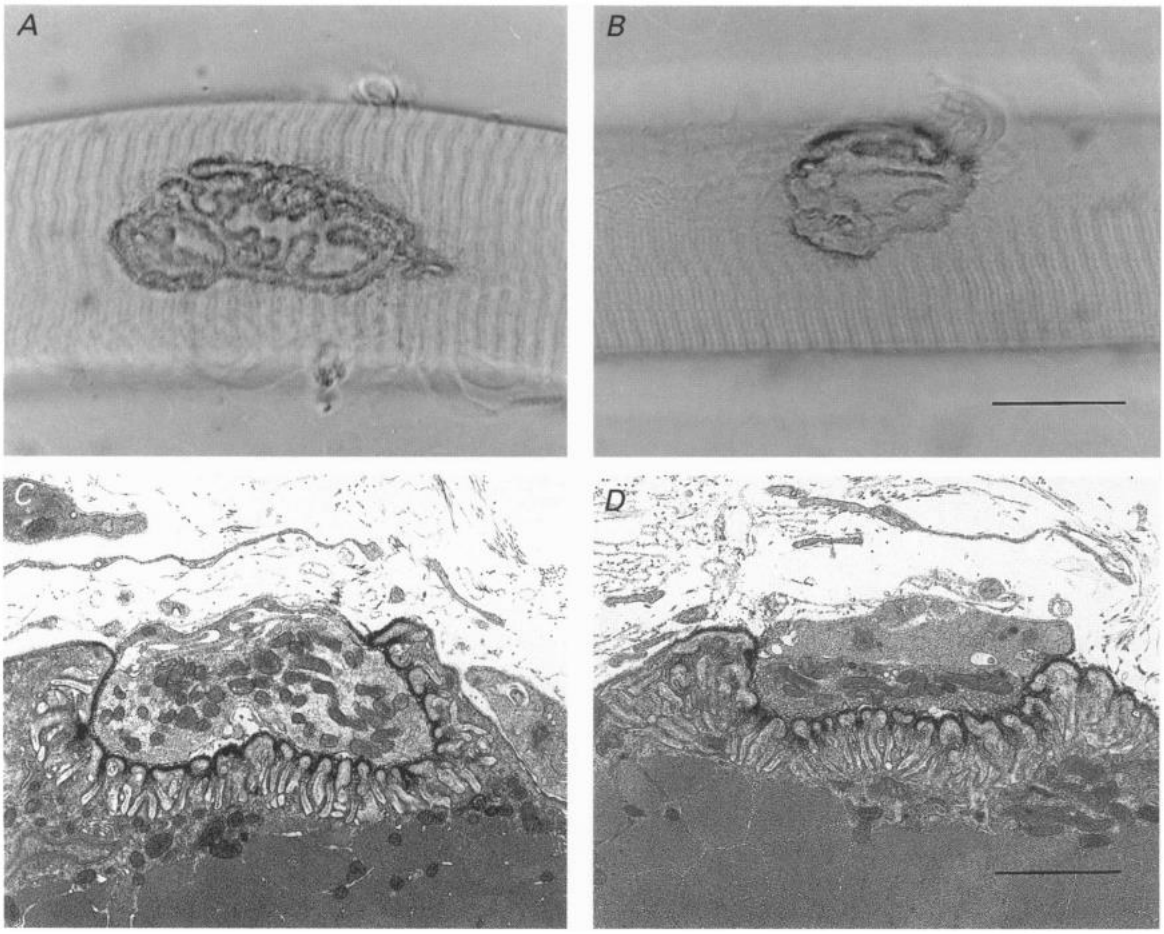

Fig. 6. *Examples of soleus (A) and EDL (B) endplates (scale bar: 20 µm). Electron micrographs of soleus (C) and EDL (D) NMJs (scale bar: 2 µm; from 32).*

1.1g NMJ maintenance

For attainment and maintenance of trophic homeostasis and muscle mass, an efficient neuromuscular transmission is required from the release of the neurotransmitter ACh by the motor neuron to the activation of the EC coupling mechanism at muscle level. There are several reports regarding the release and the neurotransmitter activity, but the knowledge of the molecular mechanisms responsible for stabilization of the NMJ are still matter of investigations.

Certainly, there is a dynamic organization of nAChRs at the NMJ. In the fully differentiated skeletal muscle, the nAChRs are ligand-gated channels localized and confined within the postsynaptic membrane. From a molecular point of view, the “adult” nAChR is composed by 5 protein subunits: 2α, β, δ, ε. During embryonic muscle development and before synaptogenesis, although some receptors form spontaneous clusters (pre-patterned), nAChRs are distributed throughout the membrane of the muscle cells. In addition, the “embryonic” nAChR expressed in developing skeletal muscle fibers are characterized by a ɣ subunit in place of the ε subunit of the adults[33]. From the functional point of view, electrophysiological experiments reveal that the $\alpha_2\beta\delta\varepsilon$ isoform has a higher single channel conductance and a shorter mean open time[34,35] (Fig. 7).

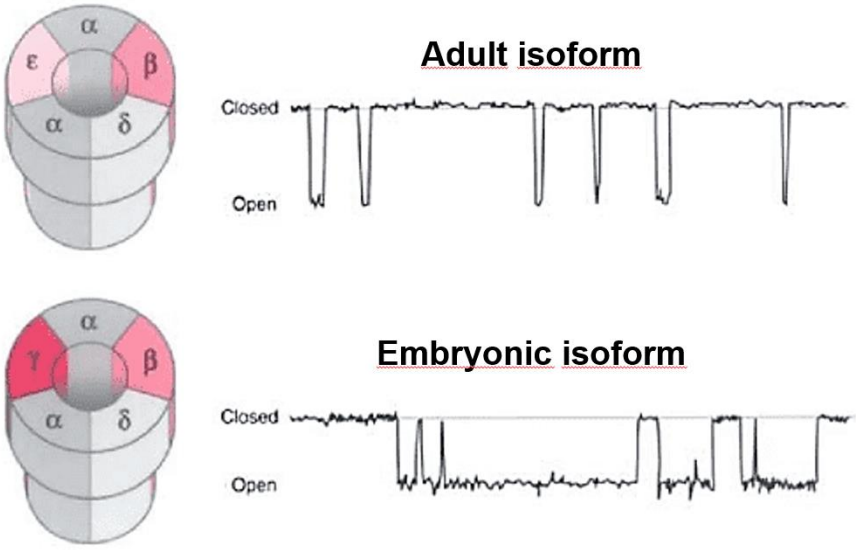

Fig. 7. *Left, subunit composition of adult and embryonic nAChRs isoforms. Right, representative electrophysiological traces of single channel openings of the adult and embryonic nAChR isoforms (modified from 39).*

Distribution and stability of the nAChRs at the endplate are controlled by both release of soluble factors from the motor nerve endings and electrical activity of the muscle fiber[36–39].

The high density of nAChRs in the postsynaptic membrane is the result of a specific gene expression of the nAChR subunits confined to the subsynaptic nuclei, controlled by the neural agrin released by the nerve terminals. Neural agrin is a motoneuron-derived large proteoglycan playing a central role in the NMJ development and maturation. Neural agrin controls growth and stabilization of the endplate nAChRs[38] and the distribution and expression of a number of extracellular matrix-associated proteins, cytoplasmic and membrane components of the postsynaptic apparatus[40,41]. It acts via a receptor complex consisting of the muscle-specific tyrosine kinase MuSK[42] and the low-density lipoprotein receptor-related protein LRP4. Lrp4 acts as co-receptor[43,44] and the MuSK/Lrp4 complex controls a multifaceted signaling pathway inducing and maintaining nAChR clustering at the endplate[45] (Fig. 8).

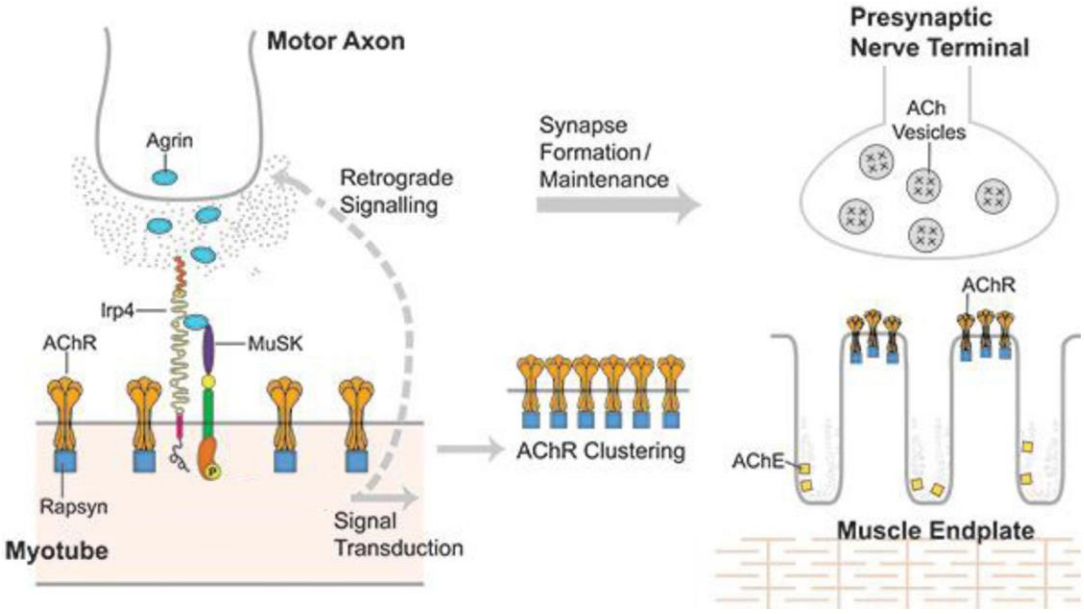

Fig. 8. *The role of neural agrin in the NMJ development. The growing motor axon releases neural agrin likely in an activity-dependent manner. When it reaches a developing myotube, neural agrin binds to the receptor complex MuSK/Lrp4 rp4 and activates the downstream cascade controlling the AChR clustering and stabilization at the endplate level of the NMJ (modified from 45).*

In particular, the localization of nAChRs at the end plate is mediated by regulated interactions with multiple scaffolding molecules, which participate to the regulation of the number, density and stability of receptors at the synapse. The neural agrin-promoted clusterization of nAChRs is mediated by Rapsyn, a 43-kDa protein regulating the agrin signaling. It links β-dystroglycan anchoring the nAChRs to components of cytoskeletal complex. Rapsyn is also crucial for synapse formation; indeed, knock-out mice lacking rapsyn die within hours after birth[46,47] (Fig. 9).

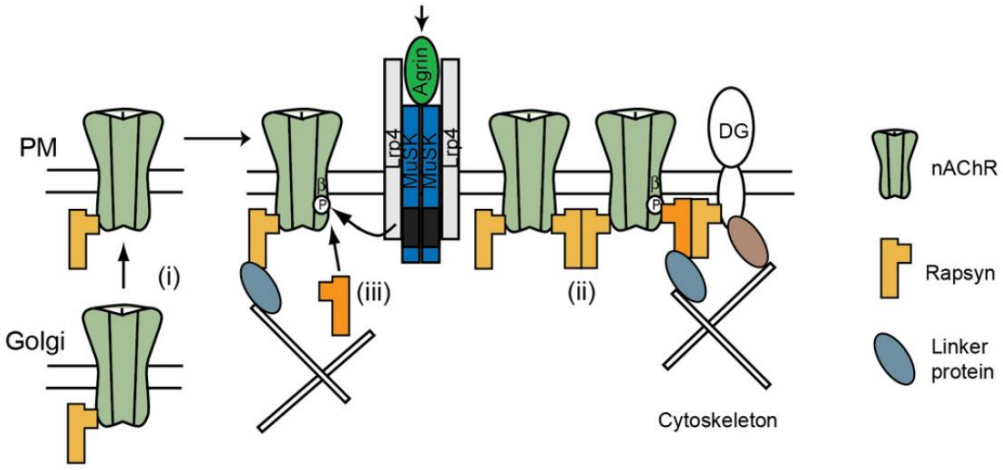

Fig. 9. *Rapsyn interactions at the endplate level. Rapsyn associates with the nAChR in the Golgi apparatus (i) and form pre-formed complexes with nAChRs on the plasmalemma (PM). Agrin-MuSK/Lrp4 signaling induces nAChR clustering via rapsyn dimerization (ii) and by promoting the binding of rapsyn to the nAChR phosphorylated βY390 motif (iii). Recruitment of additional rapsyn may require a chaperone protein (not shown). These two mechanisms create rapsyn bridges between nAChRs and anchored nAChRs to transmembrane and cytoskeletal scaffolding proteins. The stoichiometry of rapsyn/nAChR complexes is an important determinant of the density and stability of nAChRs in the postsynaptic membrane (modified from 47).*

1.1h The physio-pathological changes of the NMJ

A proper activity of NMJ appears to be crucial for the maintenance of the skeletal muscle structure and function. Altered motoneuron discharge causes an altered release of neurotrophic factors and the latter differently affect the functional profile of the skeletal muscle[48]. Neurotrophic factors[76], as well as firing activity[77], contribute to modulate phenotype and muscle contractile properties, as revealed by the fact that slow muscles cross-reinnervated by a fast motor neuron acquire fast contractile properties and vice versa.

Denervation (caused by neurodegenerative diseases or acute trauma) is responsible for rapid skeletal muscle fiber degeneration leading to the activation of atrophy-related pathway and to functional and structural changes in skeletal muscle, such as alterations in myofibrillar expression, shorter half-life of the nAChRs (from several days in normal innervated animals to 24 h[49]), expression switch from adult ε-nAChRs to embryonic γ-nAChRs, altered nAChR clustering and impaired EC process[50,51].

Aging is associated to a functional denervation of the skeletal muscles, causing a decreased skeletal muscle mass and functional capacity (sarcopenia) with a shift from fast-to-slow fiber. Muscle mass decreases approximately from 3 to 8% every 10 years after the age of 30, and the percentage of muscle loss becomes larger after sixsties[52,53]. This involuntary loss of muscle mass, strength, and function is one of the reasons of disability in older people. Sarcopenia, such as many gene-related muscular dystrophies, share defects at the nerve–muscle synapse, such as, NMJs fragmentation and altered characteristics of nAChRs and neural agrin signaling[54,55] (Fig. 10).

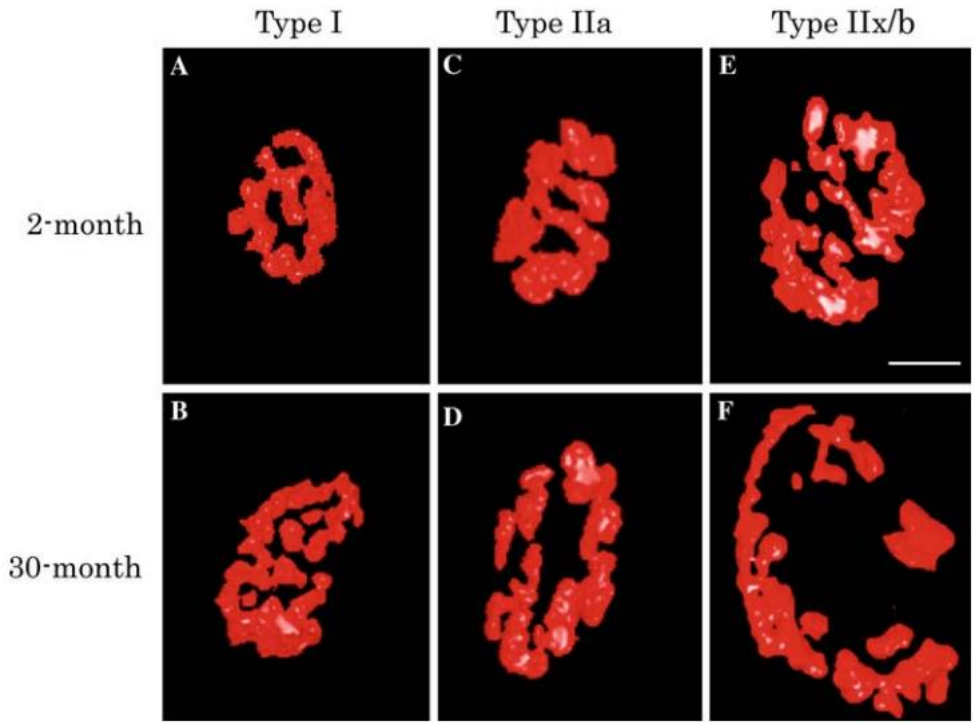

***Fig. 10**. 3D images of endplate in different fiber type from 2-month-old (A, C, E) and 30-month-old (B, D, F) rats (from 55).*

1.1i IP_3-sensitive Ca^{2+} stores

Ca^{2+} is a well-known versatile second messenger, controlling several and different cellular processes. In the skeletal muscle, it has a central role in the contraction event. Subcellular fractionation and immunocytochemistry[56] confirmed the interpretation of SR as a specialized ER compartment[57–59]. As previously described, when the EC coupling mechanism is triggered, a release of Ca^{2+} from intracellular SR is mediated by the voltage-dependent activation of the DHPRs-RyR1 complexes present at the triadic level.

Interestingly, in mammalian skeletal muscle, also inositol trisphosphate (IP_3) was reported to release Ca^{2+} from isolated SR fractions[60] and, in frog muscles, IP_3 was found to be released by electrical stimulation (ES) and to induce fiber contractions[61]. However, the role of the IP_3-sensitive store and the IP_3 receptors (R)-mediated Ca^{2+} release in the skeletal muscle physiology remains to be partially unknown. It is known that the IP_3R activation generates long-lasting $[Ca^{2+}]_i$ transients but their role is still matter of debate.

Skeletal muscle fibers have all the biochemical machinery for generation and catabolism of inositol phosphates as revealed by *in situ* hybridization and immunohistochemistry[62]. [^{3}H]-IP_3 binding revealed that IP_3Rs are preferentially expressed in slow oxidative (type I) and fast oxidative glycolytic (type IIA) fibers[62] and more recent immunofluorescent studies[63,64] confirmed the abovementioned observation.

In the skeletal muscle, the prevalent isoform of the IP_3R is the IP_3R-1[64], capable to amplify postsynaptic Ca^{2+} signals. This isoform is suggested to play a key role in NMJ development and maintenance, homeostatic regulation of neuromuscular transmission and synaptic gene expression[65]. High levels of IP_3Rs were found in postsynaptic component of NMJ, in particular surrounding motor endplate nuclei, and close to nAChRs of the endplate gutters[66]. Junctions were observed in muscle fibers between the subsynaptic folds and the rough SR at a large distance from myofibrils, indicating a particular role for such structures in the regulation of the nAChR gene expression[67]. Furthermore, subsynaptic folds were observed to continue into the T-tubular system[68]. The tubular network closed to the synaptic folds branches out to participate in the formation of triad-like structures and generation of subsynaptic local IP_3-controlled Ca^{2+}

changes[69]. It is interesting to note that, in cultured myotubes, the motor nerve activity induces slow Ca^{2+} transients at the NMJ level, which are not involved in contraction[70] and that appear to regulate neural agrin-induced nAChR clustering[71].

Localized Ca^{2+} signaling at the endplate level was suggested to be mediated by the interplay between nAChRs activity and the IP_3R[72]. In pathological condition, an overactivation of nerve terminal-associated cholinergic receptors leads to NMJ degeneration[65,72]. In synapses between neurons, the scaffold protein Homer has been shown to interact with the IP_3Rs[73–75]. In the skeletal muscle, Homer proteins were also found at the subsynaptic level[63]. Therefore, IP_3R-Homer interaction could participate in shaping local Ca^{2+} signals beneath the postsynaptic membrane[76] (Fig. 11).

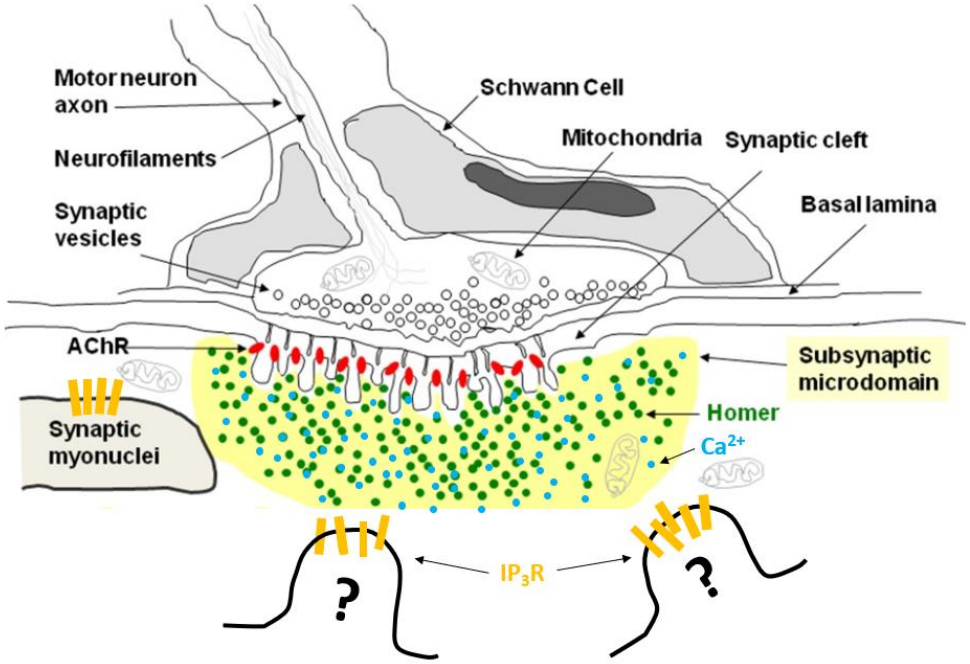

***Fig.11**. Image representing Homer protein, IP_3Rs and Ca^{2+} distribution at the subsynaptic region (modified from 76).*

1.2 Electrical stimulation

It is well established that electrical activity initiates specific molecular signaling pathways enhancing the communication between nerve and muscle and promoting not only to fiber contractions but also developmental changes, myoblast orientation, muscle fiber phenotype. Exogenous electrical pulse stimulation (EPS) could prevent the effects of denervation at the endplate level. In extra synaptic regions, electrical activity is the predominant signal that 'shut off' the expression of the fetal ɣ-nAChRs during development[35,77]. Motor innervation plays a crucial role not only in the stabilization of AChRs in the postsynaptic membrane preventing the loss of end-plate membrane structure[78], but also in promoting the recycling of internalized AChRs into the synaptic membrane.

People affected by disabling diseases, sarcopenia or upon surgery due to road accidents are often unable to move and are usually forced to remain immobile for a long period of time. Since physical activity is essential to maintain normal functioning muscles, prolonged immobilization leads to muscle strength (hyposthenia) and muscle mass (hypotrophy) reduction, which could reach 50% after six weeks of posture in bed. EPS is highly used for physiotherapeutic and rehabilitative purposes, to improve the physical condition, such as contractility and metabolism of patients, potentially restoring part of physiological body compositions and functions, movement included.

In clinical settings, EPS can be used for many different conditions, for example to improve muscle strength, to reduce edema, to increase range of motion, to decrease atrophy, especially in old people, and healing tissues[79]. Over the years the use of EPS has expanded into many fields such as in sports, for training and muscle recovery, and in aesthetic treatments for lymphatic drainage and body fat reduction. Nowadays, it represents a useful and potential tool in regenerative medicine to implement stimuli for muscle tissues, thanks to its effectiveness, safety and easy use.

1.2a Exercise models

The beneficial health-related effects of exercise are well recognized. The choice of appropriate type, repetition, duration, and intensity of the exercises are determinant for favoring a specific glycolytic or oxidative metabolic profile, and fiber types potentiation[80]. *In vivo*, EPS induces exercise-like effects depending on the frequency, duration, and intensity of electrical stimulation pulses[81,82].

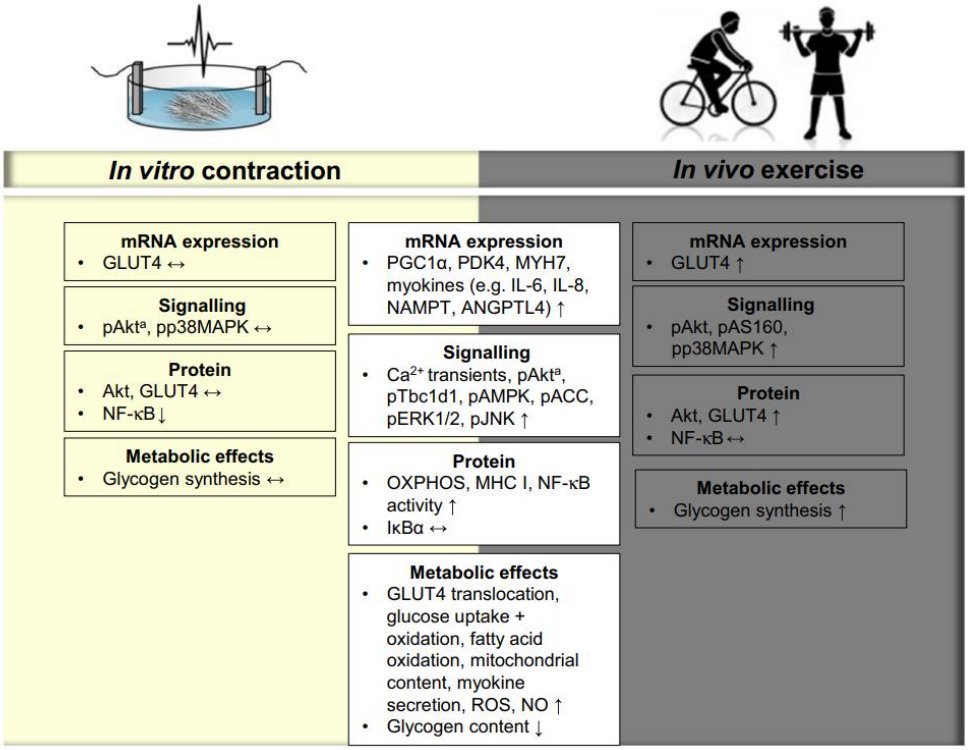

Fig 12*. In vitro EPS effects compared with the effects of in vivo exercise. Overlapping effects are presented in the middle white column. The specific effects observed in vitro and in vivo are shown in the two outer columns (from 81).*

Using various *in vivo* and *in vitro* models, numerous studies have investigated the cellular mechanism behind the usage/efficacy of EPS.

Starting from 1970' experiments, EPS of cultured skeletal muscle cells represents a tool to study muscle cell behavior, to identify myokines release and to study the role of denervation/reinnervation on AChRs regulation[83]. Today, human EPS protocols applied to 2D muscle cell cultures are used also to study, *in vitro*, what exactly happen at

molecular level during regular physical activity and which ultrastructural components and functional correlation are involved in health promotion (Fig. 12). Moreover, the cell culture systems combined with EPS offer the possibility to isolate muscle cells from other cell types, eliminating the interference of paracrine effects by other organs and thus to analyze the exercise-like effects in a controlled environment.

C2C12 skeletal muscle cell line was firstly used as exercise cell model[84]. Continuous EPS for 24 h at 1 Hz[84] induced visible C2C12 contraction as well as activation of both AMP-activated protein kinase (AMPK) cascade and mitogen-activated protein kinases (MAPK) pathway, which mediated several cellular processes such as proliferation, differentiation, apoptosis, stress responses, angiogenesis, glucose uptake, insulin sensitivity *in vivo*. Interleukin-6 (IL-6), C-X-C motif, chemokine (CXCL) 1 and CXCL5 release was also detected like in contracting skeletal muscle *in vivo*.

In 2016, Jaatinen et al. showed that EPS could change cell structure and adhesion properties in mouse myoblasts[85]. Moreover, both cardiac and skeletal muscle alignment and differentiation are known to be influenced by EPS[86].

Different types of exercises affect differently the skeletal muscle *in vivo* by activating different signaling pathways. Low load endurance exercise is characterized by oxygen delivery induced by capillary and mitochondrial activity[87–91], whereas high-load strength type of exercise leads to growth of muscle fibers with a rise in contractile proteins[92,93]. High intensity exercises were reproduced *in vitro*[94] with EPS consisting in 200 ms trains at 100 Hz given every 5th second for 5 min to evaluate the metabolic effects of an acute high intensity bout of exercise. Glucose uptake, consumption of ATP and phosphocreatine (PCr) with an increase in cell production of lactate were observed[95]. However, if EPS protocols are able to mimic *in vitro* an endurance-type or resistance-type of exercise *in vivo* is still matter of investigation. In isolated human myotubes, long lasting (2-48 h) and low frequencies (1 Hz 2 ms) stimulations showed a cytoskeleton reorganization, the AMPK activation, IL-6 increased secretion[96]. Low and high frequency EPS appear to activate separate signaling pathways depending also on the duration of EPS protocol (Fig. 13).

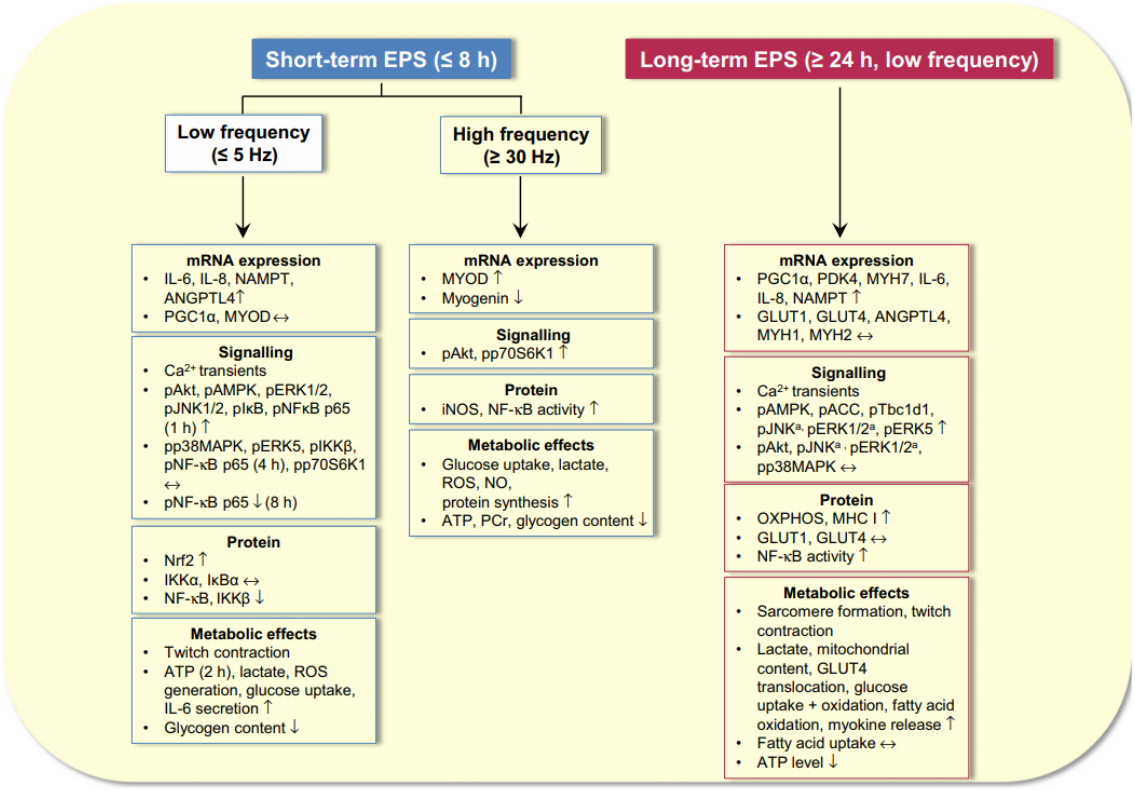

Fig. 13. *Effects of short-term vs. long-term EPS on signaling pathways, mRNA expression, protein level and metabolism measured directly after completing the EPS protocol (from 81).*

1.2b The importance of EPS parameters

The EPS devices deliver pulses in waveform patterns composed by square or rectangular waves. Monophasic pulses have only one phase and the current flow is unidirectional; biphasic currents consists of two phases, each occurring on opposite side of the baseline. If these two phases are equal in their magnitude, duration and shape, the resulting pulse is considered as symmetrical biphasic [97]. (Fig. 14). Balanced biphasic electrical stimulation have the advantage to prevent an excessive charge accumulation at the electrodes, that otherwise could prevent current flow from the stimulating electrodes[98]. Importantly, with balanced biphasic stimulation, the electrical charge delivered during one phase would be withdrawn during the opposite phase, resulting in no net charge accumulation.

Pulse duration can be increased to potentially recruit more fibers in the surrounding area in order to reduce atrophy. Comparing different pulse durations, it was observed that wider pulse widths produced stronger contractions than the narrow ones, helping atrophy reduction and producing fatigue-resistant contractions for rehabilitation[99].

The intensity/amplitude (usually reported in mA or mV, depending on the stimulator output) of single pulses are proportional to the number of activated fibers. Recruiting more motor units results in a stronger contraction force. However, high pulse intensity induces pain and, therefore, it is usually less tolerated[79].

The frequency of electrical pulses is responsible for different effects. In clinics, protocols between 2 and 4 Hz favor the trophism of muscle mass and improve the microcirculation. In addition, at a frequency of 4 Hz, the body produces enkephalins, which raise the pain threshold. Increasing the frequency to 8 Hz rises the pain threshold and elicits positive effects such as an intense relaxing effect on the stimulated area, improvement of local blood circulation, a decrease in toxic metabolites and an improvement in tissue oxygenation. From 18 and 40 Hz mainly slow fibers are activated. This type of stimulation is equivalent to the muscular work of a continuous running of medium intensity, through which aerobic capacity is improved without any oxygen deficit. Between 60 Hz and 80 Hz, depending on the pulse width, intermediate and fast fibers are recruited causing an increase in the muscle strength. Frequencies between 80 Hz and 120 Hz recruit the fast fibers and are indicated to improve strength and speed.

Proper stimuli are also necessary to activate the so called excitation-transcription (ET) coupling, controlling the gene expression profile in the skeletal muscle fibers[64]. Such ET coupling was at least in part based on IP_3-mediated slow Ca^{2+} signals, which follow the RyR1-dependent fast Ca^{2+} transient responsible for the contractile activity. The amplitudes of the slow Ca^{2+} signals are proportional to the frequencies of stimulation, reaching maximal values from 10 to 20 Hz[64]. Experimental results indicate that IP_3 production and activation of IP_3Rs are probably maximal at 20 Hz[64]. Even an increase in the number of pulses in the train increased the slow Ca^{2+} response: an increased number of depolarizing events elicits more easily the slow Ca^{2+} response.

During the EPS, motor unit recruitment is usually nonselective, compromising the natural rate of fatigue resistance[100]. In our laboratory, in collaboration with Giuliano Taccola,

from the International School of Advanced Studies, we tested an innovative EPS “noisy” protocol, called EMGstim, in an exercise model of cultured skeletal muscle cells. Such protocol derived from human gastrocnemius medialis electromyographic recordings, during an overground locomotion at a freely selected speed (1 m/s; Fig. 15)[101]. The EMGstim was characterized by biphasic voltage pulses of various duration, amplitude and frequency, and it was capable of eliciting contractions *in vitro* mouse myotubes, more efficiently than “regular” conventional stimulation protocols. In details, action potentials firing at 1 Hz was detected in myotubes, time locked with their contractions at a lower stimulus strength than regular 1 Hz, 1 ms pulse stimulations. Moreover, EMGstim protocol was able to promote muscle progenitor cell differentiation via the release of endogenous ATP[102]. Such “noisy” EPS protocol, in which pulses change continuously their amplitude, duration and frequency, was suggested to recruit motor units with different thresholds at different times. Thus, the use of “noisy” protocols in human patients could have the advantage to limit the common occurrence of pain and fatigue, typical of the regular high frequency stimulations.

More in general, the optimization of EPS parameters, including electrode material, electrode placement, and the use of variable parameters in the pulse patterns, could improve the therapeutic benefits obtained by this technique.

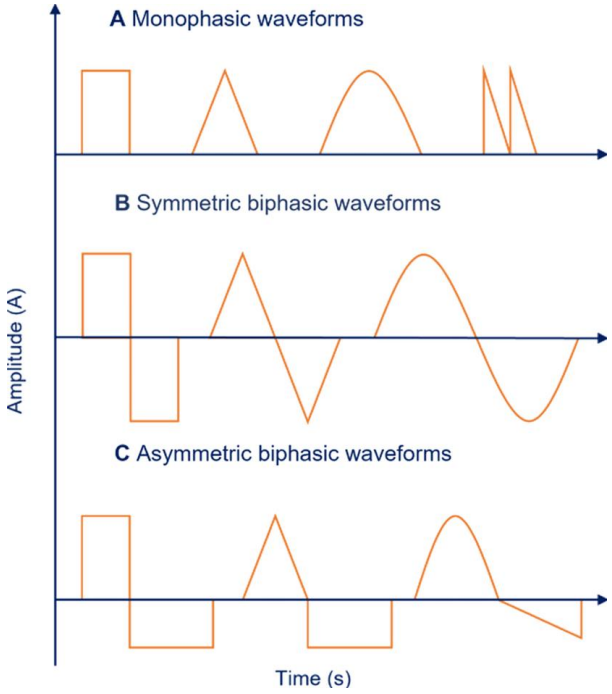

Fig. 14. *Different shapes and waveforms of pulsed electrical current. (A) Examples of monophasic waveforms above the zero baseline. (B) Examples of biphasic waveforms. (C) Examples of asymmetric and/or charged unbalanced (from 103).*

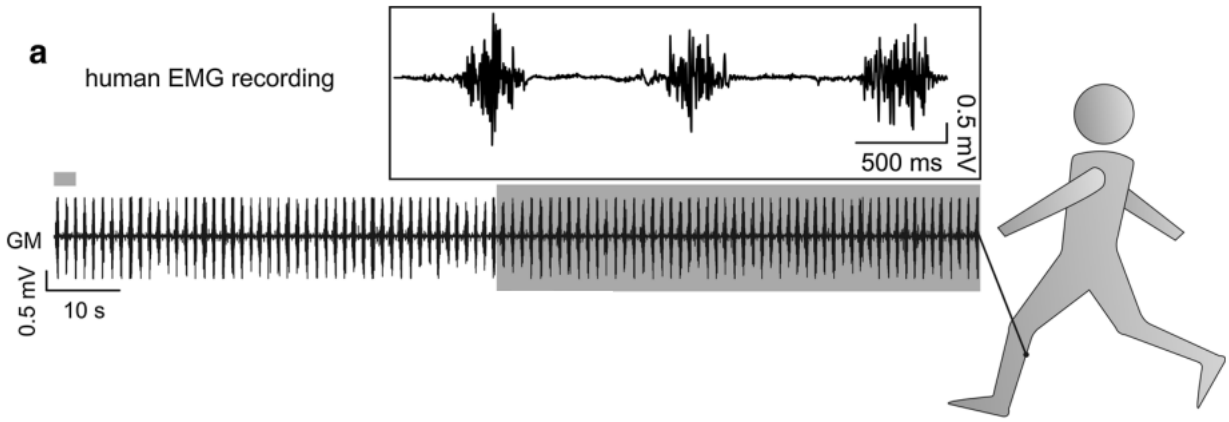

Fig. 15. *The EMGstim protocol design. A 60 s segment trace (grey box), sampled from a human EMG recording is taken in order to design off-line, the noisy stimulation pattern EMGstim. The inset shows an expanded part of the EMGstim (corresponding to upper gray rectangle) to reveal the stochastic nature of the protocol (Modified from 101).m*[101]

1.2c Skeletal muscle as an endocrine organ

Beside the classical and more known functions of locomotion and energy production, the skeletal muscle is also classified as an endocrine organ. The skeletal muscle fibers synthesize, express and release multiple factors, called myokines, which exert paracrine, autocrine and/or endocrine effects also on peripheral and remote organs[103]. Nowadays, the hypothesis is that a synergistic crosstalk among nervous, endocrine, immune and skeletal muscle systems is needed to maintain the body homeostasis (Fig. 16)[104].

Even if the skeletal muscle secretes hundreds of myokines, the majority are still not sufficiently characterized. Only few of them have been studied for their biological activity and function. Brain-derived neurotrophic factor (BDNF), myostatin, the group of IL-4, IL-6, IL-7, IL-8 and IL-15, irisin and insulin-like Growth Factor-1 (IGF-1) are the best known. How their synthesis and release are controlled is still matter of investigation, but there are experimental evidences in favor of a contractile-dependent mechanism[105–107].

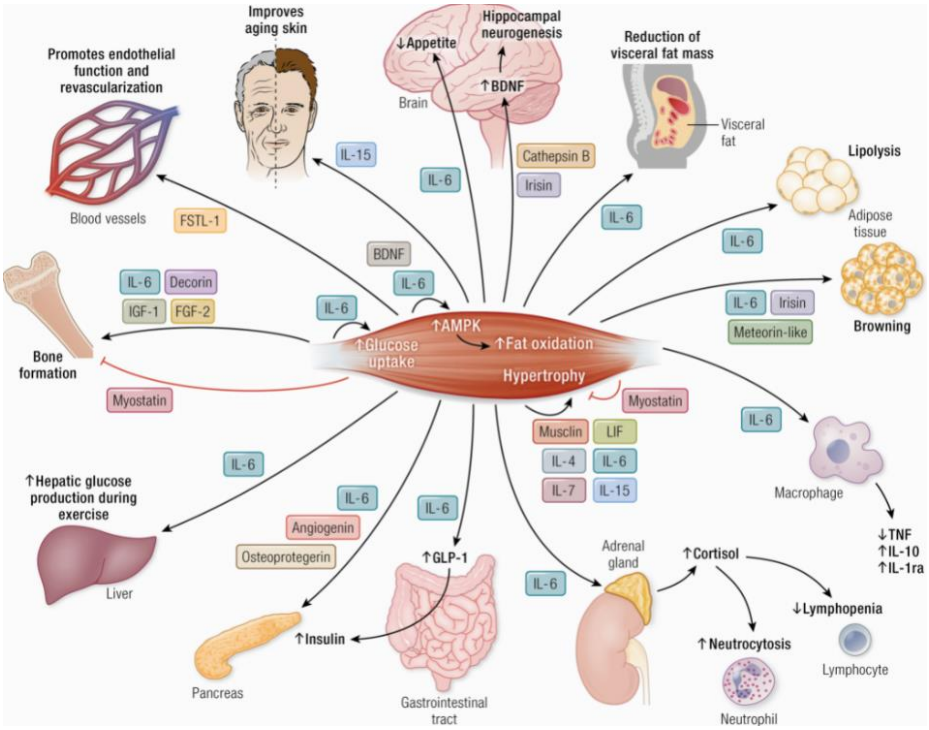

Fig. 16. *Myokines crosstalk with organs. Different myokines affect muscle itself, brain, adipose, immune system, gut, pancreatic beta-cell, liver, bone, vascular bed, and skin (rom 104).*

During contraction, muscle cells undergo mechanical strain, causing the activation of specific gene expression programs, such as myogenesis, differentiation and hypertrophy. In recent years, mechano-transduction has aroused the interest of researchers, who study the skeletal muscle physiology. An emerging hypothesis is that mechanoreceptors could be involved in several mechanisms converting the contractile activity into intracellular signaling cascades. Interestingly, the expression of mechanosensitive channels was found to be inversely proportional to the expression of atrophy-related genes Klfl5 and IL-6 in denervated or immobilized muscle fibers[108]. Moreover, there are data indicating that the mechanosensitive channels control the basal $[Ca^{2+}]_i$ even when the cell is relaxed.

2. AIMS OF THE STUDY

Functional innervation of skeletal muscle cells is required to guarantee a physiological development and maintenance of trophic homeostasis and muscle mass. Upon denervation, skeletal muscle alterations include changes at different levels, such as metabolic, biochemical and structural. Impairments in nerve-muscle communication due to ageing, disuse or injuries produce alterations in electrophysiological muscle membrane properties, Ca^{2+} release mechanisms, nAChRs distribution, EC coupling mechanism, muscle fiber type composition and release of myokines.

The aim of my research project was to investigate the different aspects of electrical stimulation/activity in cultured skeletal muscle cells. In particular, my research activity was organized in two phases.

The first part of my research focused on the effects of electrical activity at the NMJ level. Because EPS mimics nerve activity inducing muscle cell contraction, it has been proposed as a tool to counteract the related NMJ denervation-changes. We investigated the role of electrical activity *vs* neural agrin in controlling the subsynaptic IP_3R1-sensitive compartment. Moreover, since the expression and distribution of some scaffold proteins are dependent on nerve and muscle activity, we investigated the role of the scaffold protein Homer 2 in the stabilization of the NMJ using a transgenic Homer $2^{-/-}$ mice model.

The second part of my research set out to investigate the EPS-induced modulation of myokine release. We focused our attention on the myokine IL-6, known to be released upon contraction and to increase at the systemic level during exercise[109–111]. In particular, we investigated the possible involvement of the mechanosensitive Piezo 1 channels in the myokine release during EPS-induced muscle cell contraction and the ability of the pharmacological compound Yoda 1 to mimic the EPS-induced myokine release.

3. PUBLISHED RESULTS

3.a Studies on subsynaptic IP_3Rs and scaffold protein Homer 2 and their emerging role in the NMJ stability

Muscle electrical activity induced by motor neuron represents an essential factor in regulating the expression, the distribution and the stability of nAChR at the endplate level. Indeed, since electrical activity controls nAChRs half-life and turnover[112–114], denervation causes a fragmentation of the endplate. This phenomenon is associated with an alteration of the NMJ electrical properties due to the isoform switch from adult ε-nAChRs to embryonic γ-nAChRs[50,51], characterized by a reduced Ca^{2+} permeability, conductance and slower kinetics.

Electrical activity, through postsynaptic membrane depolarization, has been proposed to induce synaptic Ca^{2+} signals related to the so-called ET coupling mechanism based on an IP_3R-mediated Ca^{2+} release controlling the regulation of gene expression[115–118]. At the endplate level, sarcoplasmic/endoplasmic reticulum elements are localized close to the walls of the synaptic folds, forming subsynaptic triads[69] and/or junctions of unknown function[67]. IP_3Rs[66] were found to be localized around subsynaptic nuclei and close to nAChRs on the crests of the postsynaptic folds[66]. In pathophysiological conditions, upon denervation, an abnormal activity of IP_3Rs and rearrangement of the endplate region, are described[72]. At the endplate level, the prevalent isoform IP_3R1 is involved in controlling synaptic gene expression, development and maintenance of NMJ structure and function, as determined by RNA interference-mediated gene silencing[65]. A role of IP_3R1 in modulating cholinergic transmission at the NMJ has been therefore proposed[64,65].

All these observations raise the question of whether and how innervation and nerve-driven electrical activity control the subsynaptic IP_3R1-sensitive membrane compartment, fundamental in the NMJ stabilization. To investigate this intriguing aspect, we used both *in vivo* (denervated EDL) and *in vitro* models (cultured FDB skeletal muscle fibers) of denervation. Briefly, endplate nAChRs and the corresponding subsynaptic IP_3R1s-stained volumes were analyzed using confocal fluorescence microscopy. Flash photolysis experiments of caged IP_3 were performed to investigate the effects of

denervation on the local subsynaptic IP_3-mediated Ca^{2+} signals at functional level. In addition, since both electrical muscle activity and neural agrin maintain the endplate apparatus[34,119,120], we also investigated if the subsynaptic distribution of IP_3R1s was under the control of one of both of them. Our results demonstrated that IP_3R1 distribution is highly sensitive (even more than nAChRs) to the absence of nerve activity. EPS was able to counteract, although partially, the denervation-induced reduction of the IP_3R1-stained volume in the subsynaptic region.

In skeletal muscle, the scaffold proteins Homer interact with IP_3R and RyR1, playing a central role in Ca^{2+} signaling, development, and adaptation of muscle fibers. Many Homer isoforms are expressed in skeletal muscles fiber, depending on the phenotype. It was demonstrated that Homer 2 is able to antagonize protein degradation[121] and denervation/atrophy experiments demonstrated a rapid reduction of Homer 2 expression. In humans, Homer 2 levels were downregulated after prolonged (60 days) bedrest[122]. However, it remains still partially unclear the role of Homer 2 in skeletal muscle adaptation and/or whether and how Homer 2 modulates the structure of muscle endplate. We took advantage of the availability of the transgenic Homer $2^{-/-}$ mice to investigate this aspect. The observed upregulation of atrophy-related genes in Homer $2^{-/-}$ mice confirmed the role of Homer 2 in muscle catabolism. Morphometry analysis in Homer $2^{-/-}$ mice revealed a decrease in CSA of SOL and not of EDL and FDB muscles suggesting a type-specific signaling involved in atrophy. Using confocal immunofluorescence microscopy, we also observed a reduction in the endplate volume in isolated FDB Homer $2^{-/-}$ fibers. Briefly, our results suggest that, the scaffold protein Homer 2 could play an important role at the NMJ level integrating different downstream signaling pathways controlled by NMJ and involved in the maintenance of the cell trophism.

JGP Journal of General Physiology

ARTICLE

Excitation–Contraction Coupling

Nerve-dependent distribution of subsynaptic type 1 inositol 1,4,5-trisphosphate receptor at the neuromuscular junction

Pompeo Volpe[1], Alessandra Bosutti[2], Alessandra Nori[1], Riccardo Filadi[1,3], Gaia Gherardi[1], Gabor Trautmann[4], Sandra Furlan[3], Gabriele Massaria[2], Marina Sciancalepore[2], Aram Megighian[1], Paola Caccin[1], Annalisa Bernareggi[2], Michele Salanova[4,5], Roberta Sacchetto[6], Dorianna Sandonà[1], Paola Pizzo[1,3], and Paola Lorenzon[2]

Inositol 1,4,5-trisphosphate receptors (IP_3Rs) are enriched at postsynaptic membrane compartments of the neuromuscular junction (NMJ), surrounding the subsynaptic nuclei and close to nicotinic acetylcholine receptors (nAChRs) of the motor endplate. At the endplate level, it has been proposed that nerve-dependent electrical activity might trigger IP_3-associated, local Ca^{2+} signals not only involved in excitation–transcription (ET) coupling but also crucial to the development and stabilization of the NMJ itself. The present study was undertaken to examine whether denervation affects the subsynaptic IP_3R distribution in skeletal muscles and which are the underlying mechanisms. Fluorescence microscopy, carried out on in vivo denervated muscles (following sciatectomy) and in vitro denervated skeletal muscle fibers from flexor digitorum brevis (FDB), indicates that denervation causes a reduction in the subsynaptic IP_3R1-stained region, and such a decrease appears to be determined by the lack of muscle electrical activity, as judged by partial reversal upon field electrical stimulation of in vitro denervated skeletal muscle fibers.

Introduction

Motor innervation is required for the maturation and maintenance of diversity of both slow-twitch and fast-twitch fibers, thus regulating the contractile properties of skeletal muscle fibers, in part through the effect of electrical activity on the expression of distinct myosins. Motor innervation is also required for the attainment and maintenance of trophic homeostasis and muscle mass (Tintignac et al., 2015), with inactivity and denervation being paramount causes of skeletal muscle atrophy (Carlson, 2014).

Efficient neuromuscular transmission requires complex machineries both at pre- and postsynaptic compartments of the neuromuscular junction (NMJ). The motorneuron has developed molecular strategies to tune the adequate release of neurotransmitter acetylcholine (ACh); the skeletal muscle fiber has adopted strategies to maximize the binding of ACh to nicotinic acetylcholine receptors (nAChRs) to trigger action potentials and to turn on the excitation–contraction (EC) coupling apparatus.

Expression, distribution, and stability of nAChR at the endplate are controlled by both the release of soluble factors from motor nerve endings and the electrical activity of muscle fibers (Duclert and Changeux, 1995; Missias et al., 1996; Sanes and Lichtman, 2001; Li et al., 2018; Shi et al., 2012). Skeletal muscle denervation causes nAChR cluster dispersal at the endplate zone, reduction in the half-life of synaptic nAChRs, and isoform switch from adult ε-nAChRs to embryonic γ-nAChRs, the latter being diffusely distributed over the muscle plasma membrane (Midrio, 2006; Wu et al., 2014).

Among nerve-derived chemical messengers, a key role is played by the proteoglycan agrin (McMahan, 1990) via the activation of the Lrp4/MuSK receptor complex (Li et al., 2018).

[1]Department of Biomedical Sciences and Interdepartmental Research Center of Myology (cirMYO), University of Padova, Padova, Italy; [2]Department of Life Sciences, University of Trieste, Trieste, Italy; [3]National Research Council, Neuroscience Institute, Padova, Italy; [4]Charité-Universitätsmedizin Berlin, Corporate Member of Freie Universität Berlin, Humboldt-Universität zu Berlin and Berlin Institute of Health, Institute of Integrative Neuroanatomy, Berlin, Germany; [5]Neuromuscular Signaling, Center of Space Medicine Berlin, Berlin, Germany; [6]Department of Comparative Biomedicine and Food Science, University of Padova, Padova, Italy.

Correspondence to Pompeo Volpe: pompeo.volpe@unipd.it

This work is part of a special issue on excitation–contraction coupling.

Neural agrin controls the growth and stabilization of the endplate nAChRs (Sanes and Lichtman, 2001) and the distribution and expression of a number of other components of the postsynaptic apparatus (Wallace, 1989; Meier et al., 1997; Briguet and Ruegg, 2000).

As to the regulating effect of the electrical activity, direct muscle stimulation alone is able to prevent the denervation effects at the endplate level. In denervated active/stimulated muscles, electrical activity prevents the denervation-induced decline of metabolic nAChR stability and the loss of endplate structure, and also suppresses the expression of the fetal γ-nAChRs (Brenner and Rudin, 1989). Moreover, direct muscle stimulation counteracts the reduction in the endplate nAChR density induced by blockade of the neuromuscular transmission (Akaaboune et al., 1999). The effects of the induced electrical activity are mediated by an increase in intracellular Ca^{2+} concentration ($[Ca^{2+}]_i$), through either ligand-gated, L-type channels or intracellular Ca^{2+} stores, and are, at least in part, dependent on nAChRs phosphorylation (Martinez-Pena y Valenzuela and Akaaboune, 2021).

The electrical activity of muscle fibers also exerts its role by changes in $[Ca^{2+}]_i$, definitely unrelated to RyR-Ca^{2+} channels responsible for Ca^{2+} release from the SR during EC coupling (Ríos and Pizarro, 1991): evidence is accruing in favor of an inositol 1,4,5-trisphosphate receptor (IP_3R)-mediated Ca^{2+} signaling in the activity-dependent regulation of muscle gene expression (Araya et al., 2003), a process referred to as excitation–transcription (ET) coupling, through which skeletal muscle fibers decode the motoneuron stimulation pattern into a specific gene expression profile and phenotype (Casas et al., 2022).

The presence of all the intermediate steps involved in the metabolism of phosphoinositides, from synthesis to degradation of IP_3 (Milani et al., 1988; Hidalgo and Jaimovich, 1989), the presence of IP_3Rs, as shown by in situ hybridization, immunohistochemistry, and $[^3H]$-IP_3 binding (Moschella et al., 1995), provides a role for IP_3 in skeletal muscle function highly likely (Volpe et al., 1985; Vergara et al., 1985), although unrelated to proposals concerning the role of IP_3 as a chemical messenger for EC coupling (Somlyo, 1985; Blaauw et al., 2012).

IP_3R immunofluorescence analysis shows a staining pattern indicative of the localization of IP_3Rs at the Z-line in murine muscles different from that of type 1 RyRs. In addition, subcellular fractionation experiments show IP_3R to be enriched in longitudinal SR but not in terminal cisternae containing RyRs (Salanova et al., 2002; Powell et al., 2003). IP_3Rs are also enriched at postsynaptic components of the NMJ, surrounding the subsynaptic nuclei and close to nAChRs of the motor endplate (Powell et al., 2003). At the endplate level, IP_3R1 is the prevalent isoform and is involved in synaptic gene expression, as determined by RNA interference-mediated IP_3R1 gene silencing (Zhu et al., 2011). IP_3R1s could be placed either in walls of the synaptic folds, subsynaptic triads (Dauber et al., 2000), and/or junctions of unknown function between subsynaptic folds and rough SR (Dauber et al., 1999).

Nerve-driven electrical activity might trigger IP_3-associated, local Ca^{2+} signals in NMJ involved not only in gene regulation but also crucial to the development and stabilization of the NMJ itself (Powell et al., 2003). In more detail, a functional interplay between nAChRs activity and IP_3R1-driven Ca^{2+} release has been proposed to be responsible for localized subsynaptic Ca^{2+} signaling (Zayas et al., 2007; Zhu et al., 2011). In pathophysiological conditions, abnormal activity of IP_3Rs could also be responsible for Ca^{2+} overload observed in the slow-channel myasthenic syndrome (Zayas et al., 2007) and for NMJ degeneration during excessive cholinergic activation (Zhu et al., 2011).

Although hypotheses have been formulated for the presence and role of subsynaptic IP_3R-driven Ca^{2+} signaling in innervated skeletal muscle fibers, it is not known whether and how innervation controls the subsynaptic IP_3R1 membrane compartment. Based on the significant rearrangement of the endplate region following denervation and the supposed functional interaction between endplate nAChRs and IP_3R1s, the present study was undertaken to examine whether denervation affects the subsynaptic IP_3R1 distribution and to unveil the mechanisms controlling the expression and localization of subsynaptic IP_3R1s. Fluorescence microscopy carried out on in vivo denervated muscles (sciatectomy) and in vitro denervated adult skeletal muscle fibers (cultured flexor digitorum brevis [FDB] muscle fibers) indicates that denervation caused a reduction in the subsynaptic IP_3R1-stained region and that such a decrease appeared to be determined mainly by the lack of muscle electrical activity.

Materials and methods

Animals

Wistar rats and C57BL/6 mice were housed in certified animal facilities at the Universities of Padova and Trieste, respectively, in a 12-h light/12-h dark cycle, bred, and fed ad libitum within the guidelines and rules of the European legislation (2010/63/EU).

In vivo denervation procedure

6-wk-old female Wistar rats (140–160 g of body weight) were anesthetized before surgery and were treated with antibiotics and pain reliever drugs after surgery, as specified in *Aut. Min.* 1089-2020. Denervation procedure, i.e., sciatectomy, was performed on the right leg as previously described (Bortoloso et al., 2006) according to the recommendations provided by the European Convention for the Protection of Vertebrate Animals used for Experimental and Scientific Purposes (Council of Europe No. 123, Strasbourg, 1985) and authorized by the Animal Care Committee of the University of Padova and the Italian Health Ministry, in agreement with the European legislation (2010/63/EU), as per *Aut. Min.* 1089-2020. 9 d after sciatectomy, rats were sacrificed and extensor digitorum longus (EDL) muscles were dissected from both left (contralateral, control) and right (denervated) legs.

Isolation of adult skeletal muscles fibers

Single adult skeletal muscle fibers were obtained from the dissociation of FDB muscles of 6–8-wk-old C57BL/6 male mice (20–25 g of body weight). Mice were sacrificed by cervical

dislocation as approved by the local Animal Care Committee of the University of Trieste and the Italian Health Ministry, in agreement with the European legislation (2010/63/EU).

FDB muscle fibers were isolated from both hindlimb foot muscles of a single mouse for each independent preparation. Immediately after excision, FDB muscles were treated with type I collagenase 0.3% (*w/v*; Sigma-Aldrich) for 1 h in ice and 1 h at 37°C in Tyrode's solution containing (in mM) 137 NaCl, 2.7 KCl, 1 $MgCl_2$, 1.8 $CaCl_2$, 0.35 Na_2HPO_4, 12 $NaHCO_3$, 25.5 HEPES, and 5.5 *D*-glucose, pH 7.4 NaOH, plus 100 U/ml penicillin, 100 µg/ml streptomycin, and 10% FBS (Gibco). Single fibers (750–900 for each mouse) were isolated by mechanical dissociation with Pasteur pipettes with decreasing tip diameters and allowed to settle on Matrigel-coated (1 mg/ml; Corning) glass coverslips in 35-mm Petri dishes.

In vitro denervation of adult skeletal muscle fibers

Denervation effects at the endplate region were induced in vitro (Grohovaz et al., 1993) by culturing single adult FDB muscle fibers for up to 7 d in a medium composed of DMEM high glucose enriched (Sigma-Aldrich) supplemented with horse serum (5%; Gibco), *L*-glutamine (2 mM), penicillin (100 IU/ml), and streptomycin (100 µg/ml) at 37°C in a 100% humid air atmosphere containing 5% CO_2. The medium was renewed every 3 d. In these experimental conditions, progressive disarray of the endplate and the appearance of the fetal γ-nAChR isoform occurred after in vivo denervation (Henderson et al., 1987; Tarpey et al., 2018; Gupta et al., 2020). According to the experimental purposes, cultures were maintained in Tyrode's solution at 37°C in a 100% humid air atmosphere containing 5% CO_2 (control conditions) or underwent specific treatments (neural agrin exposure or field electrical stimulation; see below).

Neural agrin treatment of adult, cultured skeletal muscle fibers

The addition of 1 nM recombinant C-terminal fragment of rat agrin-z^+ (550-AG; R&D Systems) to the culture medium started 24 h after dissociation. Each experimental point was obtained from skeletal muscle fibers isolated from the same animal and cultured in the absence (control) or the presence of neural agrin. Renewal of the medium was performed every 3 d and 1 nM neural agrin was added, where applicable, at each medium change.

Field electrical stimulation of adult, cultured skeletal muscle fibers

The effect of field electrical stimulation was analyzed by comparing adult skeletal muscle fibers isolated from the same animal, cultured at 37°C in a 100% humid air atmosphere containing 5% CO_2 in the absence (control) and the presence of electrical stimulation. Electrical stimulation was delivered to muscle fibers using a Grass S88 stimulator (Grass Instruments). The stimulator was connected to a device constituted by a 6-well plate with two connection cards associated with two parallel platinum–iridium electrodes (0.2 mm in diameter) in each well, placed 2 cm apart and positioned 1–2 mm over the cells. Field electrical stimulation was performed daily, for 5 h, and started from 24 h after dissociation. Capacitors in series with the electrodes allowed the delivery of biphasic single pulses of 1 ms width at a frequency of 1 Hz. The medium was renewed every 3 d.

nAChR and IP_3R1 staining

EDL muscles from controlateral and denervated hindlimbs of each rat were dissected and rapidly frozen in liquid nitrogen. Processing and staining were carried out on 30-µm longitudinal cryosections postfixed with 4% (w/v) paraformaldehyde in PBS for 45 min at room temperature, then blocked with 10% goat serum in PBS (v/v) supplemented with Triton-X100 0.3% (v/v), followed by incubation for 48 h at 4°C with polyclonal antibodies against IP_3R1s (1:250 in PBS, PA3-901A; Thermo Fisher Scientific Life Sciences) or antibodies raised against a synthetic peptide corresponding to IP_3R1 aa 1829–1848 developed by Volpe et al. (1993). Sections were extensively washed in PBS and stained with goat anti-rabbit IgG–Alexa Fluor 488 conjugated secondary antibodies (1:500 in PBS; A11034; ThermoFisher Scientific Life Sciences) together with 2 µg/ml snake toxin α-bungarotoxin (α-BuTX) Alexa Fluor 555 conjugate (B35451; ThermoFisher Scientific Life Sciences) overnight. After the secondary antibodies and the toxin were removed, slides were washed three times and mounted using Pro Long antifade with DAPI mounting medium (Thermo Fisher Scientific Life Sciences).

In single FDB muscle fibers, nAChRs and IP_3R1s labeling was carried out from 24 h up to 7 d after dissociation. Fixation was carried out on coverslips with a solution of 4% (w/v) paraformaldehyde in PBS for 15 min at 4°C. Fibers were then permeabilized in PBS + Triton-X100 0.3% (v/v) for 15 min and incubated in a blocking solution containing PBS plus 2% BSA (Sigma-Aldrich) for 30 min. IP_3R1s were stained with either rabbit polyclonal anti-IP_3R1s antibodies PA3-901A (Thermo Fisher Scientific Life Sciences) or antibodies developed by Volpe et al. (1993). Rabbit polyclonal anti-IP_3R1s antibodies were diluted 1:100 in blocking solution, and cell incubation was performed overnight at 4°C. Muscle fibers were incubated for 1 h at room temperature with the secondary goat anti-rabbit Alexa Fluor 568 conjugated antibody (1:500 in PBS; A11036; Thermo Fisher Scientific Life Sciences) and Hoechst solution (1:2,000 in PBS; Thermo Fisher Scientific Life Sciences). nAChRs were labeled by 2.5 µg/ml Alexa Fluor 488–α-BuTX in PBS supplemented with 0.1% BSA (v/v) for 1 h at room temperature. After staining, fibers were washed three times with PBS and finally rinsed with distilled water and mounted on a microscope glass.

Analysis of nAChR and IP_3R1 staining

In single FDB muscle fibers, the distribution of nAChRs and IP_3R1s was analyzed on images acquired by a Nikon C1 confocal microscope using a Plan-Apochromat 60×/1.4 (NA) oil-immersion objective. Optical images were collected at either 0.30 or 0.35 µm z resolution by sequential line scanning. Volumetric analysis of the endplate nAChRs and corresponding subsynaptic IP_3R1s staining was carried out by applying Fiji ImageJ software (ver 2.1.0/1.53c, National Institutes of Health). For each endplate, a stack of images was collected through the entire depth containing the α-BuTX visible signal. The region of

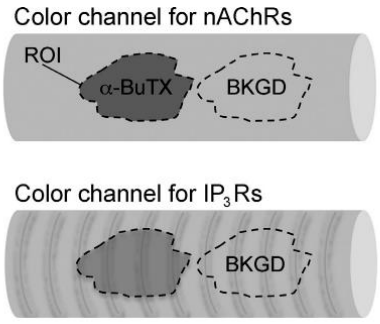

Figure 1. **Measurement of nAChR- and IP_3R-stained volumes.** The sketch shows the selection of the ROI as an endplate profile identified by α-BuTX labeling and an example of where the ROI was set to calculate the background value (BKGD) for each stack of the color channel.

interest (ROI) for the measurements was set by projecting through the *z*-axis planes the most intense pixels of the α-BuTX signal. Endplate and subsynaptic IP_3R1 volumes were calculated in the same ROI in the corresponding color channels (Fig. 1). To each stack of images, a threshold was applied to eliminate the fluorescent noise, and the background signal was subtracted. The background signal of each color channel was calculated in the ROI set as close as possible to the endplate avoiding inhomogeneous cell regions (BKGD; Fig. 1). The α-BuTX- and IP_3R-stained volumes were calculated as the sum of subtracted α-BuTX– and IP_3R1-stained images of each z-stack, taking into account the step size of acquisition.

In EDL cryosections, the analysis of nAChR and IP_3R1 staining was performed using epifluorescence and confocal microscopy. Epifluorescence analysis was done under a Leica DMR microscope equipped with a Leica HCX PL Fluotar 40×/0.75 (NA) dry objective and using the Leica Application Suite Advanced Fluorescence 4.0.0.11706 software (LASAF). Confocal analysis was carried out by a Leica SP5 confocal inverted microscope using a Leica HCX PL Fluotar L 40×/0.60 (NA) dry objective. Confocal images were collected at 1 µm z resolution by sequential line scanning. Due to the complexity of the tissue, the irregular IP_3R1 signal made the background very variable and quantification of IP_3R1 staining unreliable, thus the volumetric analysis (as described above for FDB muscle fibers) was limited to the α-BuTX signal. As for IP_3R1 quantification, we identified the IP_3R1-free endplates, i.e., endplates in which the IP_3R1 fluorescent signal in the ROI was equal to or below the minimum background signal value measured in the corresponding fiber.

Caged IP_3 photolysis and Ca^{2+} measurements

FDB muscle fibers plated on 18-mm coverslips were incubated with 1 µM Fluo-4/AM (Life Technologies), 0.02% pluronic F-127 (Sigma-Aldrich), 200 µM sulfinpyrazone (Sigma-Aldrich), 1 µM ci-IP_3/PM (Tocris Bioscience), and 2 µg/ml α-BuTX Alexa Fluor 555 conjugate (B35451; Thermo Fisher Scientific Life Sciences) for 30 min at 37°C in mKRB medium (in mM: 140 NaCl, 2.8 KCl, 2 $MgCl_2$, 10 HEPES, and 1 $CaCl_2$, pH 7.4) supplemented with 10 mM glucose. After washing, coverslips were mounted in Ca^{2+}-free, EGTA-containing (100 µM) mKRB and visualized on an inverted microscope (Leica Microsystems DMi8 Thunder Imager 3D Cell Culture) by a 20× ultraviolet-permeable objective (HC PL FLUOTAR 340; Leica Microsystems). Fluo-4 was excited with the white line of a CoolLED pE-340^{fura} (CoolLED Limited), and the emitted fluorescence was collected with a Leica Dmi8 GFP-filter set. Where indicated, photolysis of ci-IP_3/PM was obtained by exposing the sample (300 ms) to the output of the unfiltered 340 and 380 nm lines of a CoolLED pE-340^{fura}. Fluo-4 images were acquired every 50 ms, with a 40-ms exposure time by a Hamamatsu Flash 4.0 V3 camera (Hamamatsu Photonics). After 100 s, 20 µM cyclopiazonic acid (CPA; Sigma-Aldrich) was added to release Ca^{2+} from the sarcoplasmic reticulum.

At the end of the experiments, α-BuTX Alexa Fluor 555 was excited by the 555 nm line of LED8 (Leica Microsystems) to visualize the NMJ and to select the corresponding ROIs. Images were background subtracted and analyzed with LAS X Premium (Leica Microsystems), calculating the ratio F/F_0 between the Fluo-4 fluorescence emission collected at each frame (F) and that collected at the beginning of the experiment (F_0) in the ROIs.

Statistical analysis

Results are expressed as mean ± standard error (SEM). Data were analyzed with GraphPad Prism 4.00 (GraphPadSoftware) and Origin 2019b (OriginLab Corporation). Shapiro normality test was used to determine whether sample data were drawn from a Gaussian distributed population. For parametric data, statistical significance was determined using an unpaired *t* test; for data that do not belong to a normal distribution, statistical analysis was performed using Mann–Whitney test. Relationships between volumetric analysis of the endplate and corresponding subsynaptic IP_3R1 stained volume were analyzed by Spearman's correlation test (for nonparametric data). $P < 0.05$ was considered statistically significant.

Results

Effect of in vivo denervation on the subsynaptic IP_3R1 distribution in EDL muscle

To investigate whether denervation affects the subsynaptic IP_3R1 distribution, in vivo denervation was carried out in adult rats using the classical procedure of sciatectomy. Sciatectomy evokes a rapid ensuing and irreversible muscle atrophy, as judged by a marked decrease of CSA from denervation day 3 onward (Bortoloso et al., 2006; Qiu et al., 2021, and references therein).

In longitudinal muscle sections, identification of endplate was carried out by nAChR labeling with α-BuTX, as shown in Fig. 1 A for both contralateral and denervated EDL; as judged by pretzel-like features (Fig. 2 A) and by measurements of mean nAChR-stained volumes, endplates appeared not to be changed at denervation day 9 (contralateral: 2,664.32 ± 181.42 µm^3, $n = 33$; denervated: 3,074.21 ± 183.55 µm^3, $n = 39$; Fig. 2 B), a finding in line with previous observations (Fumagalli et al., 1990; Gupta et al., 2020; Walter et al., 2021). Immune labeling of

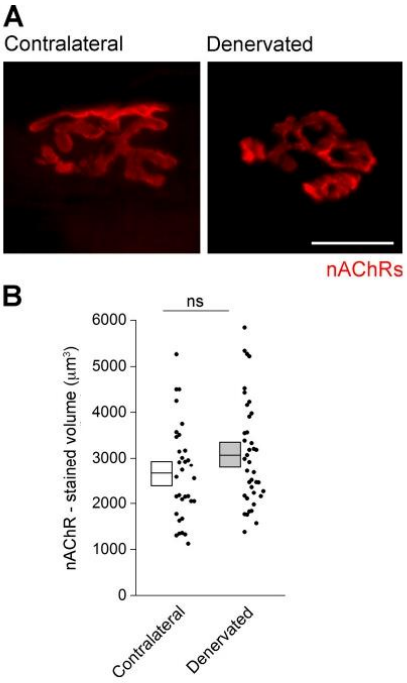

Figure 2. **No change in endplate and α-BuTX–stained volume was observed in 9-d denervated rat EDL longitudinal sections. (A)** Representative images for contralateral and denervated endplates. Scale bar, 20 µm. **(B)** nAChR-stained volumes measured in confocal images from contralateral and denervated EDL are shown as a scatter plot (contralateral: 33 endplates; denervated: 39 endplates). White and grey boxes represent the mean volume ± SEM. ns, P = 0.06, Mann–Whitney test: data are not significantly different.

contralateral EDL with anti-IP_3R1 antibodies shows a double localization pattern, i.e., at the Z-line and in the subsynaptic area (Fig. 3 A), as previously reported by Salanova et al. (2002) and Powell et al. (2003). Endplates, nuclei, and IP_3R1s were clearly detectable (Fig. 3 B). Confocal scanning of EDL samples shows that at variance with contralateral EDL (n = 33 endplates), denervation caused a change in the subsynaptic IP_3R1-immunolabeling. Tissue complexity and variable background signal discouraged any attempt at a reliable quantification, but in about 23% of the analyzed fibers (n = 39 endplates) the subsynaptic IP_3R1-immunolabeling was indistinguishable from the nearby regions or lower (representative image in Fig. 3 C; see Materials and methods for further details), and such endplates were deemed IP_3R-free.

Data obtained in vivo, although preliminary and lacking quantification of the IP_3R1-staining volume, are suggestive of a causal relationship between innervation and expression/localization of IP_3R1s at the endplates. To substantiate this hypothesis and to explore which are the mechanisms controlling the expression and localization of subsynaptic IP_3R1s, a well-established, in vitro denervation model was investigated, i.e., isolated FDB muscle fibers.

Innervated and in vitro denervated FDB adult skeletal muscle fibers: nAChR- and IP_3R1-stained volumes

The endplate nAChR- and the corresponding subsynaptic IP_3R1-stained volumes were analyzed in single FDB adult skeletal muscle fibers by confocal fluorescence microscopy after 24 h and 7 d in culture as representative of innervated and in vitro denervated muscle cell elements. In fact, FDB skeletal muscle fiber in culture is a well-established protocol to reproduce in vitro the denervation effects at the endplate level: a decreased density of nAChRs and the appearance of the fetal γ-nAChRs isoform (Grohovaz et al., 1993).

24 h after plating, confocal scanning microscopy displayed nAChRs confined to the endplate region (Fig. 4, upper panel). Analysis of the fluorescent nAChR- and IP_3R-stainings revealed a mean nAChR-stained volume of 1,100.03 ± 128.51 µm³ and a mean IP_3R1-stained volume of 473.92 ± 70.80 µm³ (n = 6 mice, 44 fibers; Fig. 4 B). The correlation plot of matched endplate nAChR- and subsynaptic IP_3R1-stained volumes indicated a direct proportionality: the larger the endplate, the larger the subsynaptic IP_3R-stained volume (Fig. 4 C, upper graph). On average, the subsynaptic IP_3R1-stained volume corresponded to ∼40% of the endplate region.

In in vitro denervated fibers, endplates displayed severe alterations, i.e., evident fragmentation (Fig. 4 A, lower panel). Mean fluorescent nAChR- and IP_3R1-stainings were reduced respectively to 425.16 ± 50.61 and 132.77 ± 25.27 µm³ (n = 6 mice, 31 fibers; Fig. 4 B). The correlation between endplate nAChR- and corresponding subsynaptic IP_3R1-stained volumes was maintained (Fig. 4 C, lower graph). However, the extent of IP_3R1-stained volume reduction was larger than that for nAChRs, and the subsynaptic IP_3R1-stained volume corresponded to ∼25% of the endplate region after 7 d of in vitro denervation.

Subsynaptic IP_3-mediated Ca^{2+} release in innervated and in vitro denervated FDB skeletal muscle fibers

To investigate whether the reduction in the subsynaptic IP_3R1-stained volume induced by in vitro denervation determined a change in the local IP_3-mediated Ca^{2+} signals, flash photolysis experiments of caged IP_3 were performed in Fluo-4 loaded fibers. Uncaging of IP_3 in in vitro denervated FDB adult skeletal muscle fibers caused a subsynaptic increase in the $[Ca^{2+}]_i$, significantly lower than in the innervated counterparts (Fig. 5 A). The mean peak values of the subsynaptic $[Ca^{2+}]_i$ variations, measured as F/F_0 (further details in Materials and methods), were 1.07 ± 0.01 in innervated (n = 44 endplates) and 1.01 ± 0.01 in in vitro denervated fibers (n = 29 endplates), corresponding to a decrease in the peak value (calculated as percentage versus basal $[Ca^{2+}]_i$) of ∼80% in in vitro denervated versus innervated fibers; Fig. 5 A). In our experimental conditions, the IP_3 photolysis entails a 1-s interruption in the acquisition (i.e., 300 ms flash and the time required to restart postflash image acquisition), thus we cannot exclude concomitant differences in Ca^{2+} release kinetics undetectable by our imaging unit.

Control experiments confirmed that UV flash pulse did not alter, per se, the levels of fluorescence (Fig. 5 A, inset).

In the analyzed Fluo-4 loaded fibers, application of 20 µM CPA, an inhibitor of sarcoplasmic reticulum Ca^{2+}-ATPase

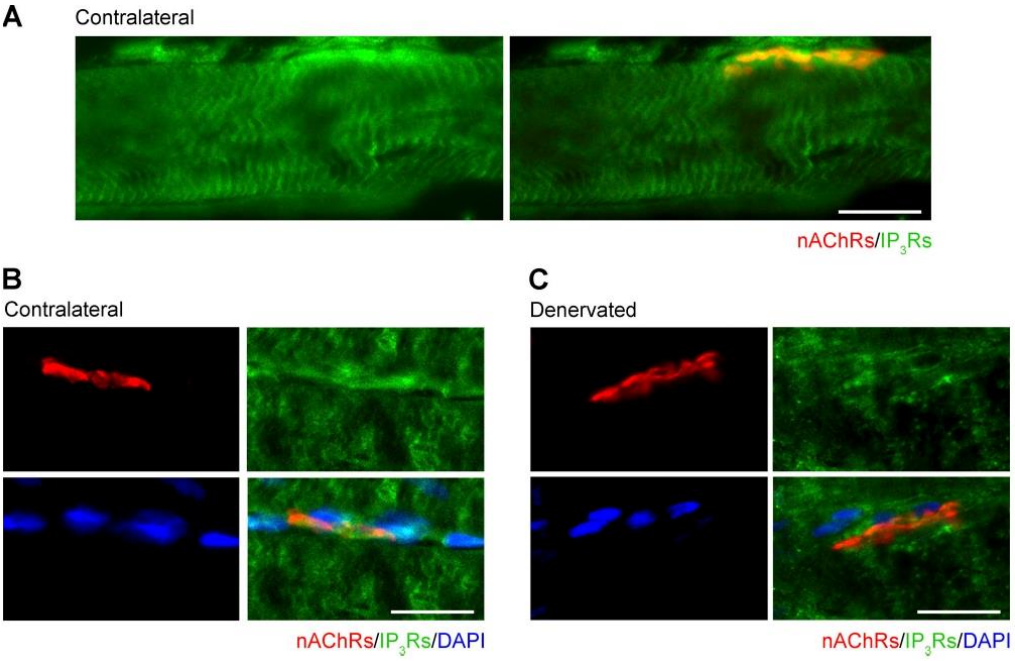

Figure 3. **Absence of subsynaptic IP_3R1s at endplate level in 9-d denervated rat EDL longitudinal sections. (A)** In the left panel, contralateral EDL labeled with anti-IP_3R1 antibodies; in the right panel, merged image after double labeling for nAChRs and anti-IP_3R1s. Scale bar, 20 µm. **(B)** Individual labeling of contralateral EDL with α-BuTX, anti-IP_3R1 antibodies, and DAPI. Scale bar, 20 µm. **(C)** Individual labeling of 9-d denervated EDL with α-BuTX, anti-IP_3R antibodies, and DAPI. Scale bar, 20 µm.

(Seidler et al., 1989), induced significantly different $[Ca^{2+}]_i$ variations in innervated and in vitro denervated fibers (Fig. 5 B). The corresponding mean area values were 101.00 ± 12.25 (n = 44 endplates) and 65.54 ± 10.77 (n = 29 endplates), respectively, indicating a decrease of ∼35% of the releasable Ca^{2+} content in in vitro denervated versus innervated fibers (Fig. 5 B).

In vitro denervated FDB adult skeletal muscle fibers: Effect of neural agrin and field electrical stimulation on nAChR- and IP_3R1-stained volumes

In innervated muscle, the maintenance of the endplate apparatus is controlled by neural agrin and electrical muscle activity (Lomo, 2003; Wu et al., 2010; Shi et al., 2012; Li et al., 2018). Some experiments were planned to investigate if neural agrin and/or muscle electrical activity control the subsynaptic distribution of IP_3R1s. To pursue this aim, we have taken advantage of isolated cultured FDB skeletal muscle fibers, which offer the possibility to work in a controlled environment (i.e., in the absence of neurotrophic factors and electrical activity) and to check the specific contribution of neural agrin and electrical activity applied experimentally in the stabilization of the subsynaptic IP_3R1s.

The effect of neural agrin was explored by comparing nAChR- and IP_3R1-stained volumes in FDB adult skeletal muscle fibers cultured up to 7 d in control conditions and in the presence of 1 nM 90 kD recombinant C-terminal fragment of rat neural agrin, which contains the binding site for Lrp4/MuSK receptor complex and induces nAChR clustering (Ferns et al., 1993). As expected, in the presence of neural agrin, the mean endplate nAChR-stained volume was larger (799.93 ± 124.69 µm³; 5 mice, 42 fibers) than in control conditions (404.52 ± 56.59 µm³; 5 mice, 28 fibers; Fig. 6). However, even if the treatment with the neurotrophic factor caused an increase in the mean IP_3R-stained volume in in vitro denervated fibers (191.32 ± 39.31 µm³; 5 mice, 42 fibers), it was statistically comparable (P = 0.18) to the mean volume measured in the control counterparts (120.73 ± 27.21 µm³; 5 mice, 28 fibers; Fig. 6).

Similar experiments were carried out to investigate the effect of the muscle electrical stimulation. Field electrical stimulation was delivered daily to the FDB adult skeletal muscle fibers in culture at a frequency of 1 Hz for 5 h. Endplate nAChRs and subsynaptic IP_3R1s volumes were measured in electrical stimulated cultured FDB skeletal muscle fibers and compared to those measured in control conditions, i.e., without electrical stimulation. 4 d of electrical stimulation determined stabilization of the endplate nAChRs: in stimulated fibers, the mean nAChR-stained volume was 441.59 ± 38.81 µm³ (6 mice, 34 fibers) versus the mean volume of 278.30 ± 39.42 µm³ (6 mice, 39 fibers) in control cultures. Field electrical stimulation stabilized also the subsynaptic IP_3R1s localization: the mean IP_3R1-stained volume was 138.20 ± 21.67 µm³ in stimulated fibers (34 fibers, 6 mice) and

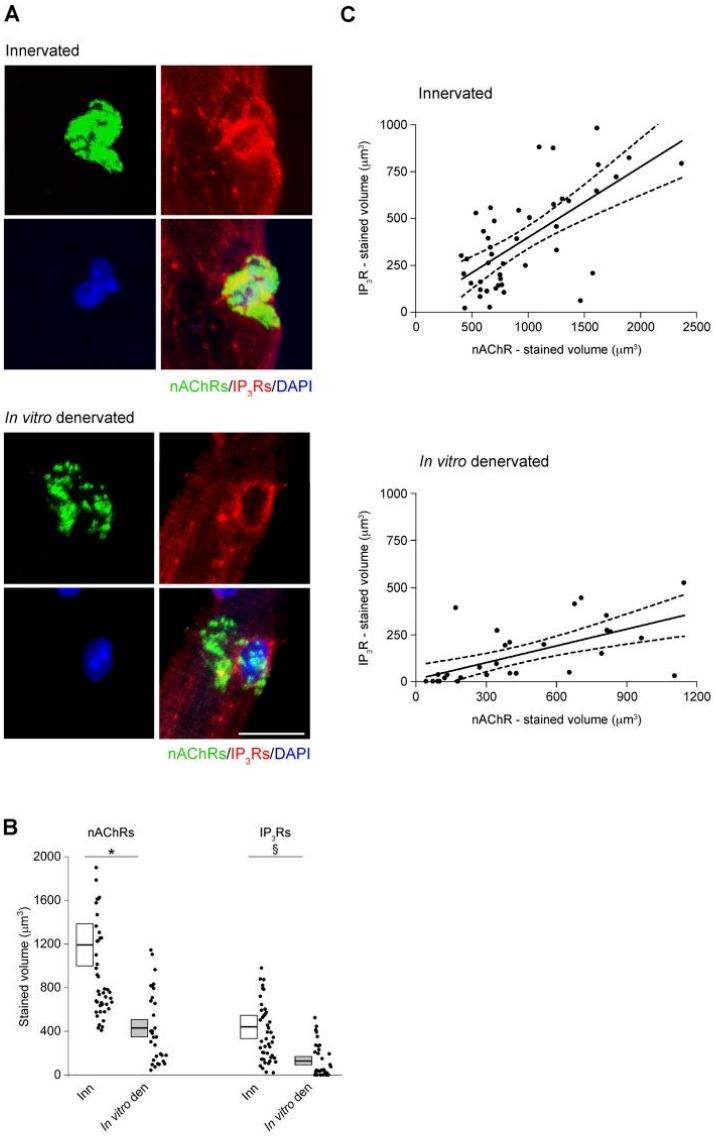

Figure 4. **nAChR- and IP_3R1-stained volumes in FDB adult skeletal muscle fibers during in vitro denervation. (A)** Top: Endplate region in a FDB adult skeletal muscle fiber as a representative image of the innervated condition (24 h after plating). nAChR staining with Alexa Fluor 488–α-BuTX revealed that nAChRs were localized at the endplate level, and immunostaining for IP_3R1s detected a subsynaptic localization of the receptor. Bottom: In vitro denervated FDB adult skeletal muscle fiber (7 d in culture) as an example of fragmented endplate and reduced subsynaptic IP_3R1s staining. Nuclei were counterstained with DAPI. Images are shown as maximum intensity projection (for details, see Materials and methods). Scale bar, 20 µm. **(B)** The nAChR- and corresponding IP_3R1-stained volumes from each of the analyzed fibers are represented as a scatter plot (n = 44 fibers). White and grey boxes represent the mean volume ± SEM calculated under the assumption that the number of analyzed animals (six mice) is an independent variable. *, P = 0.0006, unpaired t test; §, P < 0.0001, unpaired t test. **(C)** Top: Correlation plot of endplate nAChR- versus corresponding subsynaptic IP_3R1-stained volumes from the innervated FDB adult skeletal muscle fibers shown in B. R = 0.57; P < 0.0001, Spearman's rank correlation. Bottom: Correlation plot of endplate nAChR- versus corresponding subsynaptic IP_3R-stained volumes from in vitro denervated FDB adult skeletal muscle fibers shown in B. R = 0.72; P < 0.0001, Spearman's rank correlation.

56.70 ± 9.83 µm³ in control counterparts (6 mice, 39 fibers; Fig. 7 A). Although the electrical stimulation was effective on both volumes, the plot of matched endplate nAChR- versus subsynaptic IP_3R1-stained volumes indicated that the two parameters were not correlated (Fig. 7 B).

Discussion

Growing experimental evidence suggests that the motor neuron stimulation pattern encodes IP_3-dependent Ca^{2+} signals regulating muscle transcriptional activity and plasticity via the so-called ET-coupling mechanism. Direct electrical stimulation of skeletal muscle fibers reveals the existence of an IP_3-dependent signaling cascade, which originates from activation of the voltage-gated Ca^{2+} channel (Cav1.1) and proceeds via ATP release through pannexin-1 channel and activation of purinergic receptors (Casas et al., 2022). In parallel, the localization of IP_3Rs at the NMJ and the functional interplay between nAChRs activity and the subsynaptic IP_3R-induced Ca^{2+} release indicate that the nerve-mediated electrical stimulation encodes also for localized

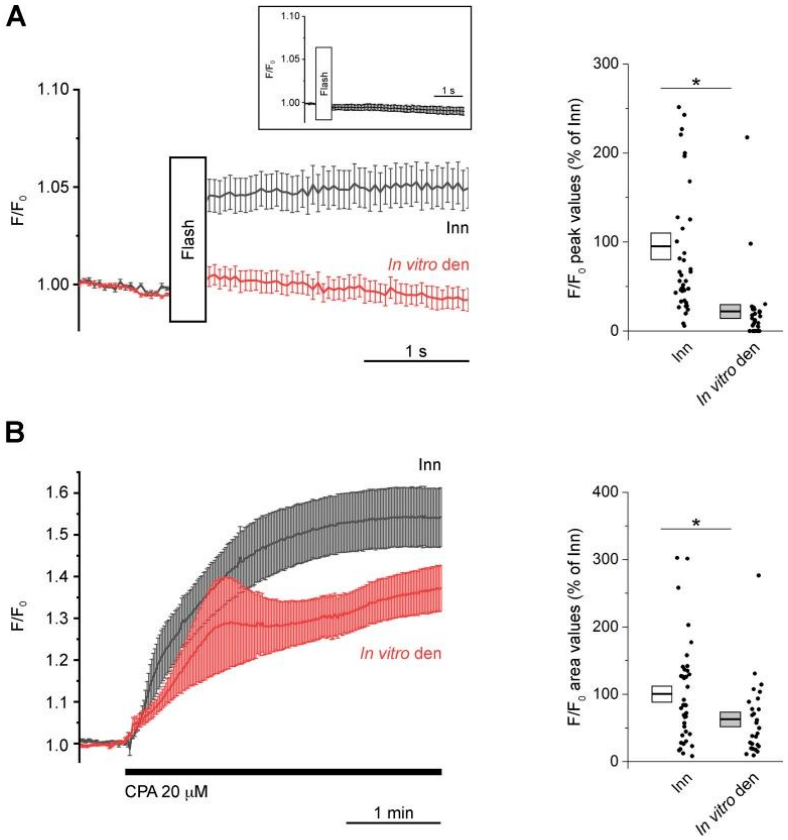

Figure 5. **Smaller subsynaptic IP_3-releasable $[Ca^{2+}]_i$ pool in in vitro denervated FDB adult skeletal muscle fibers. (A)** On the left, mean traces of subsynaptic $[Ca^{2+}]_i$ increases measured in innervated (24 h after plating; n = 44 endplates) and in in vitro denervated FDB adult skeletal muscle fibers (7 d in culture; n = 29 endplates). Trace interruption marks the time of flash photolysis of caged IP_3 (Flash). Inset: Mean trace of fluorescence measured after the UV flash in the absence of caged IP_3. On the right, the scatter plot of the normalized peak values of the $[Ca^{2+}]_i$ increases measured in in vitro denervated versus innervated fibers after flash photolysis. White and grey boxes represent the mean peak values ± SEM. *, P < 0.0001, Mann–Whitney test. **(B)** On the left, mean traces of subsynaptic $[Ca^{2+}]_i$ increases after 20 µM CPA addition upon basal $[Ca^{2+}]_i$ recovery from photolysis. On the right, scatter plot of the normalized area values of the $[Ca^{2+}]_i$ changes induced by CPA application (3.5 min) in in vitro denervated versus innervated fibers. White and grey boxes represent the mean area values ± SEM. *, P = 0.0037, Mann–Whitney test.

Ca^{2+} signals (Zayas et al., 2007; Zhu et al., 2011), which could regulate a "synaptic" ET-coupling mechanism governing the stability of the NMJ apparatus (Zayas et al., 2007; Zhu et al., 2011). If IP_3Rs are crucial in a synaptic ET-coupling, a reduction in their content/activity would impact directly on the efficient neuromuscular transmission and muscle plasticity.

As inferred from experiments carried out on in vivo denervated rat skeletal muscles obtained by sciatectomy, it appears that innervation, i.e., an anatomical intact nerve–muscle junction, controls the distribution of the subsynaptic IP_3R1s at the endplate. In denervated EDL muscle, although quantification of the IP_3R1 staining volume is lacking, a significant number of IP3R1-free endplates was observed (~23%). In this respect, preliminary experiments carried out on human muscles after 60 d of bed rest, in which a marked disuse atrophy is provoked in the presence of an intact and active nerve–muscle junction (Blottner et al., 2006), indicate that subsynaptic IP_3Rs are not changed (unpublished results). Thus, innervation appears to control distribution of IP_3R1s at the NMJ, and its role seems to be prominent also in humans. However, since there are well-known differences in the mechanism of muscle atrophy models, in particular denervation versus disuse atrophy (MacDonald et al., 2014), a further experimental investigation is needed to unveil specific genetic programs and metabolic pathways involved.

The role of innervation on subsynaptic IP_3R1 distribution was directly investigated in murine adult, isolated FDB muscle fibers. Quantification of denervation effects and investigation of the

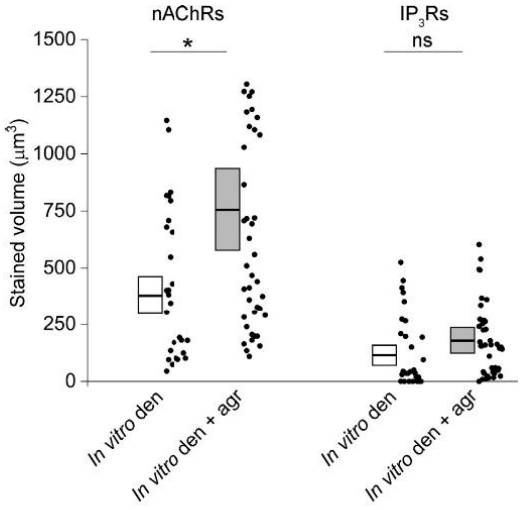

Figure 6. **Neural agrin stabilized endplate but did not prevent the decrease in the subsynaptic IP_3R1s staining in FDB adult skeletal muscle fibers during in vitro denervation.** When FDB adult skeletal muscle fibers were maintained in culture in the presence of 1 nM rat neural agrin, the endplate nAChR-stained volume was significantly larger than that of in vitro denervated FDB adult skeletal muscle fibers in control conditions. However, the subsynaptic IP_3R1-stained volume is similar to control. Data from each analyzed fiber are shown as a scatter plot (in vitro den: 28 fibers; in vitro den + agr: 42 fibers). White and grey boxes represent the mean volume ± SEM calculated under the assumption that the number of analyzed animals (five mice) is an independent variable. *, P = 0.02, unpaired *t* test. ns, P = 0.18, unpaired *t* test: data are not significantly different.

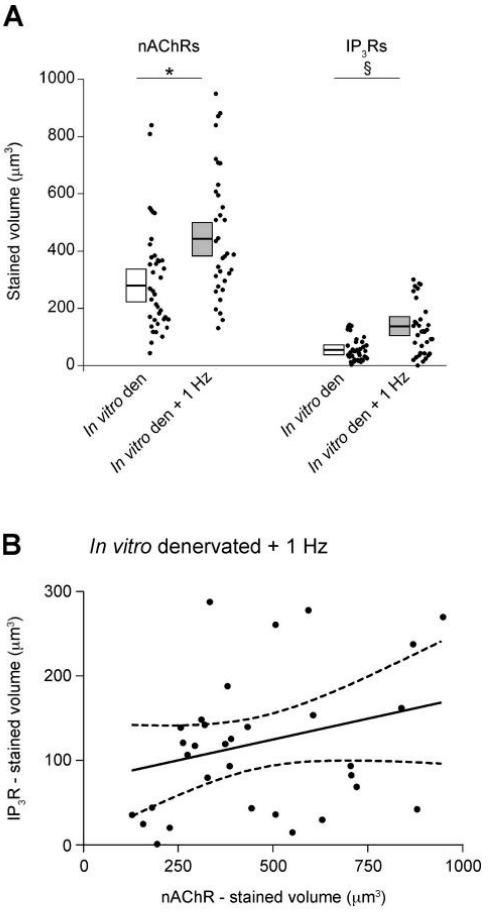

Figure 7. **Field electrical stimulation stabilized endplate and the subsynaptic IP_3R1s staining in FDB adult skeletal muscle fibers during in vitro denervation. (A)** After 4 d of electrical stimulation, both endplate nAChRs and subsynaptic IP_3R1 volumes resulted in significantly larger volumes than those of in vitro denervated FDB adult skeletal muscle fibers in control conditions. Data from each analyzed fiber are shown as a scatter plot (in vitro den: 39 fibers; in vitro den + 1 Hz: 34 fibers). White and grey boxes represent the mean ± SEM volumes calculated under the assumption that the number of analyzed animals (six mice) is an independent variable. *, P = 0.01, unpaired *t* test; §, P = 0.006, unpaired *t* test. **(B)** The plot of endplate nAChR-versus corresponding subsynaptic IP_3R1-stained volumes measured in electrically stimulated fibers, shown in A, indicated that the two parameters were not correlated in electrical stimulated FDB adult skeletal muscle fibers. R = 0.26; P = 0.14, Spearman's rank correlation.

mechanisms governing the subsynaptic distribution of IP_3R1s were pursued by comparing subsynaptic IP_3R1 in freshly isolated (innervated) and in cultured FDB fibers (in vitro denervated) maintained in different conditions.

The volumetric analysis of nAChR and IP_3R1 stainings in freshly dissociated FDB skeletal muscle fibers reveals a correlation between the endplate size and the subsynaptic IP_3R1 volume, which supports the role of subsynaptic IP_3-sensitive Ca^{2+} stores as a key amplifier of Ca^{2+} influx triggered by nAChRs activation (Zayas et al., 2007; Zhu et al., 2011). The same quantitative analysis performed on skeletal muscle fibers, upon in vitro denervation, revealed a decrease of the nAChRs-stained volume associated with a reduced IP_3R1 volume. The apparent discrepancy between the substantially conserved volume of the endplate in vivo (nAChR-stained volumes: Den, ~2,600 μm^3; Inn, ~3,074 μm^3) and the fragmentation and reduced endplate volume in vitro (nAChR-stained volumes: in vitro Den, ~470 μm^3; Inn, ~1,100 μm^3) could be due to either the short denervation time in vivo (Fumagalli et al., 1990; Gupta et al., 2020; Walter et al., 2021) and/or the severe conditions of denervation in vitro, i.e., absence of the basal lamina (Glavinovic et al., 1987), absence of neurotrophic factors, and production of nerve-breakdown by-products, which might not occur in vivo (Cangiano, 1985).

As far as in vitro denervated muscle fibers are concerned, apart from the reduced subsynaptic IP_3R1 volume, the volumetric analysis shows a different correlation slope between IP_3R1- and nAChR-stained volumes, i.e., a more severe reduction for that referable to IP_3R1s. This in vitro finding agrees fairly well with the number of IP_3R1-free NMJs detected after in vivo

denervation before any detectable alteration at the endplate level. To the best of our knowledge, our findings indicate for the first time that a nerve-dependent regulation of the IP_3R1 distribution at the endplate level and that IP_3R1-enriched membrane compartments are even more sensitive to the motor nerve absence than nAChRs membrane domains.

Flash photolysis experiments with caged IP_3 indicate that the reduction in the subsynaptic IP_3R1 volume in in vitro denervated skeletal muscle fibers leads to local IP_3-mediated Ca^{2+} release reduced by ∼80% compared to the innervated counterparts. Interestingly, the reduced subsynaptic IP_3-mediated Ca^{2+} release seems to exclude any compensation by other IP_3R isoforms after denervation. Moreover, the slighter decrease of the $[Ca^{2+}]_i$ transient areas observed after CPA addition (∼35%) suggests that denervation might affect the mechanisms of IP_3-dependent release more than the capacity of the subsynaptic Ca^{2+} storage. In line with the intriguing hypothesis suggested by Powell et al. (2003), the precocious reduction of subsynaptic IP_3R1s and the consequent, plausible Ca^{2+} signaling alterations might bring about the inevitable NMJ destabilization. Whether or not denervation induces redistribution of IP_3R1s, downregulates expression, and/or alters the metabolic stability of subsynaptic IP_3R1s remains an open question. Denervation upregulates the lysosome, calpain, and ubiquitin–proteasome systems (Schiaffino et al., 2013), all major mechanisms of skeletal muscle catabolism; proteomic studies indicate that ∼20% of total proteins were differentially expressed significantly within 2 wk after denervation compared with control muscles (Lang et al., 2017): it remains to be ascertained whether IP_3R1 reduction is merely and only a quantitative, secondary feature of denervation-induced catabolism or whether the IP_3R1 gene is specifically repressed upon denervation, i.e., it is one of the specific atrogenes downregulated during early events of muscle atrophy. Thus far, published data do not include IP_3R among the growing list of atrogenes (cfr. Lang et al., 2017; Lecker et al., 2004; Raffaello et al., 2006; Sacheck et al., 2007).

In vitro denervation of isolated FDB skeletal muscle fibers was implemented in searching for the causative role of either neural agrin and/or electrical activity in the subsynaptic distribution of IP_3R1s.

Exogenous neural agrin added to the cell culture medium partially stabilized the endplate during in vitro denervation, whereas its effect on the denervation-induced reduction of the IP_3R1-stained subsynaptic volume did not reach statistical significance. The statistical power of <0.8 revealed that our sample size was not numerous enough to rule out a less strong agrin-mediated mechanism controlling the subsynaptic localization of IP_3R1s.

On the other hand, fiber activity induced by field electrical stimulation not only promoted the stability of the endplate during both in vitro denervation and in vivo denervation (Brenner and Rudin, 1989; Akaaboune et al., 1999) but also displayed an effect on the subsynaptic IP_3R1s. In fact, electrical stimulation counteracted, although partially, the denervation-induced reduction of the IP_3R1-stained volume, thus suggesting a prevalent activity-dependent control mechanism on subsynaptic IP_3R1s.

In our experimental conditions, each electrical pulse delivered to the fibers at 1 Hz caused a $[Ca^{2+}]_i$ transient associated with a single twitch (Bosutti et al., 2019). It is known that the stabilizing effect of electrical activity on nAChRs is mediated by an increase in $[Ca^{2+}]_i$ (Martinez-Pena y Valenzuela and Akaaboune, 2021), whereas the mechanisms regulating the subsynaptic IP_3R localization are still unknown. The larger subsynaptic IP_3R1 volume, measured in electrically stimulated denervated FDB fibers, indicates the importance of fiber activity in the control of the subsynaptic IP_3R1 membrane compartment as well. However, the lack of correlation between the IP_3R1- and nAChR-stained volumes suggests that the direct electrical stimulation was efficacious but not sufficient to coordinate growth and interplay between the two receptor compartments. Whether the physiological electrical activity triggered by the nerve ending causing nAChR activation and localized synaptic Ca^{2+} signals (Powell et al., 2003; Zayas et al., 2007; Zhu et al., 2011) is responsible for subsynaptic IP_3Rs stabilization merits future investigations.

As judged by electron microscopy, upon denervation, secondary synaptic fold density falls (Brown et al., 1982), and primary grooves reveal a flattening or, more often, collapse (Labovitz et al., 1984). Since such morphological changes appear to be reversed by electrical stimulation (Brenner and Rudin, 1989), it is tempting to speculate that IP_3R1-membrane compartments are somehow coupled to both secondary synaptic folds and primary grooves. As to the heterotypic organelle juxtaposition, i.e., the interaction between nAChR- and IP_3R1-membrane compartments, identification of putative contact sites awaits further experimental investigation by way of specific sensor site probes (Cieri et al., 2018) in presence and absence of innervation. Moreover, considering the recent experimental evidence in favor of a possible role of Homer 2 scaffold protein in the endplate remodeling and plasticity (Lorenzon et al., 2021), Homer 2 could be one of the molecular players linking nAChRs to IP_3R1s.

In conclusion, this study provides evidence that the subsynaptic IP_3R1 distribution at the endplate level is controlled by innervation through a prevailing mechanism based on electrical activity. This opens a new scenario in which *IP3R1* could be included in the growing list of atrogenes. Whether the IP_3R1 downregulation causes an altered synaptic ET-coupling mechanism contributing to impaired neuromuscular transmission and muscle atrophy remains to be assessed.

Acknowledgments

Eduardo Ríos served as editor.

The authors thank Dr. Michela Soardi for performing preliminary experiments and Prof. Lucio Torelli (University of Trieste) for assistance in the statistical analysis.

This study was supported by funds from ASI NEMUCO (DC-VUM-2016-068) to P. Volpe and P. Lorenzon.

The authors declare no competing financial interests.

Author contributions: P. Volpe and P. Lorenzon designed the study, carried out experiments and analyses, and wrote the manuscript. A. Megighian, A. Nori, R. Filadi, G. Gherardi, S.

Furlan, P. Caccin, R. Sacchetto, D. Sandonà, G. Trautmann, M. Salanova, A. Bosutti, G. Massaria, A. Bernareggi, and M. Sciancalepore carried out experiments and statistical analyses. P. Pizzo discussed experiments and revised the manuscript. All the authors revised and approved the manuscript.

Submitted: 13 February 2022
Revised: 30 August 2022
Accepted: 9 September 2022

References

Akaaboune, M., S.M. Culican, S.G. Turney, and J.W. Lichtman. 1999. Rapid and reversible effects of activity on acetylcholine receptor density at the neuromuscular junction in vivo. *Science*. 286:503–507. https://doi.org/10.1126/science.286.5439.503

Araya, R., J.L. Liberona, J.C. Cárdenas, N. Riveros, M. Estrada, J.A. Powell, M.A. Carrasco, and E. Jaimovich. 2003. Dihydropyridine receptors as voltage sensors for a depolarization-evoked, IP_3R- mediated, slow calcium signal in skeletal muscle cells. *J. Gen. Physiol.* 121:3–16. https://doi.org/10.1085/jgp.20028671

Blaauw, B., P. Del Piccolo, L. Rodriguez, V.H. Hernandez Gonzalez, L. Agatea, F. Solagna, F. Mammano, T. Pozzan, and S. Schiaffino. 2012. No evidence for inositol 1, 4, 5-trisphosphate-dependent Ca^{2+} release in isolated fibers of adult mouse skeletal muscle. *J. Gen. Physiol.* 140:235–241. https://doi.org/10.1085/jgp.201110747

Blottner, D., M. Salanova, B. Puttmann, G. Schiffl, D. Felsenberg, B. Buehring, J. Rittweger, and J. Rittweger. 2006. Human skeletal muscle structure and function preserved by vibration muscle exercise following 55 days of bed rest. *Eur. J. Appl. Physiol.* 97:261–271. https://doi.org/10.1007/s00421-006-0160-6

Bortoloso, E., N. Pilati, A. Megighian, E. Tibaldo, D. Sandonà, and P. Volpe. 2006. Transition of Homer isoforms during skeletal muscle regeneration. *Am. J. Physiol. Cell Physiol.* 290:C711–C718. https://doi.org/10.1152/ajpcell.00217.2005

Bosutti, A., A. Bernareggi, G. Massaria, P. D'Andrea, G. Taccola, P. Lorenzon, and M. Sciancalepore. 2019. A "noisy" electrical stimulation protocol favors muscle regeneration in vitro through release of endogenous ATP. *Exp. Cell Res.* 381:121–128. https://doi.org/10.1016/j.yexcr.2019.05.012

Brenner, H.R., and W. Rudin. 1989. On the effect of muscle activity on the end-plate membrane in denervated mouse muscle. *J. Physiol.* 410:501–512. https://doi.org/10.1113/jphysiol.1989.sp017546

Briguet, A., and M.A. Ruegg. 2000. The Ets transcription factor GABP is required for postsynaptic differentiation in vivo. *J. Neurosci.* 20:5989–5996. https://doi.org/10.1523/jneurosci.20-16-05989.2000

Brown, M.C., W.G. Hopkins, R.J. Keynes, and I. White. 1982. A comparison of early morphological changes at denervated and paralyzed endplates in fast and slow muscles of the mouse. *Brain Res.* 248:382–386. https://doi.org/10.1016/0006-8993(82)90599-6

Cangiano, A. 1985. Denervation supersensitivity as a model for the neural control of muscle. *Neuroscience*. 14:963–971. https://doi.org/10.1016/0306-4522(85)90268-4

Carlson, B.M. 2014. The biology of long-term denervated skeletal muscle. *Eur. J. Transl. Myol.* 24:3293. https://doi.org/10.4081/ejtm.2014.3293

Casas, M., G. Jorquera, C. Morales, and E. Jaimovich. 2022. On the molecular mechanism of excitation- transcription coupling in skeletal muscle. *J. Gen. Physiol.* 154:e2021ecc41. https://doi.org/10.1085/ecc41

Cieri, D., M. Vicario, M. Giacomello, F. Vallese, R. Filadi, T. Wagner, T. Pozzan, P. Pizzo, L. Scorrano, M. Brini, and T. Calì. 2018. Splics: A split green fluorescent protein-based contact site sensor for narrow and wide heterotypic organelle juxtaposition. *Cell Death Differ.* 25:1131–1145. https://doi.org/10.1038/s41418-017-0033-z

Dauber, W., T. Voigt, and A. Heini. 1999. Junctions between subsynaptic folds and rough sarcoplasmic reticulum of muscle fibres. *J. Muscle Res. Cell Motil.* 20:697–701. https://doi.org/10.1023/a:1005521529855

Dauber, W., T. Voigt, X. Härtel, and J. Mayer. 2000. The T-tubular network and its triads in the sole plate sarcoplasm of the motor end-plate of mammals. *J. Muscle Res. Cell Motil.* 21:443–449. https://doi.org/10.1023/a:1005614917564

Duclert, A., and J.P. Changeux. 1995. Acetylcholine receptor gene expression at the developing neuromuscular junction. *Physiol. Rev.* 75:339–368. https://doi.org/10.1152/physrev.1995.75.2.339

Ferns, M.J., J.T. Campanelli, W. Hoch, R.H. Scheller, and Z. Hall. 1993. The ability of agrin to cluster AChRs depends on alternative splicing and on cell surface proteoglycans. *Neuron*. 11:491–502. https://doi.org/10.1016/0896-6273(93)90153-i

Fumagalli, G., S. Balbi, A. Cangiano, and T. Lomo. 1990. Regulation of turnover and number of acetylcholine receptors at neuromuscular junctions. *Neuron*. 4:563–569. https://doi.org/10.1016/0896-6273(90)90114-u

Glavinovic, M.I., S. Lee, and R. Miledi. 1987. Effect of collagenase treatment and subsequent culture on rat muscle fiber acetylcholinesterase activity. *J. Neurosci. Res.* 18:519–524. https://doi.org/10.1002/jnr.490180403

Grohovaz, F., P. Lorenzon, F. Ruzzier, and R. Zorec. 1993. Properties of acetylcholine receptors in adult rat skeletal muscle fibers in culture. *J. Membr. Biol.* 136:31–42. https://doi.org/10.1007/BF00241487

Gupta, R., J.P. Chan, J. Uong, W.A. Palipsis, D.J. Wright, S.B. Shah, S.R. Ward, T.Q. Lee, and O. Steward. 2020. Human motor endplate remodeling after traumatic nerve injury. *J. Neurosurg.* 18:1–8. https://doi.org/10.3171/2020.8.JNS201461

Henderson, L.P., J.D. Lechleiter, and P. Brehm. 1987. Single channel properties of newly synthesized acetylcholine receptors following denervation of mammalian skeletal muscle. *J. Gen. Physiol.* 89:999–1014. https://doi.org/10.1085/jgp.89.6.999

Hidalgo, C., and E. Jaimovich. 1989. Inositol trisphosphate and excitation-contraction coupling in skeletal muscle. *J. Bioenerg. Biomembr.* 21:267–281. https://doi.org/10.1007/BF00812072

Labovitz, S.S., N. Robbins, and M.A. Fahim. 1984. Endplate topography of denervated and disused rat neuromuscular junctions: Comparison by scanning and light microscopy. *Neuroscience*. 11:963–971. https://doi.org/10.1016/0306-4522(84)90207-0

Lang, F., S. Aravamudhan, H. Nolte, C. Türk, S. Hölper, S. Müller, S. Günther, B. Blaauw, T. Braun, and M. Krüger. 2017. Dynamic changes in the mouse skeletal muscle proteome during denervation-induced atrophy. *Dis. Models Mech.* 10:881–896. https://doi.org/10.1242/dmm.028910

Lecker, S.H., R.T. Jagoe, A. Gilbert, M. Gomes, V. Baracos, J. Bailey, S.R. Price, W.E. Mitch, and A.L. Goldberg. 2004. Multiple types of skeletal muscle atrophy involve a common program of changes in gene expression. *FASEB J.* 18:39–51. https://doi.org/10.1096/fj.03-0610com

Li, L., W.-C. Xiong, and L. Mei. 2018. Neuromuscular junction formation, aging, and disorders. *Annu. Rev. Physiol.* 80:159–188. https://doi.org/10.1146/annurev-physiol-022516-034255

Lomo, T. 2003. What controls the position, number, size, and distribution of neuromuscular junctions on rat muscle fibres. *J. Neurocytol.* 32:835–848. https://doi.org/10.1023/B:NEUR.0000020627.18156.b1

Lorenzon, P., S. Furlan, B. Ravara, A. Bosutti, G. Massaria, A. Bernareggi, M. Sciancalepore, G. Trautmann, K. Block, D. Blottner, et al. 2021. Preliminary observations on skeletal muscle adaptation and plasticity in Homer $2^{-/-}$ mice. *Metabolites*. 11:642. https://doi.org/10.3390/metabo11090642

MacDonald, E.M., E. Andres-Mateos, R. Mejias, J.L. Simmers, R. Mi, J.-S. Park, S. Ying, A. Hoke, S.-J. Lee, and R.D. Cohn. 2014. Denervation atrophy is independent from Akt and mTOR activation and is not rescued by myostatin inhibition. *Dis. Models Mech.* 7:471–481. https://doi.org/10.1242/dmm.014126

Martinez-Pena y Valenzuela, I., and M. Akaaboune. 2021. The metabolic stability of the nicotinic acetylcholine receptor at the neuromuscular junction. *Cells*. 10:358. https://doi.org/10.3390/cells10020358

McMahan, U.J. 1990. The agrin hypothesis. *Cold Spring Harbor Symp. Quant. Biol.* 55:407–418. https://doi.org/10.1101/sqb.1990.055.01.041

Meier, T., D.M. Hauser, M. Chiquet, L. Landmann, M.A. Ruegg, and H.R. Brenner. 1997. Neural agrin induces ectopic postsynaptic specializations in innervated muscle fibers. *J. Neurosci.* 17:6534–6544. https://doi.org/10.1523/jneurosci.17-17-06534.1997

Midrio, M. 2006. The denervated muscle: Facts and hypotheses. A historical review. *Eur. J. Appl. Physiol.* 98:1–21. https://doi.org/10.1007/s00421-006-0256-z

Milani, D., P. Volpe, and T. Pozzan. 1988. D-myo-inositol 1, 4, 5-trisphosphate phosphatase in skeletal muscle. *Biochem. J.* 254:525–529. https://doi.org/10.1042/bj2540525

Missias, A.C., G.C. Chu, B.J. Klocke, J.R. Sanes, and J.P. Merlie. 1996. Maturation of the acetylcholine receptor in skeletal muscle: Regulation of the AChR gamma-to-epsilon switch. *Dev. Biol.* 179:223–238. https://doi.org/10.1006/dbio.1996.0253

Moschella, M.C., J. Watras, T. Jayaraman, and A.R. Marks. 1995. Inositol 1, 4, 5-trisphosphate receptor in skeletal muscle: Differential expression in myofibres. *J. Muscle Res. Cell Motil.* 16:390–400. https://doi.org/10.1007/BF00114504

Powell, J.A., J. Molgó, D.S. Adams, C. Colasante, A. Williams, M. Bohlen, and E. Jaimovich. 2003. IP_3 receptors and associated Ca^{2+} signals localize to satellite cells and to components of the neuromuscular junction in skeletal muscle. *J. Neurosci.* 23:8185–8192. https://doi.org/10.1523/jneurosci.23-23-08185.2003

Qiu, J., L. Wu, Y. Chang, H. Sun, and J. Sun. 2021. Alternative splicing transitions associate with emerging atrophy phenotype during denervation-induced skeletal muscle atrophy. *J. Cell. Physiol.* 236:4496–4514. https://doi.org/10.1002/jcp.30167

Raffaello, A., P. Laveder, C. Romualdi, C. Bean, L. Toniolo, E. Germinario, A. Megighian, D. Danieli-Betto, C. Reggiani, and G. Lanfranchi. 2006. Denervation in murine fast-twitch muscle: Short-term physiological changes and temporal expression profiling. *Physiol. Genom.* 25:60–74. https://doi.org/10.1152/physiolgenomics.00051.2005

Ríos, E., and G. Pizarro. 1991. Voltage sensor of excitation-contraction coupling in skeletal muscle. *Physiol. Rev.* 71:849–908. https://doi.org/10.1152/physrev.1991.71.3.849

Sacheck, J.M., J.P.K. Hyatt, A. Raffaello, R.T. Jagoe, R.R. Roy, V.R. Edgerton, S.H. Lecker, and A.L. Goldberg. 2007. Rapid disuse and denervation atrophy involve transcriptional changes similar to those of muscle wasting during systemic diseases. *FASEB J.* 21:140–155. https://doi.org/10.1096/fj.06-6604com

Salanova, M., G. Priori, V. Barone, E. Intravaia, B. Flucher, F. Ciruela, R.A.J. McIlhinney, J.B. Parys, K. Mikoshiba, and V. Sorrentino. 2002. Homer proteins and $InsP_3$ receptors co-localise in the longitudinal sarcoplasmic reticulum of skeletal muscle fibres. *Cell Calcium.* 32:193–200. https://doi.org/10.1016/s0143416002001549

Sanes, J.R., and J.W. Lichtman. 2001. Induction, assembly, maturation and maintenance of a postsynaptic apparatus. *Nat. Rev. Neurosci.* 2:791–805. https://doi.org/10.1038/35097557

Schiaffino, S., K.A. Dyar, S. Ciciliot, B. Blaauw, and M. Sandri. 2013. Mechanisms regulating skeletal muscle growth and atrophy. *FEBS J.* 280:4294–4314. https://doi.org/10.1111/febs.12253

Seidler, N.W., I. Jona, M. Vegh, and A. Martonosi. 1989. Cyclopiazonic acid is a specific inhibitor of the Ca^{2+}-ATPase of sarcoplasmic reticulum. *J. Biol. Chem.* 264:17816–17823. https://doi.org/10.1016/s0021-9258(19)84646-x

Shi, L., A.K.Y. Fu, and N.Y. Ip. 2012. Molecular mechanisms underlying maturation and maintenance of the vertebrate neuromuscular junction. *Trends Neurosci.* 35:441–453. https://doi.org/10.1016/j.tins.2012.04.005

Somlyo, A.P. 1985. The messenger across the gap. *Nature.* 316:298–299. https://doi.org/10.1038/316298b0

Tarpey, M.D., A.J. Amorese, N.P. Balestrieri, T.E. Ryan, C.A. Schmidt, J.M. McClung, and E.E. Spangenburg. 2018. Characterization and utilization of the flexor digitorum brevis for assessing skeletal muscle function. *Skeletal Muscle.* 8:14. https://doi.org/10.1186/s13395-018-0160-3

Tintignac, L.A., H.R. Brenner, and M.A. Rüegg. 2015. Mechanisms regulating neuromuscular junction development and function and causes of muscle wasting. *Physiol. Rev.* 95:809–852. https://doi.org/10.1152/physrev.00033.2014

Vergara, J., R.Y. Tsien, and M. Delay. 1985. Inositol 1, 4, 5-trisphosphate: A possible chemical link in excitation-contraction coupling in muscle. *Proc. Natl. Acad. Sci. USA.* 82:6352–6356. https://doi.org/10.1073/pnas.82.18.6352

Volpe, P., G. Salviati, F. Di Virgilio, and T. Pozzan. 1985. Inositol 1, 4, 5-trisphosphate induces calcium release from sarcoplasmic reticulum of skeletal muscle. *Nature.* 316:347–349. https://doi.org/10.1038/316347a0

Volpe, P., D. Biral, P. Pizzo, G. Salviati, and A. Margreth. 1993. Ontogenesis of chick iris intrinsic muscles: Evidence for a smooth-to-striated muscle transition. *Dev. Biol.* 159:441–449. https://doi.org/10.1006/dbio.1993.1254

Wallace, B.G. 1989. Agrin induced specializations contain cytoplasmic, membrane, and extracellular matrix- associated components of the postsynaptic apparatus. *J. Neurosci.* 9:1294–1302. https://doi.org/10.1523/jneurosci.09-04-01294.1989

Walter, L.A., L.P. Blake, Y.S. Gallot, C.J. Arends, R.S. Sozio, S.M. Onifer, and K.R. Bohnert. 2021. Effect of denervation on XBP1 in skeletal muscle and the neuromuscular junction. *Int. J. Mol. Sci.* 23:169. https://doi.org/10.3390/ijms23010169

Wu, H., W.C. Xiong, and L. Mei. 2010. To build a synapse: Signaling pathways in neuromuscular junction assembly. *Development.* 137:1017–1033. https://doi.org/10.1242/dev.038711

Wu, P., A. Chawla, R.J. Spinner, C. Yu, M.J. Yaszemski, A.J. Windebank, and H. Wang. 2014. Key changes in denervated muscles and their impact on regeneration and reinnervation. *Neural Regen. Res.* 9:1796–1809. https://doi.org/10.4103/1673-5374.143424

Zayas, R., J.S. Groshong, and C.M. Gomez. 2007. Inositol-1, 4, 5-triphosphate receptors mediate activity induced synaptic Ca^{2+} signals in muscle fibers and Ca^{2+} overload in slow-channel syndrome. *Cell Calcium.* 41:343–352. https://doi.org/10.1016/j.ceca.2006.07.007

Zhu, H., B.J. Bhattacharyya, H. Lin, and C.M. Gomez. 2011. Skeletal muscle IP_3R_1 receptors amplify physiological and pathological synaptic calcium signals. *J. Neurosci.* 31:15269–15283. https://doi.org/10.1523/JNEUROSCI.3766-11.2011

metabolites

MDPI

Article

Preliminary Observations on Skeletal Muscle Adaptation and Plasticity in Homer 2$^{-/-}$ Mice

Paola Lorenzon [1], Sandra Furlan [2], Barbara Ravara [3], Alessandra Bosutti [1], Gabriele Massaria [1], Annalisa Bernareggi [1], Marina Sciancalepore [1], Gabor Trautmann [4], Katharina Block [4], Dieter Blottner [4], Paul F. Worley [5], Sandra Zampieri [3,6], Michele Salanova [4] and Pompeo Volpe [3,*]

1 Dipartimento di Scienze della Vita, Università di Trieste, I-34077 Trieste, Italy; plorenzon@units.it (P.L.); bosutti@units.it (A.B.); GABRIELE.MASSARIA@phd.units.it (G.M.); abernareggi@units.it (A.B.); msciancalepore@units.it (M.S.)
2 Istituto di Neuroscienze del Consiglio Nazionale delle Ricerche, Sezione di Padova, I-35121 Padova, Italy; sfurlan@bio.unipd.it
3 Dipartimento di Scienze Biomediche, Università di Padova, I-35121 Padova, Italy; barbara.ravara@unipd.it (B.R.); sanzamp@unipd.it (S.Z.)
4 Institute for Integrative Neuroanatomy, Neuromuscular System, Center of Space Medicine Berlin (ZWMB), Charité Universitätsmedizin Berlin, D-10115 Berlin, Germany; gabor.trautmann@charite.de (G.T.); katharina.block@charite.de (K.B.); dieter.blottner@charite.de (D.B.); michele.salanova@charite.de (M.S.)
5 Department of Neuroscience, Johns Hopkins University School of Medicine, 725 N Wolfe Street, Baltimore, MD 21205, USA; pworley1@jhmi.edu
6 Dipartimento di Scienze Chirurgiche, Oncologiche e Gastroenterologiche, Università di Padova, I-35122 Padova, Italy
* Correspondence: pompeo.volpe@unipd.it

check for updates

Citation: Lorenzon, P.; Furlan, S.; Ravara, B.; Bosutti, A.; Massaria, G.; Bernareggi, A.; Sciancalepore, M.; Trautmann, G.; Block, K.; Blottner, D.; et al. Preliminary Observations on Skeletal Muscle Adaptation and Plasticity in Homer 2$^{-/-}$ Mice. *Metabolites* **2021**, *11*, 642. https://doi.org/10.3390/metabo11090642

Academic Editors: Viviana Moresi, Luca Madaro and Cristina Mammucari

Received: 1 July 2021
Accepted: 18 September 2021
Published: 19 September 2021

Publisher's Note: MDPI stays neutral with regard to jurisdictional claims in published maps and institutional affiliations.

Abstract: Homer represents a diversified family of scaffold and transduction proteins made up of several isoforms. Here, we present preliminary observations on skeletal muscle adaptation and plasticity in a transgenic model of Homer 2$^{-/-}$ mouse using a multifaceted approach entailing morphometry, quantitative RT-PCR (Reverse Transcription PCR), confocal immunofluorescence, and electrophysiology. Morphometry shows that *Soleus* muscle (SOL), at variance with *Extensor digitorum longus* muscle (EDL) and *Flexor digitorum brevis* muscle (FDB), displays sizable reduction of fibre cross-sectional area compared to the WT counterparts. In SOL of Homer 2$^{-/-}$ mice, quantitative RT-PCR indicated the upregulation of *Atrogin-1* and *Muscle ring finger protein 1 (MuRF1)* genes, and confocal immunofluorescence showed the decrease of neuromuscular junction (NMJ) Homer content. Electrophysiological measurements of isolated FDB fibres from Homer 2$^{-/-}$ mice detected the exclusive presence of the adult ε-nAChR isoform excluding denervation. As for NMJ morphology, data were not conclusive, and further work is needed to ascertain whether the null Homer 2 phenotype induces any endplate remodelling. Within the context of adaptation and plasticity, the present data show that Homer 2 is a co-regulator of the normotrophic *status* in a muscle specific fashion.

Keywords: Homer 2; atrophy; neuromuscular junction; skeletal muscle

1. Introduction

Homer proteins are scaffolds and transducers that play a central role in Ca^{2+} signalling, development, and adaptation in skeletal muscle [1–5]. There are three Homer genes, *Homer 1*, *Homer 2*, and *Homer 3*, each encoding for several transcripts [3,6]. Homer 1 and Homer 2 interact with both sarcoplasmic reticulum Ca^{2+} release channels, IP_3R and RYR1 [7,8], whereas Homer 1b/c also functions as an important scaffold for transient receptor potential (TRP) channels and thus regulates mechanotransduction in skeletal muscle [2]. Homer 1 proteins act as dynamic regulators of RyR1 activity, and the equilibrium between short and long Homer proteins at the receptor site defines the RyR1 channel activity [9]. Homer 1 expression is identical irrespective of the muscle type, whereas expression of Homer 2a/b appears to be

characteristic of the slow-twitch phenotype. In general terms, distribution of Homer 2 in skeletal muscles appears to be species independent and fibre type-dependent [1,3].

Homer 1 is either diffusely distributed at the I band with reinforcement of the Z line [10] or localises to the Z-disk [2]; transgenic Homer $1^{-/-}$ mice [11] exhibit a skeletal myopathy characterised by abnormal TRP channel activity [2]. Homer 2, on the other hand, displays a regular sarcomeric pattern and localises at the Z line level, away from the A-I band where E-C coupling takes place [4].

Homers appear to be key players of skeletal muscle plasticity [5]. In several experimental models of skeletal muscle atrophy, i.e., denervation and disuse (bed rest, hind limb unloading, microgravity), expression of Homer 2 is rapidly and largely inhibited. Homer 2 appears to be required for trophic homeostasis of slow-twitch skeletal muscle fibres [4]. Mechanistically, Homer 2 was shown to antagonise protein degradation in rat slow-twitch skeletal muscles. In particular, downregulation of Homer 2 is an early event of denervation atrophy, i.e., the transcript being reduced by 90% after 3 days. In addition, Homer 2 participates in the control of ubiquitinisation and ensuing proteolysis via transcriptional downregulation of *MuRF1, Muscle Atrophy F-box* (*MAFbx*)*/Atrogin-1*, and *Myogenin* [4].

Homer 2 is observed in the NMJ postsynaptic domain both in slow- and fast-twitch skeletal muscle fibres [12]. Since the Homer 2 isoform is mainly expressed in the slow-twitch fibre type, the role of Homer 2 at NMJ level has been mainly studied in predominantly slow-twitch muscles. In SOL, Homer 2 is downregulated after either denervation or disuse, suggesting a neuronal control mediated by muscle activity. Moreover, at the postsynaptic compartment of NMJ, Homer 2 co-localises and interacts with NFATc1 indicating that Homer 2 translates neuromuscular synaptic input to the calcineurin-NFAT signalling cascade [12].

NMJ stability requires correct expression, proper turnover, and cluster distribution of nicotinic acetylcholine receptors (nAChRs), processes controlled by release of soluble factors from motor nerve endings and electrical activity of muscle fibres [13–15]. The interplay among NMJ activity, Ca^{2+} influx through nAChR, and its amplification via Ca^{2+} release from intracellular IP_3R-sensitive stores is being unveiled [16]. Since IP_3Rs are enriched at the endplate of skeletal muscle fibres, the current hypothesis is that IP_3-induced Ca^{2+} release has a major effect on junctional nuclei and synaptic gene expression [17]. At the NMJ level, the role of Homer 2 still is an open issue, and it is not known whether and how it modulates the structure and/or function of endplate. However, Homer 2 might potentially behave as both scaffold and transducer.

Availability of transgenic Homer $2^{-/-}$ mice [18] allows for further molecular investigation of the trophic role of Homer 2 in skeletal muscle. Moreover, the KO model lends itself as a precious tool to dissect the role of Homer 2 in structure/function of the NMJ.

2. Results

2.1. SOL, EDL, and FDB Morphometry in WT and Homer $2^{-/-}$ Mice

An established index of the skeletal muscle trophic state is the fibre cross-sectional area (CSA; [19]), as determined by morphometry in haematoxylin and eosin (H-E)-stained transverse cryosections. Analysis was carried out on transverse sections of SOL and FDB muscles derived from either Homer $2^{-/-}$ and WT mice [20].

In SOL muscles from Homer $2^{-/-}$ mice, mean CSA was decreased by about 24%, as compared to that of WT mice. No significant changes were detected in EDL and FDB muscles (Figure 1 and Table 1). Moreover, SOL from Homer $2^{-/-}$ mice (Figure 1, right, upper panel) contained smaller fibres interdispersed within a homogeneous matrix.

2.2. Quantitative RT-PCR Analysis of MuRF1 and Atrogin-1 Genes in SOL of WT and Homer $2^{-/-}$ Mice

Skeletal muscle atrophy upregulates both *MuRF1* and *Atrogin-1* genes [21,22], which encode E3-ubiquitin ligases and are causally involved in denervation atrophy [23]. *Homer 2* replacement, as referred to above, partially counteracted denervation-induced upregulation of both *MuRF1* and *Atrogin-1* genes in rat SOL [4]; thus, hypotrophy/atrophy of SOL from

Homer $2^{-/-}$ mice might be due to the lack of constitutive downregulatory activity exerted by Homer 2. Measurements of *MuRF 1* and *Atrogin-1* transcripts were carried out by quantitative RT-PCR in SOL derived from Homer $2^{-/-}$ mice. The results show that both *MuRF 1* and *Atrogin-1* genes were significantly upregulated by approximately 35% as compared to the WT muscle (Figure 2).

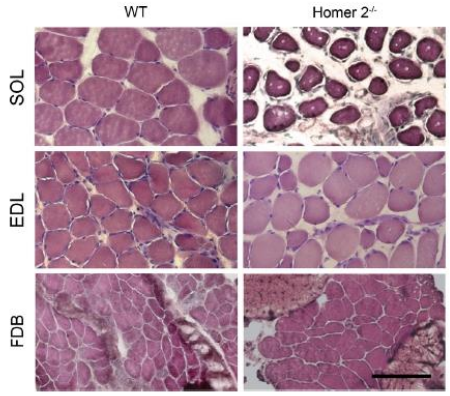

Figure 1. Light microscopy of SOL, EDL, and FDB cryosections from WT and Homer $2^{-/-}$ mice. Representative haematoxylin and eosin staining of transverse sections of SOL (upper panels), EDL (middle panels), and FDB (lower panels) from WT and Homer $2^{-/-}$ mice. In EDL of Homer $2^{-/-}$ mice, some angular fibres were observed. Scale bar = 100 μm.

Table 1. SOL, EDL, and FDB morphometry in WT and Homer $2^{-/-}$ mice.

Muscle	WT	Homer $2^{-/-}$	Δ	*p*
SOL CSA (μm^2)	1779.00 ± 30.98 (924)	1353.00 ± 23.92 (622)	−23.92%	<0.0001
EDL CSA (μm^2)	1681.44 ± 31.22 (829)	1722.00 ± 40.63 (745)	+2.41%	0.4162
FDB CSA (μm^2)	400.00 ± 9.57 (670)	414.50 ± 8.51 (950)	+7.42%	0.2606

Data are expressed as mean ± SEM. In parentheses, number of analysed fibres for each experimental group. Statistical differences were determined by unpaired *t*-test. Data were from 3 animals for both WT and Homer $2^{-/-}$.

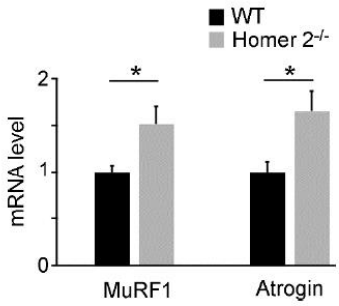

Figure 2. Quantitative RT-PCR analysis of mRNA levels for *MuRF1* and *Atrogin-1* in SOL from WT and Homer $2^{-/-}$ mice. Values are expressed as the fold change over WT after GeNorm normalisation. Each histogram represents the data obtained from 8 different animals per experimental group. Data are expressed as mean ± SEM. Statistical differences were determined by unpaired *t*-test. * $p < 0.05$ vs. the respective WT control.

These data strengthen previous observations on the role of Homer 2 as co-regulator of SOL skeletal muscle normotrophic *status*.

Levels of *Homer 1b/c* and *Homer 1a* mRNA transcripts were also measured in total RNA extracted from SOL of either WT or Homer $2^{-/-}$ mice. No adaptive changes were detected with respect to the prevalent Homer 1 isoforms expressed in skeletal muscles (data not shown).

2.3. Homer Immunoreactivity in SOL from WT and Homer $2^{-/-}$ Mice

Investigation on the presence of Homer was specifically carried out at the NMJ in SOL from WT and Homer $2^{-/-}$ mice using confocal microscopy. SOL cryosections were double stained with a pan-Homer antibody and Alexa-555-α-BuTX (Figure 3A). Using confocal immunofluorescence microscopy, Homer immunoreactivity resulted decreased by about 25% under the NMJ of Homer $2^{-/-}$ mice, confirming the localisation of Homer 2 isoform at the subsynaptic level (Figure 3B). The persistence of the other Homer isoforms whose transcription was found to be unchanged (see above) well explains the partial decrease of the immunoreactivity detected by the isoform non-selective pan-Homer antibody.

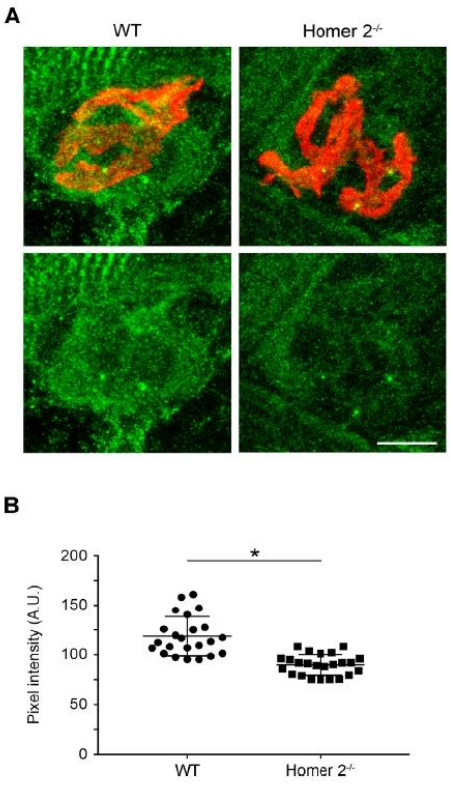

Figure 3. Homer immunoreactivity at the NMJ of SOL cryosections from WT and Homer $2^{-/-}$ mice. (**A**) SOL cryosections were stained for Homer using a pan-Homer antibody (green) and for nAChRs using Alexa-555-α-BuTX (red) as described in the Materials and Methods section. Confocal microscopy revealed a reduced immunoreactivity for Homer in the NMJ subsynaptic region in Homer $2^{-/-}$ compared to WT mice (lower panels). Scale bar, 10 μm. (**B**) Data are shown as pixel intensity at the NMJ junction from either WT and Homer $2^{-/-}$ mice. Data were obtained from 3 animals per each experimental group, and at least 23 endplates per group was analysed. Data are expressed as mean ± SEM. Statistical differences were determined by unpaired *t*-test. * $p < 0.05$ vs. the respective WT control.

2.4. Endplate Volume in Intact SOL and EDL from WT and Homer 2$^{-/-}$ Mice

Given the reported subsynaptic localisation (see above, and [12]), KO of Homer 2 gene might generate effects at the endplate. Thus, the endplate volume was estimated in intact and frozen SOL and EDL muscles from WT and Homer 2$^{-/-}$ mice. To do this, cryosections were stained with Alexa-555-α-bungarotoxin (α-BuTX) in order to label nAChRs. Under the prevailing experimental conditions and assumptions detailed in the Materials and Methods section, α-BuTX-positive regions show the "pretzel-like" structure characteristic for the mouse endplate (Figure 4A) [24]. The α-BuTX-stained volume did not change in SOL of Homer 2$^{-/-}$ mice (Figure 4B, left hand panel), whereas it was slightly but significantly increased in EDL (Figure 4B, right hand panel).

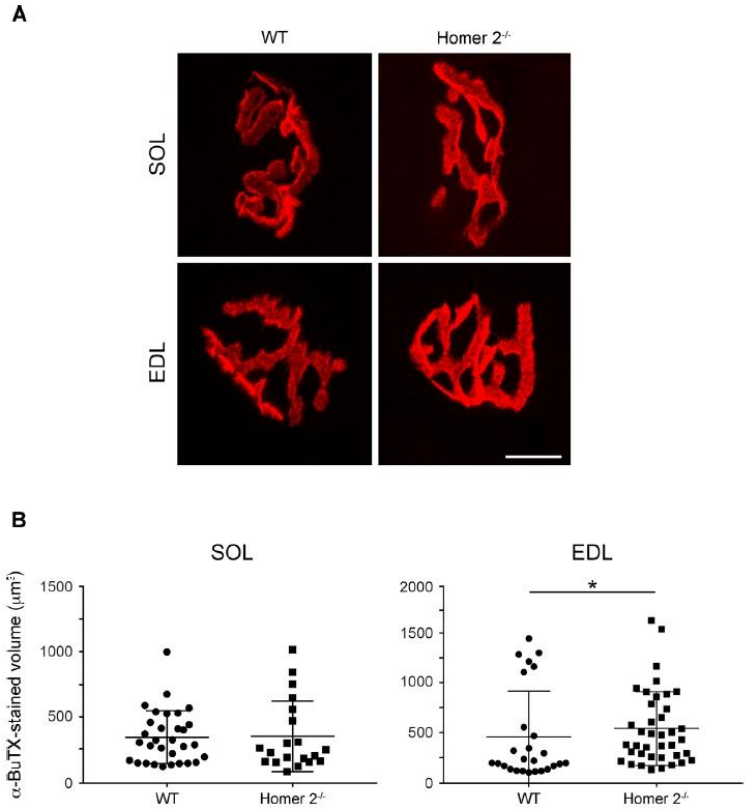

Figure 4. Endplate volume in either SOL and EDL from WT and Homer 2$^{-/-}$ mice. (**A**) SOL and EDL cryosections were stained for nAChRs with Alexa-555-α-BuTX (see the Materials and Methods section for details). Scale bar, 10 μm. (**B**) The endplate volume was calculated both in SOL and EDL as described in the Section 4 [24]. For each group, SOL and EDL from 4 mice were analysed and at least 20 endplates per group were examined. Data are expressed as mean ± SEM. Statistical differences were determined by Mann–Whitney test. * $p < 0.05$ vs. the respective WT control.

2.5. The Endplate Volume in Single FDB Fibres from WT and Homer 2$^{-/-}$ Mice

Isolated FDB skeletal muscle fibres from either WT or Homer 2$^{-/-}$ mice were stained with Alexa-488-α-BuTX to evaluate the endplate volume at single cell level. As in intact EDL and SOL muscles, confocal scanning microscopy detected nAChRs confined to the endplate region (Figure 5A) and organised in a pretzel-like structure in muscle fibres from WT and Homer 2$^{-/-}$ mice (Figure 5B). Analysis of the fluorescent signals reveals that the

mean α-BuTX-stained volume was reduced by about 30% in Homer $2^{-/-}$ FDB skeletal muscle fibres, as compared to WT fibres (see also Figure 5C), formally resembling the effects of in vivo denervation [25–28]. A set of experiments was carried out in FDB muscle fibres maintained in culture to recapitulate the denervation effects in vitro [29]. In in vitro denervated fibres, endplates displayed more severe alterations, i.e., evident fragmentation and larger reduction in the mean α-BuTX-stained volume (approximately 45%).

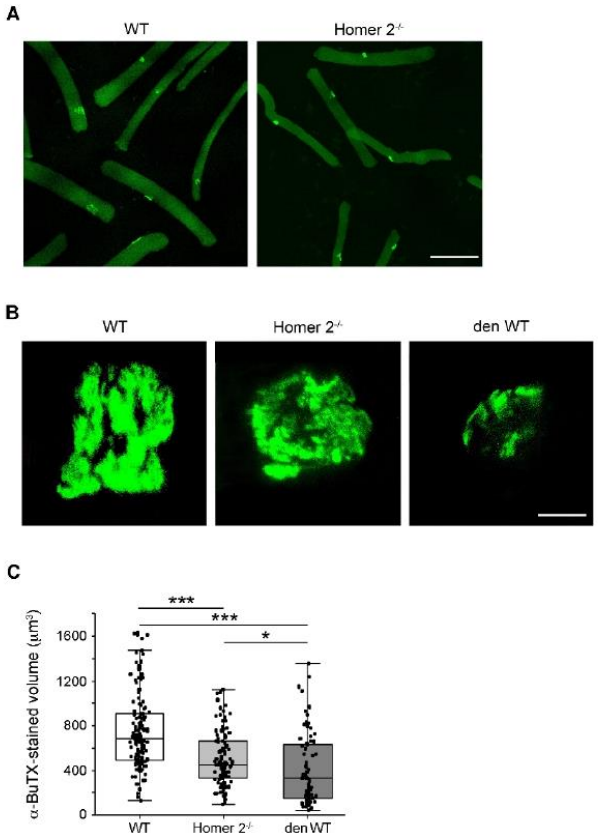

Figure 5. The endplate morphology in WT and Homer $2^{-/-}$ FDB muscle fibres. (**A**) nAChR staining with Alexa-488-α bungarotoxin (α-BuTX) showed that nAChRs were localised at the endplate level in WT as well as in Homer $2^{-/-}$ muscle fibres. Scale bar, 150 μm. (**B**) A pretzel-like structure was appreciable in both WT and Homer $2^{-/-}$ muscle fibres, whereas the endplate appeared more disarrayed in in vitro denervated WT FDB muscle fibres (i.e., 7-days cultured; den WT). Scale bar, 10 μm. (**C**) Volumetric analysis of the α-BuTX staining showed a significant decrease in the volume measured in Homer $2^{-/-}$ compared to WT (Homer $2^{-/-}$: 501.86 ± 23.48 μm^3, n = 107 fibres from 5 mice; WT: 752.82 ± 30.13 μm^3, n = 129 fibres from 16 mice). The decrease in volume resulted larger in den WT (404.55 ± 37.10 μm^3, n = 74 fibres from 12 mice) than in Homer $2^{-/-}$. Data are expressed as mean ± SEM. Data were analysed using one-way ANOVA, and significant differences were analysed by Dunn's multiple comparisons test; * $p < 0.05$, *** $p < 0.001$.

2.6. Patch Clamp Experiments in Single FDB Fibres from Homer $2^{-/-}$ Mice

Following FDB dissociation, the exposure of the endplate region makes feasible the electrophysiological recording of the nAChR activity [26,29]. A set of patch clamp experiments was carried out in the cell-attached configuration in order to ascertain which

nAChR isoforms are present at the endplate region of Homer $2^{-/-}$ FDB muscle fibres. ACh (200 nM) was used in the recording pipette solution. The activity of single nAChR channels was measured in membrane patches at the level of the endplate region (Figure 6A), identifiable by phase-contrast microscopy as a roughness of the cell surface [30]. The unitary current amplitude distribution was best fitted by a single Gaussian curve and the open-time distribution by a single exponential, revealing the presence of a single type of nAChR channel (Figure 6B). Values of mean single-channel conductance and time constant confirmed the exclusive presence of the adult ε-nAChR isoform in Homer $2^{-/-}$ muscle fibres, as in the case of WT muscle fibres (Figure 6C; see also [27]). This is in contrast with the in vitro denervated WT counterpart in which the embryonic γ-nAChR isoform was also expressed (Figure 6C; see also [27]), as it occurs in vivo for denervated skeletal muscle [26].

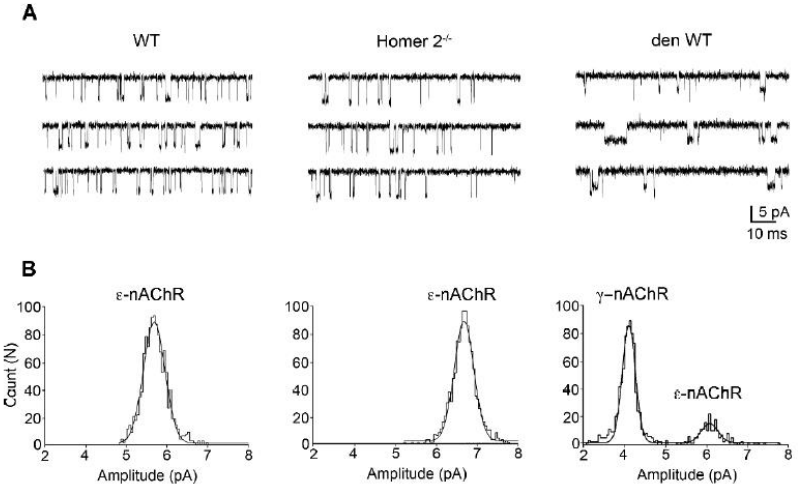

C

	Conductance (pA)		τ (ms)	
	ε-nAChR	γ-nAChR	ε-nAChR	γ-nAChR
WT	51.83 ± 3.31 (4)	-	1.06 ± 0.05 (16)	-
Homer $2^{-/-}$	54.17 ± 1.23 (33)	-	1.30 ± 0.07 (43)	-
den WT	54.37 ± 3.38 (4)	37.15 ± 1.58 (7)	1.58 ± 0.16 (4)	τ_1: 1.55 ± 0.29 (7) τ_2: 5.95 ± 1.08 (7)

Figure 6. Single-channel activity of nAChRs recorded from FDB endplates. (**A**) Representative single nAChR channel activity evoked by 200 nM ACh at the endplate regions of WT, Homer $2^{-/-}$, and in vitro denervated WT FDB muscle fibres (i.e., 7-days cultured; den WT). At a pipette potential of +60 mV, channel openings appeared as downward deflections. (**B**) Corresponding unitary current amplitudes with the best fits superimposed. The analysis revealed the presence of the adult ε-nAChR openings alone in WT and Homer $2^{-/-}$ and the coexistence of adult ε-nAChR and foetal γ-nAChR openings in den FDB muscle fibres. (**C**) Mean values of conductance and time constants of the nAChR openings in WT, Homer $2^{-/-}$, and den WT muscle fibres. Data are expressed as mean ± SEM. In parentheses, the number of the analysed recordings. Data were from 3 mice for WT, 15 mice from Homer $2^{-/-}$, and 7 mice for den WT. The statistical analysis performed using one-way ANOVA and Tukey's post hoc test revealed no statistical differences among groups.

3. Discussion

Changes in skeletal muscle mass may result from either changes in protein turnover, reflecting the balance between protein synthesis and protein degradation, or changes in cell turnover, reflecting the balance between myonuclear accretion and myonuclear loss [31].

Skeletal muscle atrophy occurs when protein degradation rates exceed protein synthesis and takes place in a variety of conditions, including starvation, disuse, denervation, cancer cachexia, and aging. Two major protein degradation pathways, the proteasomal and the autophagic-lysosomal pathways, are involved during muscle atrophy and variably contribute to the loss of muscle mass. Moreover, satellite cells and myonuclei may undergo apoptosis during muscle atrophy [31,32].

Skeletal muscle fibre types are differentially sensitive to specific pathophysiologic atrophy signals. For example, red, slow-twitch oxidative fibres have a higher rate of protein synthesis and degradation and are more resistant to fasting than white, fast-twitch glycolytic fibres. In contrast, slow-twitch fibres are more sensitive to inactivity, microgravity, and denervation-induced atrophy [33].

Our observations indicate that SOL muscle has adapted to genetic lack of *Homer 2*. The *Homer 2* null phenotype is characterised by upregulation of the atrophy master genes *Murf1* and *Atrogin-1*, and 2-month-old mice display clear-cut atrophy. Thus, there appears to be a solid link between either downregulation or absence of *Homer 2* and initiation of muscle catabolism. If Homer 2 contributes to the normotrophic *status* of SOL muscle, genetic lack of *Homer 2* might very well determine hypotrophy rather than atrophy.

In a previous report [4], an almost complete disappearance of Homer 2 was detected after 14-day denervation of rat SOL muscle in parallel with the decrease of both muscle mass and fibre CSA, indicating that the extent of muscle atrophy caused by denervation was likewise conspicuous. Moreover, *Homer 2* replacement by transient transfection of denervated SOL muscle with plasmidic-Homer 2 cDNA was able to partially reverse fibre CSA decrease by about 20–30% [4]. On the basis of these findings, SOL of Homer $2^{-/-}$ mice was expected to be atrophic for congenital lack of *Homer 2*. The extent of hypotrophy/atrophy observed in Homer $2^{-/-}$ mice was smaller than that induced by denervation. This observation suggests that the normotrophic *status* of SOL muscle is dependent upon constitutive Homer 2 expression in combination with additional, independent factors linked to the innervated condition of the muscle.

In SOL muscle of Homer $2^{-/-}$ mice, the decrease of CSA was accompanied by an apparent thickening of the extracellular matrix. At steady state, in 2-month-old Homer $2^{-/-}$ mice, is this due to either necrosis, apoptosis, lack of satellite cell proliferation, or a combination thereof? Apoptosis is a hallmark of atrophy [31,32] and might explain at least in part such a reduction. Fibrous proliferation would imply a certain degree of preceding muscle necrosis, regeneration, and exhaustion of regeneration. Interference of satellite cell proliferation by Homer 2 might be postulated on the account of our own previous findings on rat SOL regeneration, showing that expression levels of *Homer 2* were positively and linearly related to muscle mass increase during regeneration: *Homer 2* is expressed by myogenic cells during regeneration and increase of *Homer 2b* during regeneration is associated to muscle mass recovery [3]. Moreover, *Homer 2* mRNA and protein were found to be transiently expressed at high levels in whole embryo at developmental stage E14.5 [1]; lack of such a spike might alter the overall skeletal muscle developmental program.

Another interesting finding was that in Homer $2^{-/-}$ EDL and FDB muscles, no significant changes in CSA were detected. Assessment of different Homer 2 controlled routes in different muscles awaits additional experimental work and could contribute to the identification of putative fibre type-specific signalling pathways controlling atrophy.

Because of their unique molecular properties that allow for clustering and functional modulation of different interacting partners, Homer proteins, and in particular Homer 2 at the subsynaptic domain, could play an important role at the NMJ integrating different downstream signalling pathways controlled by as yet unknown presynaptic signalling mechanisms. Two relevant biological questions are in order: (1) Is there a relationship be-

tween NMJ activity, or even NMJ disruption, and initiation of muscle catabolism mediated by Homer 2? (2) Is there a relationship between NMJ activity and muscle development and differentiation mediated by Homer 2?

The present results indicate that the null *Homer 2* phenotype did not entail changes in the nAChRs isoform localisation and expression. Adaptation in Homer $2^{-/-}$ does not perturb the expression of the adult ε-nAChR isoform, which remains detectable only at endplate level. However, downstream effects in the nAChR signalling pathway cannot be fully excluded.

On the contrary, data pertaining to morphological changes of endplate in Homer $2^{-/-}$ mice appeared not yet conclusive and conflicting. The apparent discrepancy between data from tissue specimens (Figure 4) and isolated FDB muscle fibres (Figure 5) might be due to at least four different reasons: (1) muscle type and lack of direct identification of fibre type; (2) experimental milieu, frozen muscles vs. isolated and cultured fibres; (3) innervation status (muscle specimens) vs. lack of innervation (isolated fibres); (4) methodology of volumetric analysis. Further work is needed to reconcile the conflicting result, but it is entirely possible, although speculative, that endplate in Homer $2^{-/-}$ muscle fibres might be more vulnerable to the lack of motor innervation than the WT counterpart.

Since 2005, data in the literature indicate the pivotal role of Homer 2 in muscle differentiation, trophism, and plasticity [1–5,11,12,34]. The present data are in line with the increasing evidence that Homer 2 regulates a few, key transcriptional programs of atrophy. However, more experimental work is needed to better characterise the signalling pathways activated in both slow- and fast-twitch fibres and the integrative function of Homer 2, if any, in the NMJ activity-driven control of skeletal muscle trophism.

4. Materials and Methods

4.1. Mice and Transgenic Mice

KO mice for *Homer 2* [18] have been generated as described and generously provided by Paul F. Worley (Johns Hopkins School of Medicine, Baltimore, MD, USA); C57BL/6 mice were used to produce *Homer 2* heterozygotes that were crossed to generate WT and Homer $2^{-/-}$ mice. Even though the WT littermates could show phenotypic properties different from the commercially available C57BL/6 mice, this procedure is commonly used to obtain mice with a more similar genotype except for the gene of interest. All mice used in the present study were bred and housed in the certified animal facility at the University of Trieste. Mice had free access to food and water and were maintained in a 12 h light/12 h dark cycle. Mice between 6 and 9 weeks of age were used for the experiments; body weight of WT and Homer $2^{-/-}$ mice was determined, and no difference was detected between the two experimental groups. For muscle dissection, mice were sacrificed by cervical dislocation as approved by the local Animal Care Committee and in agreement with the European legislation (2010/63/EU).

4.2. Morphometry

The hindlimb EDL, SOL, and FDB muscles were excised from WT and Homer $2^{-/-}$ mice, placed in OCT, and quickly frozen in liquid nitrogen. Cryosections from any muscle were stained with haematoxylin and eosin (Sigma-Aldrich, Darmstadt, Germany). Morphometry was carried out using ImageJ software (ver 1.42 q, National Institute of Health, Bethesda, MD, USA). Images at magnification 10× were acquired using a Zeiss AxioSkop microscope connected to a Leica DC 300F camera. Cross-sectional area (CSA) of the muscle fibres (μm^2) was calculated from cross-sections. CSA was estimated by outlining the profile on the monitor screen using a computer mouse.

4.3. RNA Extraction and Quantitative RT-PCR

Frozen tissue samples were ground to a fine powder under liquid nitrogen, and total RNA was extracted using Trizol method, following the manufacturer's instructions and including a glycogen co-precipitating step. Reverse transcription was performed on 1 μg

of total RNA by using a SuperScript VILO cDNA Synthesis Kit (ThermoFisher Scientific, Waltham, Massachusetts, MA, USA).

Specific primers for Homer1A and Homer1B/C were designed with the Primer3 software (Whitehead Institute for Biomedical Research, Cambridge, MA, USA; http://frodo.wi.mit.edu/ (accessed on 15 January 2021)), and their thermodynamic specificity was determined using BLAST sequence alignments (U.S. National Center for Biotechnology Information (NCBI), Bethesda, MD, USA) and Vector NTI® Software (Thermo Fisher Scientific, Waltham, Massachusetts, MA, USA). Primers sequences for *MuRF1*, *Atrogin-1*, *Cyclophilin A* (*PPIA*), *TATA-box-binding protein (TBP1*), and *hypoxanthine-guanine phosphoribosyltransferase* (*HPRT1*) were already published in [34]. Quantitative RT-PCR was performed in triplicate in a CFX96 Thermal Cycler (Bio-Rad, Hercules, CA, USA) using SYBR Green chemistry. A melt-curve analysis was performed at the end of each experiment to verify that a single product per primer pair was amplified. *PPIA*, *TBP*, and *HPRT1* were used as reference genes, and normalisation was performed using GeNorm software (V3.5, 2007, https://genorm.cmgg.be (accessed on 15 January 2021)).

Primers sequences were as follows:

MuRF-1 (Trim63)	Fw 5′-ACCTGCTGGTGGAAAACATC-3′ Rv 5′-CTTCGTGTTCCTTGCACATC-3′
Atrogin-1 (Fbxo32)	Fw 5′-GCAAACACTGCCACATTCTCTC-3′ Rv 5′-CTTGAGGGGAAAGTGAGACG-3′
Homer 1a	Fw 5′-GAAGTCGCAGGAGAAGATGG-3′ Rv 5′-GAACTTCCATATTTATCCA-3′
Homer 1b/c	Fw 5′- GAAGTCGCAGGAGAAGATGG-3′ Rv 5′-TAGCTCAGCCTCCCAGTGTT-3′
PPIA	Fw 5′-AGCATGTGGTCTTTGGGAAGGTG-3′ Rv: 5′-CTTCTTGCTGGTCTTGCCATTCC-3′
TBP1	Fw: 5′-TCAAACCCAGAATTGTTCTCC-3′ Rv: 5′-AACTATGTGGTCTTCCTGAATCC-3′
HPRT1	Fw: 5′-CTCATGGACTGATTATGGACAGGAC-3′ Rv: 5′-GCAGGTCAGCAAAGAACTTATAGCC-3′

4.4. Staining and Image Analysis of SOL and EDL Muscles

EDL and SOL were isolated from WT and Homer $2^{-/-}$ mice, quickly frozen in liquid nitrogen, and then cut to 10 µm and 30 µm thick sections at the middle portion of the muscle belly, then fixed with 4% (*w*/*v*) paraformaldehyde at RT for 10 min.

For the analysis of the endplate volume, after permeabilisation with a blocking buffer (0.3% Triton, 2% goat serum, and 2% Albumin in TBS, pH 7.4) for 60 min at RT, the 30 µm thick sections were incubated at 4 °C for 48 h with anti-Dystrophin primary antibody (0.076mg/mL in blocking buffer; rabbit Abcam, Cambridge, UK), followed by a 48 h incubation at 4 °C with Alexa-488-secondary antibody (0.2 µg/mL; goat-anti-rabbit ThermoFisher Scientific). At the end, the sections were incubated with Alexa-555-α-BuTX (1µg/mL, ThermoFisher Scientific) for 90 min at RT.

Immunostaining for Homer was carried out using 10 µm thick sections by incubation for 24 h at 4 °C with the primary rabbit anti-Homer antibody (propriety of Dr. Michele Salanova, 0.05 mg/mL), followed by an incubation with the same Alexa-488-goat-anti-rabbit secondary antibody used for the 30 µm thick sections.

Labelled 10 µm and 30 µm thick sections were mounted with a non-curing Mounting medium (ThermoFisher Scientific) and stored at 4 °C for further imaging. Cell nuclei were counterstained by 4′,6-diamidino-2-phenylindole (DAPI, 1:50; Sigma-Aldrich). Labelled sections were imaged using an SP8 confocal laser-scanning microscope (Leica Biosystems, Wetzlar, Germany). Image acquisition was carried out with the 63X/1.3 (NA) using an oil-immersion objective. Optical images were collected at 0.44 µm z resolution by sequential line scanning. Regions of interest (ROIs) were defined as α-BuTX-positive regions that resembled the "pretzel-like" morphology. ROIs were scanned at the *z*-axis throughout the whole thickness of the stained tissue. 3D image reconstruction and image analysis

were carried out with the Leica 3D Analysis Tool, allowing us to measure the NMJ volume and α-BuTX-signal intensity. Homer signal intensity was measured in the region 5–10 µm below the α-BuTX-positive signal, between the subsynaptic nuclei and the nAChRs.

4.5. Isolation of Muscles Fibres from FDB Muscles

Freshly isolated muscle fibres were obtained from the dissociation of FDB muscles of 6 to 8-weeks old Homer $2^{-/-}$ and WT male mice. FDB muscle fibres were isolated from both hindlimb foot muscles of a single mouse for each preparation. Briefly, immediately after the isolation, FDB muscles were enzymatically treated for 1 h in ice and 1 h at 37 °C with Type I collagenase 0.3% (*w*/*v*; Sigma-Aldrich), in Tyrode's solution containing (in mM): NaCl 137, KCl 2.7, $MgCl_2$ 1, $CaCl_2$ 1.8, Na_2HPO_4 0.35, $NaHCO_3$ 12, HEPES 25.2, D-glucose 5.5, pH 7.4 NaOH plus 100 U/mL penicillin, 100 µg/mL streptomycin, and 10% foetal bovine serum (Gibco, Burlington, ON, Canada). Single fibres (750–900 for each mouse) were isolated by mechanical dissociation with Pasteur pipettes with decreasing tip diameters and allowed to settle on Matrigel-coated (1 mg/mL; Corning, Tewksbury, MA, USA) glass coverslips accommodated in 35-mm Petri dishes. Cultures were maintained in the physiological saline as above at 37 °C in a humid air atmosphere containing 5% CO_2. According to the experimental purpose, denervation effects on the endplate were induced in vitro [29] by culturing isolated FDB muscle fibres for 7 days in a medium composed by DMEM high glucose enriched (Sigma-Aldrich) supplemented with horse serum (5%; Gibco), L-glutamine (2 mM), penicillin (100 IU/mL), and streptomycin (100 µg/mL), at 37 °C in a humid air atmosphere containing 5% CO_2. In these experimental conditions, a disarrangement of the endplate and the appearance of the foetal γ-nAChR isoform occurred as after in vivo denervation [25–27].

4.6. nAChRs Staining and Image Analysis of Isolated FDB Fibres

nAChRs staining was conducted in FDB muscle fibres 24 h or 7 days after dissociation according to the experimental aims. Cells were fixed with a solution of 4% (*w*/*v*) paraformaldehyde in PBS for 15 min at 4 °C. Fibres were incubated in a blocking solution containing PBS plus 2% bovine serum albumin (BSA; Sigma-Aldrich) for 30 min. nAChRs were labelled by Alexa-488-α-BuTX (ThermoFisher Scientific; 2.5 µg/mL in PBS supplemented with 0.1% BSA, for 1 h at RT). Cells were mounted on microscope slides.

Distribution of nAChRs and morphology of the endplates were analysed on images acquired by a Nikon C1 confocal microscope equipped with an argon laser (457, 477, 488, and 514 nm lines), a 561 nm and a 640 nm diode laser, and a Plan-Apochromat 60X/1.4 (NA) oil-immersion objective. Optical images were collected at either 0.30 or 0.35 µm z resolution by sequential line scanning.

Volumetric endplate analysis was carried out applying Fiji ImageJ software (ver 2.1.0/1.53c, National Institute of Health, Bethesda, MD, USA), quantifying the α-BuTX-stained volume. For each endplate, a stack of images was collected through the entire depth containing the α-BuTX visible signal. The region of interest (ROI) for the measurement of the endplate volume was set by projecting through the *z*-axis planes the most intense pixels of the α-BuTX signal. To each stack of images, a threshold was applied to eliminate the fluorescent noise and the background signal subtracted. The α-BuTX-stained volume was calculated as the sum of α-BuTX-stained volume of each z-stack, taking in account the step size of acquisition.

4.7. nAChRs Single Channel Recordings in Isolated FDB Fibres

Single-nAChR recordings were carried out by patch clamp technique in the cell-attached configuration on the endplate region identifiable by phase contrast microscopy as a distinct roughness of the fibre surface [27]. According to the experimental aim, electrophysiological recordings were performed on freshly isolated Homer $2^{-/-}$ and WT muscle fibres and on WT muscle fibres after 7 days of culturing (in vitro denervated). Single-channel recordings were performed using an Axopatch 200 amplifier (Molecular

Devices, Union City, CA, USA) after achieving a giga seal and when the baseline was stable. Signals were sampled at 50 kHz, filtered at 2 kHz with a low pass Bessel filter, and analysed by the pCLAMP 8.0 software package (Molecular Devices, Union City, CA, USA), using a threshold crossing criterion. All records were performed in the presence of 200 nM of ACh (Sigma-Aldrich), and for each stable patch, more than 500 events were analysed [30]. The open time distribution was best fitted with one or more exponentials if appropriate by maximum likelihood method. Lifetimes of the channel openings were expressed as time constants (τ) of the exponential curves. Single-channel conductance was estimated from the slope of the regression line obtained by plotting the current amplitude against the pipette potentials (Vp) at +60, +80 mV, and +100 mV.

Author Contributions: Study concept: P.L. and P.V.; experiment performance data collection and analysis: A.B. (Annalisa Bernareggi), A.B. (Alessandra Bosutti), S.F., B.R., G.M., G.T., K.B. and M.S. (Marina Sciancalepore); drafting manuscript P.L. and P.V.; critical evaluation and revision of the manuscript P.L., P.V., S.Z., D.B., P.F.W., and M.S. (Michele Salanova). All authors have read and agreed to the published version of the manuscript.

Funding: The research was supported by grants Programma-Contratto ASI, 2018-13-U.0-NEMUCO to Pompeo Volpe and Paola Lorenzon; No. 50WB1421/1718/2029 (to D.B.) and 50WB1826 (NEMUCO to M.S.) from Federal Department of Economy and Energy (BMWi) through Deutsches Zentrum fuer Luft- und Raumfahrt (DLR e.V., Bonn-Oberkassel, Germany).

Institutional Review Board Statement: The animal protocol was approved by the Institutional Animal Care and the Italian Minister of Health (8B687.N.X46).

Informed consent Statement: Not applicable.

Data Availability Statement: Data are contained within the article.

Conflicts of Interest: The authors declare that they have no conflict of interest.

References

1. Stibert, J.A.; Tabatabaei, N.; Howkins, A.F.; Hawke, T.; Worley, P.F.; Williams, R.S.; Rosenberg, P. Homer modulates NFAT-dependent signaling during muscle differentiation. *Dev. Biol.* **2005**, *287*, 213–224. [CrossRef]
2. Stiber, J.A.; Zhang, Z.S.; Burch, J.; Eu, J.P.; Zhang, S.; Truskey, G.A.; Seth, M.; Yamaguchi, N.; Meissner, G.; Shah, R.; et al. Mice lacking Homer1 exhibit a skeletal myopathy characterized by abnormal transient receptor potential channel activity. *Mol. Cell Biol.* **2008**, *28*, 2637–2647. [CrossRef]
3. Bortoloso, E.; Pilati, N.; Megighian, A.; Tibaldo, E.; Sandonà, D.; Volpe, P. Transition of Homer isoforms during skeletal muscle rigeneration. *Am. J. Physiol. Cell Physiol.* **2006**, *290*, C711–C718. [CrossRef] [PubMed]
4. Bortoloso, E.; Megighian, A.; Furlan, S.; Gorza, L.; Volpe, P. Homer 2 antagonizes protein degradation in slow-twitch skeletal muscles. *Am. J. Physiol. Cell Physiol.* **2013**, *304*, C68–C77. [CrossRef] [PubMed]
5. Salanova, M.; Volpe, P.; Blottner, D. Homer protein family regulation in skeletal muscle and neuromuscular adaptation. *IUBMB Life* **2013**, *65*, 769–776. [CrossRef] [PubMed]
6. Fagni, L.; Worley, P.F.; Ango, F. Homer as both a scaffold and transduction molecule. *Sci. STKE* **2002**, *137*, re8. [CrossRef]
7. Duncan, R.S.; Hwang, S.Y.; Koulen, P. Effects of Vesl/Homer proteins on intracellular signaling. *Exp. Biol. Med.* **2005**, *230*, 527–535. [CrossRef]
8. Jardin, I.; López, J.J.; Berna-Erro, A.; Salido, G.M.; Rosado, J.A. Homer proteins in Ca^{2+} entry. *IUBMB Life* **2013**, *65*, 497–504. [CrossRef]
9. Feng, W.; Tu, J.; Pouliquin, P.; Cabrales, E.; Shen, X.; Dulhunty, A.; Worley, P.F.; Allen, P.D.; Pessah, I.N. Dynamic regulation of ryanodine receptor type 1 (RyR1) channel activity by Homer 1. *Cell Calcium* **2008**, *43*, 307–314. [CrossRef]
10. Volpe, P.; Sandri, C.; Valle, G.; Nori, A.; Bortoloso, E. Topology of Homer 1a and Homer 1c in C_2C_{12} myotubes and transgenic skeletal muscle fibers. *Biochem. Biophys. Res. Commun.* **2004**, *316*, 884–892. [CrossRef] [PubMed]
11. Yuan, J.P.; Kiselyov, K.; Shin, D.M.; Chen, J.; Shcheynikov, N.; Kang, S.H.; Dehoff, M.H.; Schwarz, M.K.; Seeburg, P.H.; Muallem, S.; et al. Homer binds TRPC family channels and is required for gating of TRPC1 by IP_3 receptors. *Cell* **2003**, *114*, 777–789. [CrossRef]
12. Salanova, M.; Bortoloso, E.; Schiffl, G.; Gutsmann, M.; Belavý, D.L.; Felsenberg, D.; Furlan, S.; Volpe, P.; Blottner, D. Expression and regulation of Homer in human skeletal muscle during neuromuscular junction adaptation to disuse and exercise. *FASEB J.* **2011**, *25*, 4312–4325. [CrossRef]
13. Buonanno, A.; Fields, R.D. Gene regulation by patterned electrical activity during neural and skeletal muscle development. *Curr. Opin. Neurobiol.* **1999**, *9*, 110–120. [CrossRef]

14. Sanes, J.R.; Lichtman, J.W. Induction, assembly, maturation and maintenance of a postsynaptic apparatus. *Nat. Rev. Neurosci.* **2001**, *11*, 791–805. [CrossRef]
15. Lin, S.; Landmann, L.; Ruegg, M.A.; Brenner, H.R. The role of nerve- versus muscle-derived factors in mammalian neuromuscular junction formation. *J. Neurosci.* **2008**, *28*, 3333–3340. [CrossRef]
16. Zayas, R.; Groshong, J.S.; Gomez, C.M. Inositol-1,4,5-triphosphate receptors mediate activity-induced synaptic Ca^{2+} signals in muscle fibers and Ca^{2+} overload in slow-channel syndrome. *Cell Calcium* **2007**, *41*, 343–352. [CrossRef] [PubMed]
17. Zhu, H.; Bhattacharyya, B.J.; Lin, H.; Gomez, C.M. Skeletal muscle IP_3R1 receptors amplify physiological and pathological synaptic calcium signals. *J. Neurosci.* **2011**, *31*, 15269–15283. [CrossRef]
18. Shin, D.M.; Dehoff, M.; Luo, X.; Hyeok Kang, S.; Tu, J.; Nayak, S.K.; Ross, E.M.; Worley, P.F.; Muallem, S. Homer 2 tunes G protein–coupled receptors stimulus intensity by regulating RGS proteins and PLCβ GAP activities. *J. Cell Biol.* **2003**, *162*, 293–303. [CrossRef] [PubMed]
19. Briguet, A.; Courdier-Fruh, I.; Foster, M.; Meier, T.; Magyar, J.P. Histological parameters for the quantitative assessment of muscular dystrophy in the *mdx*-mouse. *Neuromuscul. Disord.* **2004**, *14*, 675–682. [CrossRef] [PubMed]
20. Wang, T.; Xu, Y.-Q.; Yuan, Y.-Y.; Xu, P.-W.; Zhang, C.; Fan, L.; Wang, L.-N.; Yin, C.; Zhang, L.; Cai, X.-C.; et al. Succinate induces skeletal muscle fiber remodeling via $SUNCR_1$ signaling. *EMBO Rep.* **2019**, *20*, e47892. [CrossRef]
21. Bodine, S.C.; Latres, E.; Baumhueter, S.; Lai, V.K.; Nunez, L.; Clarke, B.A.; Poueymirou, W.T.; Panaro, F.J.; Na, E.; Dharmarajan, K.; et al. Identification of ubiquitin ligases required for skeletal muscle atrophy. *Science* **2001**, *294*, 1704–1708. [CrossRef]
22. Gomes, M.D.; Lecker, S.H.; Jagoe, R.T.; Navon, A.; Goldberg, A.L. Atrogin-1, a muscle-specific F-box protein highly expressed during muscle atrophy. *Proc. Natl. Acad. Sci. USA* **2001**, *98*, 14440–14445. [CrossRef]
23. Gomes, A.V.; Waddell, D.S.; Siu, R.; Stein, M.; Dewey, S.; Furlow, J.D.; Bodine, S.C. Upregulation of proteasome activity in muscle RING finger 1-null mice following denervation. *FASEB J.* **2012**, *26*, 2986–2999. [CrossRef]
24. Boehm, I.; Alhindi, A.; Leite, A.S.; Logie, C.; Gibbs, A.; Murray, O.; Farrukh, R.; Pirie, R.; Proudfoot, C.; Clutton, R.; et al. Comparative anatomy of the mammalian neuromuscular junction. *J. Anat.* **2020**, *237*, 827–836. [CrossRef]
25. Tarpey, M.D.; Amorese, A.J.; Balestrieri, N.P.; Ryan, T.E.; Schmidt, C.A.; McClung, J.M.; Spangenburg, E.E. Characterization and utilization of the flexor digitorum brevis for assessing skeletal muscle function. *Skelet. Muscle* **2018**, *8*, 14. [CrossRef]
26. Henderson, L.P.; Lechleiter, J.D.; Brehm, P. Single channel properties of newly synthesized acetylcholine receptors following denervation of mammalian skeletal muscle. *J. Gen. Physiol.* **1987**, *89*, 999–1014. [CrossRef]
27. Gupta, R.; Chan, J.P.; Uong, J.; Palipsis, W.A.; Wright, D.J.; Shah, S.B.; Ward, S.R.; Lee, T.Q.; Steward, O. Human motor endplate remodeling after traumatic nerve injury. *J. Neurosurg.* **2020**, *18*, 1–8. [CrossRef] [PubMed]
28. Ojeda, J.; Bermedo-García, F.; Pérez, V.; Mella, J.; Hanna, P.; Herzberg, D.; Tejero, R.; López Manzaneda, M.; Tabares, L.; Henríquez, P. The Mouse *Levator Auris Longus* Muscle: An amenable model system to study the role of postsynaptic proteins to the maintenance and regeneration of the neuromuscular synapse. *Front. Cell Neurosci.* **2020**, *14*, 225. [CrossRef] [PubMed]
29. Grohovaz, F.; Lorenzon, P.; Ruzzier, F.; Zorec, R. Properties of acetylcholine receptors in adult rat skeletal muscle fibers in culture. *J. Membr. Biol.* **1993**, *136*, 31–42. [CrossRef]
30. Bernareggi, A.; Ren, E.; Giniatullin, A.; Luin, E.; Sciancalepore, M.; Giniatullin, R.; Lorenzon, P. Adenosine promotes endplate nAChR channel activity in adult mouse skeletal muscle fibers via low affinity P1 receptors. *Neuroscience* **2018**, *383*, 1–11. [CrossRef] [PubMed]
31. Schiaffino, S.; Dyar, K.A.; Ciciliot, S.; Blaauw, B.; Sandri, M. Mechanisms regulating skeletal muscle growth and atrophy. *FEBS J.* **2013**, *280*, 4294–4314. [CrossRef] [PubMed]
32. Pallafacchina, G.; Blaauw, B.; Schiaffino, S. Role of satellite cells in muscle growth and maintenance of muscle mass. *Nutr. Metab. Cardiovasc. Dis.* **2013**, *23*, S12–S18. [CrossRef] [PubMed]
33. Wang, Y.; Pessin, J.E. Mechanisms for fiber-type specificity of skeletal muscle atrophy. *Curr. Opin. Clin. Nutr. Metab. Care* **2013**, *16*, 243–250. [CrossRef] [PubMed]
34. Gambara, G.; Salanova, M.; Ciciliot, S.; Furlan, S.; Gutsmann, M.; Schiffl, G.; Ungethuem, U.; Volpe, P.; Gunga, H.-C.; Blottner, D. Microgravity-induced transcriptome adaptation in mouse paraspinal longissimus dorsi muscle highlights insulin resistance-linked genes. *Front. Physiol.* **2017**, *8*, 279. [CrossRef]

3.b EPS-driven Piezo 1 activity and IL-6 release

The voluntary movement sustained by the skeletal muscle system prevents and counteracts muscle atrophy. More and more evidences suggest that physical exercise is also beneficial for cognitive functions, mood and brain health. Physical exercise reduces stress, anxiety, depression as well as the risk of cardiovascular disease, cancer, osteoporosis, and diabetes.

Recently, skeletal muscle has been identified as an endocrine organ, with the ability to produce and release several myokines as a consequence of the contractile activity. Myokines are responsible for a multitude of effects on a wide range of different tissues, thus establishing several muscle-organ crosstalks[123].

So far, about 650 myokines have been identified; only 5% of them are associated with a known biological function[103]. Circulating myokine levels appear to increase during physical exercise and decrease with physical inactivity. IL-6, first cloned in 1986[124], is mainly known for its role in the immune response and acute phase reactions; however, it acts also as an anti-inflammatory myokine, which regulates the growth and differentiation of various tissues[125,126]. It is known that IL-6 plasma concentration increases up to 100-fold in volunteers performing exercise[38]. The levels of released myokines are related to the percentage of muscle mass used, the intensity and the duration of the physical effort produced[127]. Taking into account that the skeletal muscles are approximately 40% of total body weight in humans and contains 50-75% of all body proteins[2], in response to contraction, skeletal muscles are considered the predominant source of the systemic increase of IL-6 induced by exercise[109,110,111].

During exercise, IL-6 stimulates the appearance in blood circulation of other anti-inflammatory cytokines, such as IL-1 and IL-10, and inhibits the production of the pro-inflammatory cytokine TNF-α both in *in vitro* and *in vivo* experiments[128,129]. In addition, IL-6 enhances lipid turnover, stimulating lipolysis as well as fat oxidation. Moreover, several studies demonstrate the beneficial autocrine/paracrine role of IL-6 acting on skeletal muscle regeneration[130–132].

EPS is able to mimic the nerve activity in cultured skeletal myotubes inducing visible cell contraction. Action potentials were elicited, time locked with EPS, triggering intracellular Ca^{2+} increase[101,133] as well as IL-6 production and release[125]. Field EPS promoted IL-6

production via ATP release, acting on purinergic receptors and activating the IP_3-dependent intracellular Ca^{2+} signals. Released IL-6 controlled its own expression[125].

During contraction, because of the mechanical strain, cation-permeable mechanosensitive channels are activated. The Piezo family of mechanosensitive channels, discovered by Ardem Patapoutian in 2010[134] (bestowed with Nobel Prize for Medicine in 2021), consists of two isoforms of non-selective Ca^{2+} permeable ion channels named Piezo 1 and Piezo 2. Many studies have shown that these channels play important functional roles in several tissues[135] (Figure 17).

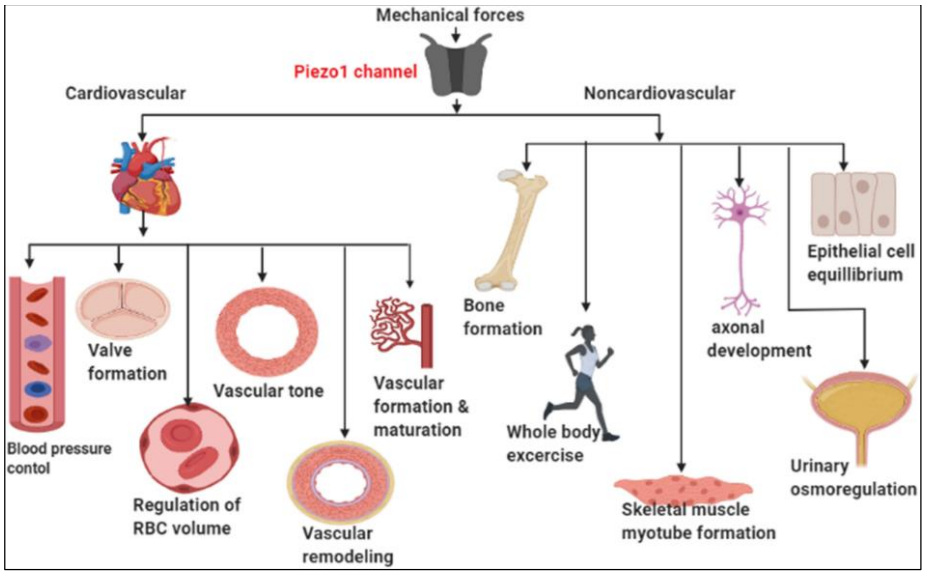

Fig. 17. *The sketch illustrates the wide range of Piezo 1 channel functions in different tissues (from 135).*

At skeletal muscle level, Piezo 1 activation was identified in a study performed on the C2C12 myogenic cell line, in which the activity of Piezo 1 channels controls the cortical actomyosin assembly, necessary for myotube formation during myogenesis[136]. A similar role of Piezo 1 channels on primary skeletal muscle cells was identified for the first time in our laboratory. By the chemical activation with the specific agonist Yoda 1, we identified the role of Piezo 1 channel activity in the transition from the proliferative myoblasts to the MyoG-positive differentiated myocytes, able to fuse into myotubes[137].

Nowadays, although the activation of Ca^{2+} signaling pathways triggered by mechanosensitive channels is well established[138], it remains still unknown their role in the myokine release during contractions. Part of my research activity was intended to investigate the possible involvement of Piezo 1 channels in IL-6 release during muscle cell contraction induced by EPS.

Our results demonstrated for the first time that mechano-activated Piezo 1 channel activity supports IL-6 release. Moreover, our data indicated that chemical activation of Piezo 1 channels could be even more efficient in inducing IL-6 release than EPS, suggesting that chemical compounds acting on Piezo 1 channels might represent promising tools to mimic muscle activity.

Biochemical and Biophysical Research Communications 623 (2022) 148–153

Contents lists available at ScienceDirect

Biochemical and Biophysical Research Communications

journal homepage: www.elsevier.com/locate/ybbrc

A preliminary study on the role of Piezo1 channels in myokine release from cultured mouse myotubes

Marina Sciancalepore [a], Gabriele Massaria [a], Federica Tramer [b], Paola Zacchi [c], Paola Lorenzon [a], Annalisa Bernareggi [a, *]

[a] Department of Life Sciences, Biophysics and Cellular Neurobiology Laboratory, University of Trieste, via Fleming 22, 34127, Trieste, Italy
[b] Department of Life Sciences, University of Trieste, via Giorgieri 1, 34127, Trieste, Italy
[c] Department of Life Sciences, University of Trieste, via Valerio 28/1, 34127, Trieste, Italy

ARTICLE INFO

Article history:
Received 4 July 2022
Accepted 14 July 2022
Available online 19 July 2022

Keywords:
Skeletal muscle cells
Electrical pulse stimulation
IL-6
Piezo1
Yoda1

ABSTRACT

It has long been known that regular physical exercise induces short and long term benefits reducing the risk of cardiovascular disease, diabetes, osteoporosis, cancer and improves sleep quality, cognitive level, mobility, autonomy in enderly. More recent is the evidence on the endocrine role of the contracting skeletal muscle. Exercise triggers the release of miokines, which act in autocrine, paracrine and endocrine ways controlling the activity of muscles but also of other tissues and organs such as adipose tissue, liver, pancreas, bones, and brain. The mechanism of release is still unclear.

Neuromuscular electrical stimulation reproduces the beneficial effects of physical activity producing physiological metabolic, cardiovascular, aerobic responses consistent with those induced by exercise. *In vitro*, Electrical Pulse Stimulations (EPS) of muscle cells elicit cell contraction and mimic miokine release in the external medium.

Here we show that, in cultured mouse myotubes, EPS induce contractile activity and the release of the myokine IL-6. Gadolinium highly reduces EPS-induced IL-6 release, suggesting the involvement of mechanical activated ion channels. The chemical activation of mechanosensitive Piezo1 channels with the specific agonist Yoda1 stimulates IL-6 release similarly to EPS, suggesting the involvement of Piezo1 channels in the control of the myokine release. The expression of Piezo1 protein in myotubes was confirmed by the Western blot analysis.

To the best of our knowledge, this is the first evidence of a Piezo1-mediated effect in myokine release and suggests a potential translational use of specific Piezo1 agonists for innovative therapeutic treatments reproducing/enhancing the benefits of exercise mediated by myokines.

1. Introduction

During the past decade numerous studies have described the endocrine role of skeletal muscle, able to produce and release several myokines during contraction including interleukins IL-6, IL-8, IL-15, Insulin-like growth factor, BDNF, myostatin, irisin and others, which bind to their receptors and activate specific signaling pathways [1]. Circulating myokine levels increase during physical exercise and decrease with physical inactivity. In particular, skeletal muscles are considered the dominant source of IL-6 production secreted into the bloodstream in response to muscle contraction [2] and, therefore, mostly responsible for the systemic increase of IL-6 induced by exercise [3,4]. IL-6 binds to the transmembrane receptor IL-6R or a soluble receptor sIL-6R. Signaling is mediated through the glycoprotein named gp130, activating intracellular signaling including cytosolic Ca^{2+} increase, production of reactive oxygen species and NF-kB pathway [5]. Higher levels of plasma IL-6 characterize intensive and long activity exercises with the use of larger muscle mass. IL-6, more known as inflammatory cytokine, is involved in a dual effect. A transient short-term action is related to its autocrine and paracrine activity required to modulate proliferation and differentiation of muscle cells [6–9]. A persistent pro-inflammatory activity is related to higher levels of the circulating miokine with a long-lasting effect associated to muscle damage

Abbreviations: EPS, Electrical pulse stimulation; IL-6, interleukin 6.

* Corresponding author. Department of Life Sciences, University of Trieste, Via A. Fleming, 22, I, 34127, Trieste, Italy.
E-mail address: abernareggi@units.it (A. Bernareggi).

https://doi.org/10.1016/j.bbrc.2022.07.059

[10,11]. Conventional and noisy Pulse Electro Stimulations (EPS) mimick the nerve activity in cultured skeletal muscle cells [12–14]. EPS elicit time-locked Ca^{2+} increases, cell contractions [13,15] and IL-6 release [16,17].

Sustaining muscle cell contractions, physical exercise as well as neuromuscular electrical stimulation are supposed to activate cation-permeable mechano-activated channels (MAs) at the skeletal muscle level eliciting Ca^{2+}-dependent signaling [18] but the mechanism promoting the miokine release during muscle contractions is still unknow. Piezo1 channels belong to the large family of the mechanically-activated (MA) channels [19]; they are activated either by mechanical and chemical stimuli [20]. The chemical activation is mediated by the specific exogenous agonist Yoda1, offering the advantage to induce the opening of Piezo1 channels in the absence of any mechanical stimulation [21].

This study aimed to investigate the possible contribution of MA channel activity in the IL-6 release in EPS stimulated skeletal muscle cells, with a particular attention on Piezo1 channels.

2. Materials and methods

2.1. Cell cultures

Primary myotube cultures were obtained starting from satellite cells derived from the hind-leg muscles of a 7-day-old male Balb/c mouse [22] killed by cervical dislocation as approved by Local Animal Care Committee and in agreement with the European legislation.

Myoblasts were seeded at 70.000 cells per dish onto matrigel-coated (0.5 mg/ml) coverslips and grown for 24 h in a Growth Medium (GM) consisting of HAM F-10 plus 20% foetal bovine serum (FBS), L-Glutamine (4 mM), penicillin (100 IU/ml) and streptomycin (100 μg/ml). To induce myoblast fusion into myotubes, GM was replaced with Differentiation Medium (DM) composed by DMEM high glucose enriched with Horse Serum (2%), L-Glutamine (2 mM), penicillin (100 IU/ml) and streptomycin (100 μg/ml). Dishes were maintained in an incubator at 37 °C in saturated humidity and in CO_2 (5%)-enriched air. The culture medium was replaced every 48 h.

2.2. EPS of cultured myotubes

EPS was carried out on day 7 differentiated myotubes plated on matrigen-coated 6-well plates. Before the EPS, in each well the medium was replaced with 1 ml Tyrode's Salt solution enriched with FBS (10%) and penicillin and streptomycin as above. During EPS, the contractile activity of myotubes was assessed by an inverted Axiovert microscope (Carl Zeiss, Germany). EPS was performed by field electrostimulation delivered by the Grass S88 stimulator (Grass Instruments, Quincy, MA) to the myotubes kept at 37 °C in saturated humidity and in CO_2 (5%)-enriched air. In each well, two handmade connection cards connected to a couple of parallel platinum-iridium electrodes (0.2 mm in diameter) were present. The couples of electrodes were placed 2 cm apart and positioned 1–2 mm over the cells. Biphasic single conventional 1 ms pulses, were delivered at the frequencies of 1, 5 and 10 Hz. The stimulus strength (strengths 6–7 V peak to peak) was set to approximately 10% above the mechanical threshold in order to induce visible myotube contractions, without causing cell damage.

2.3. Electrophysiological recordings

Changes in membrane potential elicited by EPS were recorded by single myotubes by patch-clamp technique under current clamp conditions with perforated patch clamp method. Mouse myotubes that occasionally exhibited spontaneous contractions, were discharged.

Changes in voltage were recorded by an Axopatch 200B amplifier (Axon Instruments, Foster City, CA, USA). Extracellular recording solution contained (in mM): 100 NaCl, 2.8 KCl, 2 $CaCl_2$, 2 $MgCl_2$, 10 Hepes, 10 glucose, pH 7.3. Pipette solution contained (in mM): 140 K-aspartate, 10 NaCl, 2 $MgCl_2$, 10 Hepes and 150 μg/ml amphotericin B, pH 7.3. Voltage recordings were sampled at 100 kHz and low-pass filtered at 1 Hz.

2.4. Cytotoxicity assay

During EPS, lactate dehydrogenase activity (LDH) was measured by spectrophotometric measurements of the supernatant and lysate using a LDH assay kit (In Vitro Toxicology Assay Kit, Lactic Dehydrogenase based, Sigma Aldrich) and following the manufacturer's instructions. In order to obtain the absorbance measure, the value of the background absorbance of the multi-well plates measured at 690 nm was subtracted from the absorbance measured at a wavelength of 490 nm. LDH levels (%) were calculated by dividing the amount of LDH detected in the supernatant by the total amount of LDH (detected in supernatant and lysate). Each experimental point was performed in triplicate.

2.5. IL-6 ELISA quantification

Immediately after the EPS, supernatants (1 ml) were collected from both the electrically-stimulated and control dishes, precooled at 4 °C and spun 5 min at 20,000 *g* to remove non adherent cells. Surnatants were stored at −80 °C. Cells were lysed with 400 μl lysis buffer/well (PBS + 1% TritonX-100) collected and stored at −80 °C.

IL-6 concentrations in supernatants were measured with commercially available Quantikine® ELISA kit (R&D Systems Minneapolis, MN, USA) in a Microplate reader (Synergy, BioTeck Winooski, VT).

Total proteins were extracted with lysis buffer and the protein concentration was quantified by Coomassie (Bradford) protein assay (Thermo Fisher Scientific) and used to normalize against the values obtained for cytokine release. Each experimental point was repeated at least in duplicate.

2.6. Western blotting

Myotubes were washed twice with warm PBS and incubated for 30 min at 4 °C in RIPA buffer (25 mM Tris-HCl pH = 7.6, 150 mM NaCl, 1% NP40, 0,5% Sodium Deoxycholate, 0,1% SDS, 1 mM EDTA) supplemented with 1 × EDTA-free protease inhibitor cocktail tablets (Sigma-Aldrich). After removing the insoluble material by centrifugation (13,000 *g* for 10 min at 4 °C), protein concentrations were determined by Bio-Rad DC Protein Assay. Thirty-microgram aliquots of proteins were separated by SDS-PAGE and subject to Western blotting. Proteins were transferred onto 0.22-μm nitrocellulose membranes (Amersham). Binding of nonspecific proteins to membranes was blocked by incubating the membranes in the blocking buffer consisting of 5% non-fat milk in TBS plus 0.1% Tween 20 (TBST) for 1 h at room temperature. Membranes were then incubated overnight at 4 C with rabbit polyclonal antibody against Piezo1 (NBP1-78446) diluited 1:1000 in blocking buffer. After three washes with TBST, membranes were incubated in horseradish peroxidase-conjugated secondary antibodies for 1 h. After three more washes with TBST, immunoreactive proteins on the membranes were detected by WesternBright ECL (Advasta, San Jose, CA).

2.7. Chemicals

L-Glutamine, penicillin and streptomycin were purchased from Euroclone (Milano, Italy); FBS from Gibco (Burlington, ON, Canada). Matrigel from Corning (Tewksbury, MA, USA). Unless otherwise stated, all the other chemicals were from Sigma-Aldrrich (St. Louis, MA, USA). Stock solutions of Yoda1 were reconstituted in DMSO and stored at −20 °C. According to the experimental protocol, when applied, cells were preincubated for 30 min with Yoda1 and the agonist was maintained in the bathing solution for all the duration of the experiment.

2.8. Statistical analysis

Data of *n* experiments are expressed as mean ± standard error (SEM). All statistical tests and curve fitting were performed using the software package GraphPad Prism (CA, USA) Version 8.00. Unpaired Student's *t*-test was used to compare data between two groups of normally distributed values. Mann-Whitney non parametric test was used to compare two groups of non-parametric values. The significance level was set at $P < 0.05$.

3. Results

3.1. EPS induce contractions

In a set of experiments, 7 day differentiated mice myotubes were stimulated for 4 h with regular bipolar 1 ms pulses at constant frequencies of 1, 5 and 10 Hz. At all frequencies, action potentials were observed, time-locked with EPS (Fig. 1A). As previously reported, each action potential was associated to a cell twitching [13]. Upon EPS delivery, LDH was measured in the external medium. LDH release did not differ significantly in media from stimulated compared with unstimulated myotubes (Fig. 1B). Accordingly, the observation of stimulated cells excluded a visible cell damage. The results indicated that none of the EPS protocols, used and delivered for 4 h, induced cytotoxicity.

3.2. EPS induce IL-6 production

The content of IL-6 release in the supernatants derived from EPS stimulated myotubes was measured as picrograms per total milligrams of proteins detected in the cell extract (pg IL-6/mg proteins) and normalized to that derived from the unstimulated cells.

A set of experiments was carried out to investigate on the time-dependency of the secretion. IL-6 content was assessed at 1 h and 4 h of regular 1 ms EPS delivered at 10 Hz. The entity of IL-6 released was unchanged after 1 h but it resulted significantly increased after 4 h EPS in respect to unstimulated cells (Fig. 2A).

No increase of IL-6 release was observed after 4 h at 1 Hz EPS (259.1 ± 30.03 pg/mg after 4h EPS vs 218.5 ± 25.96 pg/mg in controls); while EPS delivered at 5 Hz significantly increased the IL-6 production (216.1 ± 31.71 pg/mg vs 119.0 ± 26.19 pg/mg observed in controls) as well as at 10 Hz (315.3 ± 54.45 pg/mg protein vs 136.6 ± 18.52 pg/mg in controls, Fig. 2B).

3.3. The role of mechanosensitive Piezo1 channels in the release of IL-6

When myotubes underwent EPS at 10 Hz for 4 h in the presence of the MA channel blocker gadolinium (Gd^{3+}) [19], the release of the myokine severely decresed. In more detail, the pre-incubation (30 min) with Gd^{3+} 30 μM reduced by ~65% the EPS-induced release of IL-6 (Fig. 3A) suggesting the involvement of the MA channels in the control of the myokine secretion.

Interestingly, Piezo1 protein expression was detected in myotubes by WB analysis (Fig. 3 B). Moreover, in the absence of EPS stimulation, the pharmacological activation of Piezo1 channels by the specific agonist Yoda1 (for 4 h at 3 μM and 10 μM) increased the IL-6 release (Fig. 3C). The content of IL-6, detected at the two agonist concentrations, revealed that the chemical activation of Piezo1 mimics the effect of the EPS-induced contractile activity (see Fig. 2B).

4. Discussion

IL-6 is the cytokine with the highest plasma increase after acute physical exercise [23,24] and skeletal muscle is mostly responsible

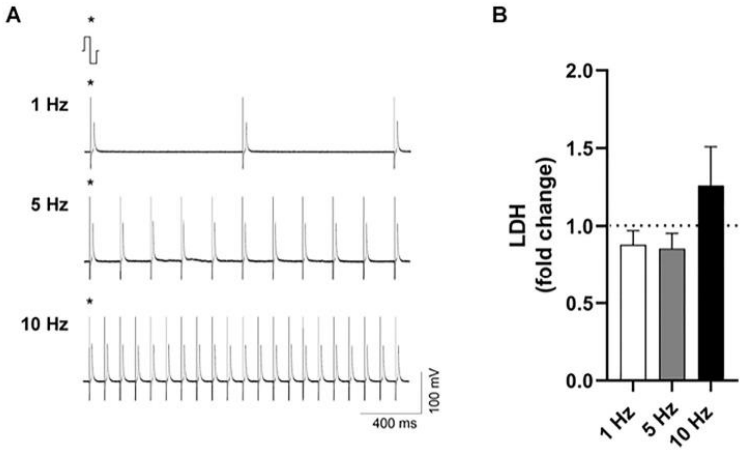

Fig. 1. EPS elicit action potentials. A. Representative traces of action potentials elicited in 7 day - differentiated myotubes by regular stimulations (1 ms biphasic pulses) at the frequences of 1, 5 and 10 Hz as indicated. Traces were sampled at 100 kHz and band-pass filtered at 1 Hz. B. LDH content in the external medium of myotubes after similar protocols of EPS ($n = 5$). LDH contents are expressed as fold changes to control values. No significant variation was observed ($P > 0.05$ vs. unstimulated).

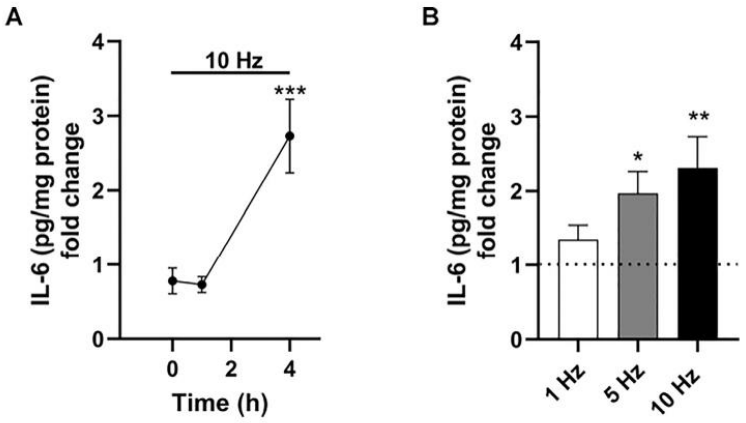

Fig. 2. EPS elicit IL-6 release. A. IL-6 release after 4 h EPS (1 ms biphasic pulses) at 1, 5 and 10 Hz expressed as fold increase to unstimulated conditions. EPS at 5 and 10 Hz significantly (*$P < 0.05$, **$P < 0.01$) increase the IL-6 secretion from 7 day - differentiated myotubes ($n = 5–10$). B. IL-6 secretion assessed at 1 and 4 h of EPS at 10 Hz expressed as fold increase in respect to unstimulated conditions, indicate a significant IL-6 secretion starting from 4 h of EPS.

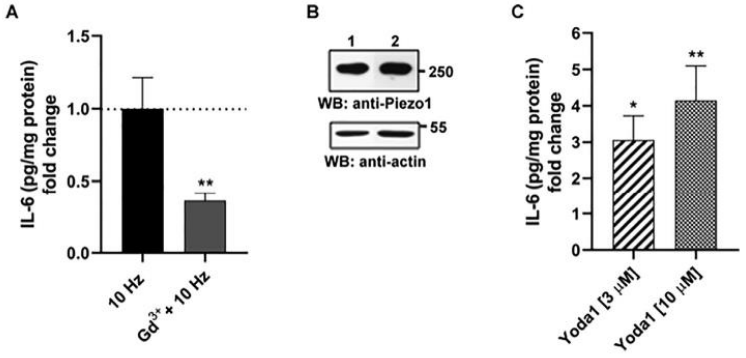

Fig. 3. Piezo1 channel expression and Yoda1-induced IL-6 release in myotubes. A. Gd3+ inhibitory effect on IL-6 release induced by 10 Hz EPS. Myotubes were stimulated with EPS at 10 Hz with and without 30 min preincubation with 30 μM Gd3+ (**$P < 0.01$). B. Western blot analysis revealed the Piezo1 expression in myotubes derived from two indipendent cultures (lane 1 and lane 2). Actin was used as loading control. C. Yoda1 at 3 μM and 10 μM increased the IL-6 production. Data are normalized to unstimulated conditions. (*$P < 0.05$, **$P < 0.01$).

for this phenomenon [3,4]. Indeed, the magnitude of the IL-6 increase is related to the individual muscle mass, duration and intensity of the exercise [25].

We previously detected in mouse myotubes the efficiency of electrostimulation protocols in promoting intracellular Ca^{2+} changes, time-locked with electric pulses and contractile activity [13]. This *in vitro* exercise model offers the advantage to explore the muscle release of myokines, without cell damage avoiding other possible myokine sources present in the intact muscles (e.g. neuronal, endocrine, immune system cells). Various studies reported electrostimulation-mediated increase in IL-6 expression and release in muscle cell lines such as C2C12 (8,26,27,28], primary human myotubes [29–31] and rodent myotubes [16,32,33]. Variability in the amount and time-course of IL-6 release has been related to the different experimental animal species, stimulation protocols, or protein detection.

The mechanisms regulating IL-6 production and secretion are not completely known. Intracellular IL-6-positive vesicles-like structures have been detected in muscle fibers at both the sarcolemma and inside the fibers in the T-tubules area, reduced in number after contraction [34]. Furthermore, exercise was recently proposed to activate lactate-dependent pH sensitive-proteases, which would alter the extracellular matrix, inducing membrane conformational changes, responsible for IL-6 release [35]. Independently from the mechanism of release, a beneficial role of IL-6 acting in autocrine/paracrine way on skeletal muscle regeneration was observed [5,8].

Regarding the mechanisms controlling IL-6 expression/release triggered by EPS, previous reports indicate that field electrostimulation of skeletal muscle cells promotes the release of extracellular ATP through pannexins [14–16] favouring IL-6 expression via IP_3-dependent intracellular Ca^{2+} signals [16]. IL-6 was suggested to be released and to autocrinally promote, though a positive feedback, IL-6 production acting on IL-6R and activation of the JAK2/STAT3 signaling [16].

During contraction, muscle cells undergo mechanical strain, causing the activation of specific signaling controlling regulation of gene expression, cell differentiation and hypertrophy [36,37]. The

contractile activity causes MA channels activation; being them Ca^{2+} permeable, they could potentially control a wide number of intracellular signaling pathways including the myokine production.

In this report, for the first time we show that MA channel activity sustains to a large extent (~65%) the IL-6 release. The lacking of specific MA channel blockers/antagonists, does not allow the identification of the specific MA channel subtypes involved, considering that many of them could be likely expressed in myotubes [38]. Recently, we identified a time-window in which the chemical activation of the mechanical sensitive Piezo1 activity promotes differentiation and fusion of the myogenic precursors [39]. Here we unveil the role of Piezo1 in controlling IL-6 release in skeletal muscle cells similarly to what reported in cardiac fibroblasts where Piezo1 activation by Yoda 1 was found to be coupled to IL-6 secretion via a p38 MAPK-dependent pathway [40]. However, patient immobilization was recently found to be associated to a downregulation of Piezo1, and an upregulation of atrophy-related genes including *Il6* via a signaling pathway mediated by the transcription factor Krüppel-like factor 15 (KLF15) [41]. The discrepancy between the reported results requires further investigation.

The comparison between the amount of IL-6 released by EPS and by the chemical activation of Piezo1 channel suggests that the chemical activation of Piezo1 channels by Yoda1 could be even more efficient than the EPS at 10 Hz in inducing the myokine release. Thus, according to that, specific pharmacological Piezo1 activation could represent a new powerfull tool to promote IL-6 release in physiological and pathological contests [42,43].

Funding

This work was supported by Interreg V-A Italia-Slovenia 2014–2020 program MEMORI-net.

Author contributions

MS, PL, and AB conceived and designed research; MS, GM and PZ, FT performed experiments; MS, GM analyzed data; MS, FT interpreted results of experiments; MS, GM and PZ prepared figures; MS and AB drafted manuscript; MS, PL and AB edited and revised manuscript; MS, GM, PZ, PL, FT and AB approved final version of manuscript.

Declaration of competing interest

The authors declare that they have no known competing financial interests or personal relationships that could have appeared to influence the work reported in this paper.

Acknowledgements

We are grateful to Andrew Constanti (UCL, School of Pharmacy, London, UK) for critically reading the manuscript.

References

[1] B.K. Pedersen, A. Steensberg, P. Keller, C. Keller, C. Fischer, N. Hiscock, G. van Hall, P. Plomgaard, M.A. Febbraio, Muscle-derived interleukin-6: lipolytic, anti-inflammatory and immune regulatory effects, Pflügers Archiv 446 (2003) 9–16, https://doi.org/10.1007/s00424-002-0981-z.

[2] B.K. Pedersen, A. Steensberg, C. Fischer, C. Keller, P. Keller, P. Plomgaard, M. Febbraio, B. Saltin, Searching for the exercise factor: is IL-6 a candidate? J. Muscle Res. Cell Motil. 24 (2003) 113–119, https://doi.org/10.1023/a:1026070911202.

[3] A. Steensberg, G. van Hall, T. Osada, M. Sacchetti, B. Saltin, B.K. Pedersen, Production of interleukin-6 in contracting human skeletal muscles can account for the exercise-induced increase in plasma interleukin-6, J. Physiol. 529 (2000) 237–242, https://doi.org/10.1111/j.1469-7793.2000.00237.x.

[4] A.D. Toft, A. Falahati, A. Steensberg, Source and kinetics of interleukin-6 in humans during exercise demonstrated by a minimally invasive model, Eur. J. Appl. Physiol. 111 (2011) 1351–1359, https://doi.org/10.1007/s00421-010-1755-5.

[5] J.E. Belizário, C.C. Fontes-Oliveira, J.P. Borges, J.A. Kashiabara, E. Vannier, Skeletal muscle wasting and renewal: a pivotal role of myokine IL-6, SpringerPlus 5 (2016) 619, https://doi.org/10.1186/s40064-016-2197-2.

[6] B. Baeza-Raja, P. Muñoz-Cánoves, p38 MAPK-induced nuclear factor-kappaB activity is required for skeletal muscle differentiation: role of interleukin-6, Mol. Biol. Cell 15 (2004) 2013–2026, https://doi.org/10.1091/mbc.e03-08-0585.

[7] F. Haddad, F. Zaldivar, D.M. Cooper, G.R. Adams GR, IL-6-induced skeletal muscle atrophy, J. Appl. Physiol. 98 (2005) 911–917, https://doi.org/10.1152/japplphysiol.01026.2004.

[8] A.L. Serrano, B. Baeza-Raja, E. Perdiguero, M. Jardí, P. Muñoz-Cánoves, Interleukin-6 is an essential regulator of satellite cell-mediated skeletal muscle, Hypertrophy 7 (2008) 33–44, https://doi.org/10.1016/j.cmet.2007.11.011.

[9] P. Muñoz-Cánoves, C. Scheele, B.K. Pedersen, A.L. Serrano, Interleukin-6 myokine signaling in skeletal muscle: a double-edged sword? FEBS J. 280 (2013) 4131–4148, https://doi.org/10.1111/febs.12338.

[10] T. Tsujinaka, J. Fujita, C. Ebisui, M. Yano, E. Kominami, K. Suzuki, K. Tanaka, A. Katsume, Y. Ohsugi, H. Shiozaki, M. Monden, Interleukin 6 receptor antibody inhibits muscle atrophy and modulates proteolytic systems in interleukin 6 transgenic mice, J. Clin. Invest. 97 (1996) 244–249, https://doi.org/10.1172/JCI118398.

[11] K.A. Baltgalvis, F.G. Berger, M.M.O. Pena, J.M. Davis, S.J. Muga, J.A. Carson, Interleukin-6 and cachexia in ApcMin/+ mice, Am. J. Physiol. Regul. Integr. Comp. Physiol. 294 (2008) R393–R401, https://doi.org/10.1152/ajpregu.00716.2007.

[12] N. Nikolić, S.S. Bakke, E.T. Kase, I. Rudberg, I.F. Halle, A.C. Rustan, G.H. Thoresen, V. Aas, Electrical pulse stimulation of cultured human skeletal muscle cells as an in vitro model of exercise, PLoS One 7 (2012), e33203, https://doi.org/10.1371/journal.pone.0033203.

[13] M. Sciancalepore, T. Coslovich, P. Lorenzon, G. Ziraldo, G. Taccola, Extracellular stimulation with human "noisy" electromyographic patterns facilitates myotube activity, J. Muscle Res. Cell Motil. 36 (2015) 349–357, https://doi.org/10.1007/s10974-015-9424-2.

[14] A. Bosutti, A. Bernareggi, G. Massaria, P. D'Andrea, G. Taccola, P. Lorenzon, M. Sciancalepore, A "noisy" electrical stimulation protocol favors muscle regeneration in vitro through release of endogenous ATP, Exp. Cell Res. 381 (2019) 121–128, https://doi.org/10.1016/j.yexcr.2019.05.012.

[15] S. Buvinic, G. Almarza, M. Bustamante, M. Casas, J. López, M. Riquelme, J.C. Sáez, J.P. Huidobro-Toro, E. Jaimovich, ATP released by electrical stimuli elicits calcium transients and gene expression in skeletal muscle, J. Biol. Chem. 284 (2009) 34490–34505, https://doi.org/10.1074/jbc.M109.057315.

[16] M. Bustamante, R. Fernández-Verdejo, E. Jaimovich, S. Buvinic, Electrical stimulation induces IL-6 in skeletal muscle through extracellular ATP by activating Ca^{2+} signals and an IL-6 autocrine loop, Am. J. Physiol. Endocrinol. Metab. 306 (2014) E869–E882, https://doi.org/10.1152/ajpendo.00450.2013.

[17] Y. Furuichi, Y. Manabe, M. Takagi, M. Aoki, N.L. Fujii, Evidence for acute contraction-induced myokine secretion by C2C12 myotubes, PLoS One 13 (10) (2018), e0206146, https://doi.org/10.1371/journal.pone.0206146.

[18] R. Squecco, H. Kern, D. Biral, K. Rossini, F. Francini, Mechano-sensitivity of normal and long-term denervated soleus muscle of the rat, Neurol. Res. 30 (2008) 155–159, https://doi.org/10.1179/174313208X281028.

[19] B. Coste, J. Mathur, M. Schmidt, T.J. Earley, S. Ranade, M.J. Petrus, A.E. Dubin, A. Patapoutian, Piezo1 and Piezo 2 are essential components of distinct mechanically activated cation channels, Science 330 (2010) 55–60, https://doi.org/10.1126/science.1193270.

[20] R. Syeda, J. Xu, A.E. Dubin, B. Coste, J. Mathur, T. Huynh, J. Matzen, J. Lao, D.C. Tully, I.H. Engels, H.M. Petrassi, A.M. Schumacher, M. Montal, M. Bandell, A. Patapoutian, Chemical activation of the mechanotransduction channel Piezo1, Elife 4 (2015), e07369, https://doi.org/10.7554/eLife.07369.

[21] J.J. Lacroix, W.M. Botello-Smith, Y. Luo, Probing the gating mechanism of the mechanosensitive channel Piezo1 with the small molecule Yoda1, Nat. Commun. 9 (1) (2018) 2029, https://doi.org/10.1038/s41467-018-04405-3.

[22] A. Irintchev, M. Langer, M. Zweyer, R. Theisen, A. Wernig, Functional improvement of damaged adult mouse muscle by implantation of primary myoblasts, J. Physiol. 500 (1997) 775–785, https://doi.org/10.1113/jphysiol.1997.sp022057.

[23] B.K. Pedersen, L. Hoffman-Goetz, Exercise and the immune system: regulation, integration and adaptation, Physiol. Rev. 80 (2000) 1055–1081, https://doi.org/10.1152/physrev.2000.80.3.1055.

[24] M.A. Febbraio, B.K. Pedersen, Muscle-derived interleukin-6: mechanisms for activation and possible biological roles, Faseb. J. 16 (2002) 1335–1347, https://doi.org/10.1096/fj.01-0876rev.

[25] H.G. Knuttgen, Strength training and aerobic exercise: comparison and contrast, J. Strength Condit Res. 21 (2007) 973–978, https://doi.org/10.1519/R-505011.1.

[26] T. Nedachi, H. Fujita, M. Kanzaki, Contractile C2C12 myotube model for studying exercise-inducible responses in skeletal muscle, Am. J. Physiol. Endocrinol. Metab. 295 (2008) E1191–E1204, https://doi.org/10.1152/ajpendo.90280.2008.

[27] H. Pan, X. Xu, X. Hao, Y. Chen, Changes of myogenic reactive oxygen species and interleukin-6 in contracting SkeletalMuscle cells, oxid, Med. Cell. Longev. 145418 (2012), https://doi.org/10.1155/2012/145418.

[28] M. Whitham, M.H. Chan, M. Pal, V.B. Matthews, O. Prelovsek, S. Lunke, A. Eiosta, H. Broenneke, J. Alber, J.C. Brüning, F.T. Wunderlich, G.I. Lancaster, M.A. Febbraio, Contraction-induced interleukin-6 gene transcription in skeletal muscle is regulated by c-Jun terminal kinase/activator protein 1, J. Biol. Chem. 287 (2012) 10771–10779, https://doi.org/10.1074/jbc.M111.310581.

[29] S. Lambernd, A. Taube, A. Schober, B. Platzbecker, S.W. Görgens, R. Schlich, K. Jeruschke, J. Weiss, K. Eckardt, J. Eckel, Contractile activity of human skeletal muscle cells prevents insulin resistance by inhibiting proinflammatory signalling pathways, Diabetologia 55 (2012) 1128–1139, https://doi.org/10.1007/s00125-012-2454-z.

[30] M. Scheler, M. Irmler, S. Lehr, S. Hartwig, H. Staiger, H. Al-Hasani, J. Beckers, M. Hrabé de Angelis, H.U. Häring, C. Weigert, Cytokine response of primary human myotubes in an in vitro exercise model, Am. J. Physiol. Cell Physiol. 305 (2013) C877–C886, https://doi.org/10.1152/ajpcell.00043.2013.

[31] J. Tarum, M. Folkesson, P.J. Atherton, F. Kadi, Electrical pulse stimulation: anin vitroexercise model forthe induction of human skeletal muscle cell hypertrophy, Exp. Physiol. 102 (2017) 1405–1413140, https://doi.org/10.1113/EP086581.32.

[32] C. Henríquez-Olguín, F. Altamirano, D. Valladares, J.R. López, P.D. Allen, E. Jaimovich, Altered ROS production, NF-κB activation and interleukin-6 gene expression induced by electrical stimulation in dystrophic mdx skeletal muscle cells, Biochim. Biophys. Acta 1852 (2015) 1410–1419, https://doi.org/10.1016/j.bbadis.2015.03.012.

[33] N. Juretić, P. García-Huidobro, J.A. Iturrieta, E. Jaimovich, N. Riveros, Depolarization-induced slow Ca2+ transients stimulate transcription of IL-6 gene in skeletal muscle cells, Am. J. Physiol. Cell Physiol. 290 (2006) C1428–C1436, https://doi.org/10.1152/ajpcell.00449.2005.

[34] H.P.M.M. Lauritzen, J. Brandauer, P. Schjerling, H.J. Koh, J.T. Treebak, M.F. Hirshman, H. Galbo, L.J. Goodyear, Contraction and AICAR stimulate IL-6 vesicle depletion from skeletal muscle fibers in vivo, Diabetes 62 (2013) 3081–3092, https://doi.org/10.2337/db12-1261.

[35] X.P. Hojman, C. Brolin, N. Nørgaard-Christensen, C. Dethlefsen, B. Lauenborg, C.K. Olsen, M.M. Åbom, T. Krag, J. Gehl, B.K. Pedersen, IL-6 release from muscles during exercise is stimulated by lactate-dependent protease activity, Am. J. Physiol. Endocrinol. Metab. 316 (2019) E940–E947, https://doi.org/10.1152/ajpendo.00414.2018.

[36] D.E. Ingber, Tensegrity: architectectural basis of cellular mechanotransduction, Annu. Rev. Physiol. 59 (1997) 575–599, https://doi.org/10.1146/annurev.physiol.59.1.575.

[37] Y. Wang, J. Song, X. Liu, J. Liu, Q. Zhang, X. Yan, X. Yuan, D. Ren, Multiple effects of mechanical stretch on myogenic progenitors, Stem Cell. Dev. 29 (2020) 336–352, https://doi.org/10.1089/scd.2019.0286.

[38] A. Franco Jr., J.B. Lansman, Stretch-sensitive channels in developing muscle cells from a mouse cell line, J. Physiol. 427 (1990) 361–380, https://doi.org/10.1113/jphysiol.1990.sp018176.

[39] A. Bosutti, A. Giniatullin, Y. Odnoshivkina, L. Giudice, T. Malm, M. Sciancalepore, R. Giniatullin, P. D'Andrea, P. Lorenzon, A. Bernareggi, Time window" effect of Yoda1-evoked Piezo1 channel activity during mouse skeletal muscle differentiation, Acta Physiol. 233 (2021), e13702, https://doi.org/10.1111/apha.13702.

[40] N.M. Blythe, K. Muraki, M.J. Ludlow, V. Stylianidis, H. T, J. Gilbert, E.L. Evans, K. Cuthbertson, R. Foster, J. Swift, J. Li, M.J. Drinkhill, Mechanically activated Piezo1 channels of cardiac fibroblasts stimulate p38 mitogen-activated protein kinase activity and interleukin-6 secretion, J. Biol. Chem. 294 (2019) 17395–17408, https://doi.org/10.1074/jbc.RA119.009167.

[41] Y. Hirata, Z. Nomura, D. Kato, Y. Tachibana, T. Niikura, K. Uchiyama, T. Hosooka, T. Fukui, K. Oe, R. Kuroda, Y. Hara, T. Adachi, K. Shibasaki, H. Wake, W. Ogawa W, A Piezo1/KLF15/IL-6 axis mediates immobilization-induced muscle atrophy, J. Clin. Invest. 132 (2022), e154611, https://doi.org/10.1172/JCI154611, 2022.

[42] H. Tang, R. Zeng, E. He, I. Zhang, C. Ding, A. Zhang, Piezo-type mechanosensitive ion channel component 1 (Piezo1): a promising therapeutic target and its modulators, J. Med. Chem. 65 (2022) 6441–6453, https://doi.org/10.1021/acs.jmedchem.2c00085.

[43] A. Bernareggi, A. Bosutti, G. Massaria, R. Giniatullin, T. Malm, M. Sciancalepore, P. Lorenzon, The state of the art of Piezo1 channels in skeletal muscle regeneration, Int. J. Mol. Sci. 23 (2022) 6616, https://doi.org/10.3390/ijms23126616.

International Journal of
Molecular Sciences

MDPI

Review

The State of the Art of Piezo1 Channels in Skeletal Muscle Regeneration

Annalisa Bernareggi [1,*], Alessandra Bosutti [1], Gabriele Massaria [1], Rashid Giniatullin [2], Tarja Malm [2], Marina Sciancalepore [1] and Paola Lorenzon [1]

[1] Department of Life Sciences, University of Trieste, 34127 Trieste, Italy; alessandra.bosutti@units.it (A.B.); gabriele.massaria@phd.units.it (G.M.); msciancalepore@units.it (M.S.); plorenzon@units.it (P.L.)
[2] A.I. Virtanen Institute for Molecular Sciences, University of Eastern Finland, 70211 Kuopio, Finland; rashid.giniatullin@uef.fi (R.G.); tarja.malm@uef.fi (T.M.)
* Correspondence: abernareggi@units.it

Abstract: Piezo1 channels are highly mechanically-activated cation channels that can sense and transduce the mechanical stimuli into physiological signals in different tissues including skeletal muscle. In this focused review, we summarize the emerging evidence of Piezo1 channel-mediated effects in the physiology of skeletal muscle, with a particular focus on the role of Piezo1 in controlling myogenic precursor activity and skeletal muscle regeneration and vascularization. The disclosed effects reported by pharmacological activation of Piezo1 channels with the selective agonist Yoda1 indicate a potential impact of Piezo1 channel activity in skeletal muscle regeneration, which is disrupted in various muscular pathological states. All findings reported so far agree with the idea that Piezo1 channels represent a novel, powerful molecular target to develop new therapeutic strategies for preventing or ameliorating skeletal muscle disorders characterized by an impairment of tissue regenerative potential.

Keywords: Piezo1; myogenesis; Yoda1; myoblasts; satellite cells; myotubes; sarcopenia; muscle atrophy

Citation: Bernareggi, A.; Bosutti, A.; Massaria, G.; Giniatullin, R.; Malm, T.; Sciancalepore, M.; Lorenzon, P. The State of the Art of Piezo1 Channels in Skeletal Muscle Regeneration. *Int. J. Mol. Sci.* **2022**, *23*, 6616. https://doi.org/10.3390/ijms23126616

Academic Editor: Manuela Malatesta

Received: 23 May 2022
Accepted: 11 June 2022
Published: 14 June 2022

1. Introduction

Mechanotransduction is defined by the ability of a cell to sense mechanical inputs and convert them into signalling events that elicit biological responses. The main molecular translators of this process are the mechanically-activated (MA) ion channels expressed in almost all tissues of the body [1].

The MA channels include a large family of ion channels able to respond to stretch, swelling, flow, and poking, for the proper growth, development, and health of cells and tissues. They are comprised of MA channels of large and of small conductance, the two-pore potassium channel (K2P) family that include TREK-1, TREK-2 and TRAAK, the ion channels OSCA/TMEM63, the Transient Receptor Potential (TRP) channels, and the Piezo1 and Piezo2 channels [1].

Skeletal muscle is a tissue heavily affected by mechanical strain that contributes to homeostasis. This suggests that the functional role of MA channels may be especially predominant in muscle compared to other non-contractile cell-types. Indeed, one of the first records of MA channel activity dates back to 1984 in chick skeletal muscle fibers [2]. Later, in 1990, studies conducted in dystrophic muscle cells underlined the first link between MA channel dysfunction and skeletal muscle pathology [3]. Since then, due to the better understanding of the variety of triggering stimuli, including, for instance, the stiffness of the substrate or pressure from expanding of surrounding tissues, MA channels have been reported in almost all types of cells, even extending to bacteria, fungi and plants, where they control physiological and pathological cellular responses [1]. Currently, it is also known that the functional role of MA channel activity is directed at detecting an excess

of stress on the sarcolemma and to act as a "safety alarm" for the reinforcement of the cytoskeleton and for preventing cell lysis [4].

One of the most interesting aspects of the role of mechanical forces in skeletal muscle physiology is the impact on regeneration, which is a critical factor for maintaining proper motor function [5]. Skeletal muscle regeneration requires an adult *myogenesis*, which is controlled by the myogenic precursors derived from a cell population named muscle satellite cells (MuSCs). These cells are critically important for regeneration, and are located between the basal lamina and the sarcolemma of adult skeletal muscle fibers [6]. They are important not only for skeletal muscle growth after birth, but also for mediating regeneration after injury. When activated, MuSCs proliferate into myoblasts able to fuse with each other into multinucleated myotubes or to damaged fibers, in order to reconstitute fiber integrity and function. Therefore, MuSCs define the regenerative potential of skeletal muscle under healthy conditions. Unfortunately, the regenerative capacity of skeletal muscle tends to decline during aging [7,8] and in pathological conditions manifests as muscular dystrophies [9,10].

MuSCs are directly and continually exposed to mechanical signals resulting from the contractile activity of the skeletal muscle fibers. Indeed, mechanical stretch represents one of the critical stimuli for the activation of MuSCs. At the molecular level, MuSC stretching is coupled to an MA channel-mediated Ca^{2+} influx that most likely controls the functional state of these cells and promotes the release of many local factors, including myokines such as hepatocyte growth factor (HGF) and the gaseous transmitter nitric oxide (NO) [11,12], which regulates the vascular functions in the muscle. Most of the locally-released factors control activation, proliferation and differentiation of MuSCs in an autocrine/paracrine manner [13]. Importantly, the reduction in MA channel activity leads to an in vitro decline in the proliferation of MuSCs [12], which is in line with the reduction of MuSCs observed in intact fibers in response to mechanical unloading [14,15]. Moreover, the activation of MA channels has been reported to contribute to anabolic signalling during acute reloading following disuse atrophy [16], suggesting that MuSCs are key players to counteract skeletal muscle atrophy during aging and in conditions of immobilization and microgravity. The pattern and the intensity of the mechanical load differently affects the MuSC cell behavior: low and tonic stimulation prevents MuSC activation, whereas stronger stimulation activates these cells, leading to a hypertrophic phenotype of the skeletal muscle tissue [8]. The signalling cascades in the MuSCs, including IGF1/IL6/JAK/STAT3, that are activated during exercise, could be mediated by IGF1 and IL6 released from the myogenic and neighbouring cells [8]. Certainly, muscle tissue is highly vascularized and the MuSCs are in close proximity with endothelial cells, suggesting a potential interplay between the two cell-types [17].

Currently, largely due to growing interest in the function of Piezo channels, it is becoming clearer how MA channels sense and transduce mechanosensitive stimuli. However, the contribution of MA channel activity and the related signalling pathways involved in the pathophysiology of MuSCs remain largely unknown. One limitation is related to the controversial nature of the mechanical "transducers" that likely include a heterogeneous population of MA channels with different sensitivities to the type of mechanical stimulations, but also to the kinetics, expression and ion permeability of these molecular transducers. In addition, the identification of the specific role of each type of MA channel is strongly limited by the poor selectivity of the physical and chemical agonists/antagonists available to discriminate the different types of ion channels.

The Piezo channel family discovered by Coste et al. in 2010 [18] consists of the two isoforms, Piezo1 and Piezo2. Piezo1 is mainly present in tissues exposed to fluid pressure and flow such as erythrocytes, vascular endothelial cells, bladder urothelial cells, and chondrocytes. Piezo1 along with Piezo2 is also expressed in sensory neurons from trigeminal [19,20] and dorsal root ganglia (DRG) [18]. Both are permeable to cations, including calcium ions, but the Piezo1-mediated currents inactivate slower than the Piezo2 –mediated currents (18).

Interestingly, the synthetic molecule Yoda1 was found to activate Piezo1 channels without the application of any mechanical force [21]. Yoda1 binds to a narrow hydrophobic pocket of the Piezo1 channel protein and stabilizes the open conformation of the ion channel. In this way, Yoda1 increases the open channel probability and the cation flux across the pore [21,22]. Later, two other agonists, Jedi1 and Jedi2, were discovered [23]. Moreover, Dooku1 was shown to reversibly block Yoda1-evoked activation of Piezo1, leaving unaltered constitutive Piezo1 activity [24].

Given the specific hypersensitivity of the Piezo1 channel to mechanical forces, the availability of the first selective chemical agonist Yoda1 provides an intriguing therapeutic prospective, making this field of research very attractive [25].

Historically, the identification of Piezo1 channels in skeletal muscle cells began with a study performed on the C2C12 myogenic cell line [26]. A few years later, our group reported the functional expression of Piezo1 in primary myogenic precursors of mouse *Flexor Digitorum Brevis* (FDB) muscle fibers [27], and later, our observation was confirmed in the *Tibialis Anterior* (TA), *Extensor Digitorum Longus* and *Soleus* muscle fibers [28–30]. Taken as a whole, these studies suggested thePiezo1 channel as the main potential mechanical transducer in the control of the intracellular signaling required for the correct development, maintenance and regeneration of skeletal muscle tissue [31,32]

Structurally, Piezo1 forms large homotrimers in the cell membrane in which each subunit contains 2500 amino acids and about 24–40 transmembrane helices. The ion channel conducts Na^+, K^+, Mg^{2+} along with a relatively large Ca^{2+} permeability [18] which can play a specific signalling role in muscle precursors. Piezo1 senses a variety of mechanical stimuli, such as shear force, cell stretching, poking and stiffness [18]. These channels also detect the membrane tension derived from the presence of an asymmetric membrane distribution of negatively charged lipids [21] or from the presence of cholesterol [33]. The latter is consistent with a modulatory role of the lipid cell membrane composition (*force-from-lipid*; [34]). Moreover, Piezo1 is modulated by the cytoskeleton, and by cell membrane interactions with the extracellular matrix (*force-from-filament*; [34]).

The aim of this review is to summarize the evidence about the role of the Piezo1 in skeletal muscle tissue, primarily focusing on their role in controlling the regenerative capability of the myogenic precursors and on how the chemical activation of Piezo1 in these cells could bring a novel powerful pharmacological tool to counteract the effect of skeletal muscle aging, disuse and injuries. This idea is complimentary to the original concept by D. Beech and colleagues on the potential development of "exercise" pills acting via Piezo1 in muscle vasculature [25].

2. The Role of Piezo1 during Adult Myogenesis

2.1. Piezo1 in MuSC Activation

The MuSCs are a heterogeneous population of cells coexisting in the same muscle fiber. Each step of the adult myogenesis is characterized by a time-specific expression of the transcription factor Pax7 and *Myogenic Regulatory* Factors (MRFs) such as MyoD, Myf5, MyoG and Mrf4 [8]. The quiescent MuSC pool includes a long-term self-renewing *stem* cell population identified by the expression of $Pax7^+$ but not Myf5 ($Pax7^+/Myf5^-$) and a *committed* short-term self-renewing population identified by the expression of Pax7 and Myf5 ($Pax7^+/Myf5^+$, Figure 1A(a) [8]).

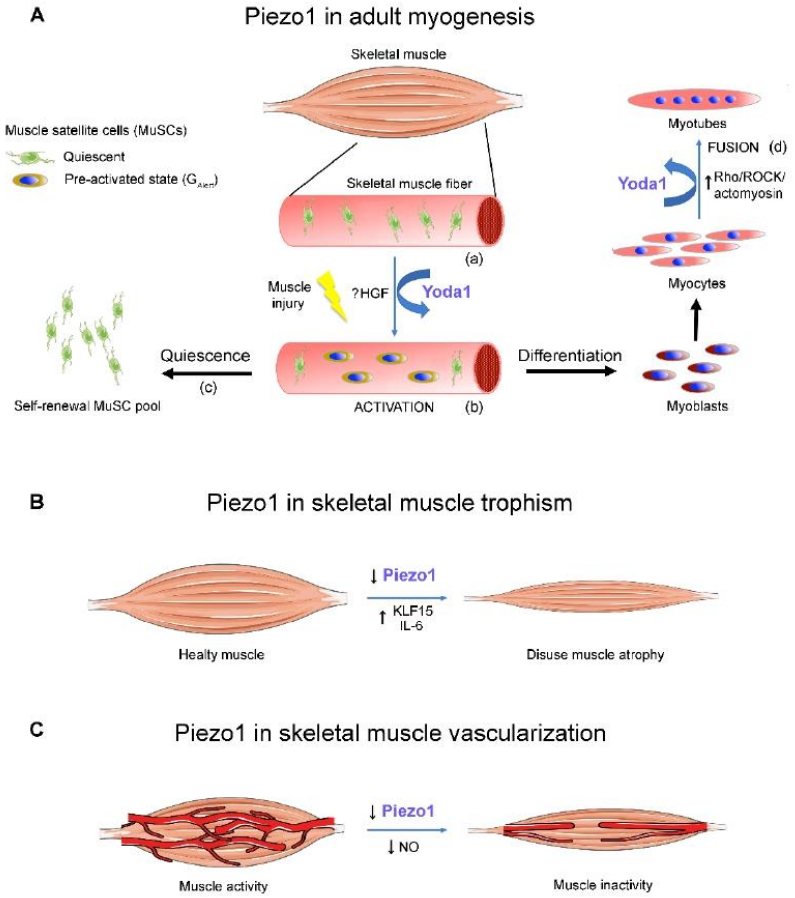

Figure 1. Role of Piezo1 in skeletal muscle. (**A**), Piezo1 controls the adult myogenesis. (**a**) Quiescent satellite cells (MuSCs) are located on intact muscle fibers. (**b**) Under muscle injury or following the Piezo1 activation by Yoda1, the MuSCs shift toward a G_{Alert} phase favouring the cell activation. (**c**) Part of the MuSCs self-renews the quiescent population; (**d**) the rest proliferates as myoblasts, differentiate into myocytes, which then fuse into multinucleated myotubes. The pharmacological activation of Piezo1 by Yoda1 promotes myocyte fusion and myotube differentiation. (**B**), A down regulation of PIEZO1 expression leads to disuse atrophy of the adult muscle. (**C**), The stimulation of the Piezo1 activity of endothelial cells and muscle cells during physical exercise sustain angiogenesis and muscle trophism.

During muscle injury, a subtype of committed MuSCs is recognizable, in a G_{Alert} reversible phase, and defines an 'alerting' pre-activated state of the cells. The G_{Alert} allows a quick activation under conditions of damage and stress, priming the MuSCs for cell cycle entry [35]. The G_{Alert} transition depends on systemic signals, and it is likely mediated by a downstream PI3K-Akt signalling, following the binding of HGF to the cMet receptor expressed by the MuSCs [35]. From a morphological point of view, the G_{Alert} phase is characterized by the lack of cell protrusions, a more circular cell shape and a larger size than its quiescent counterpart ([28], Figure 1A(b)).

According to the degree of muscle injury, the quiescent population $Pax7^{+}/Myf5^{-}$ can divide either symmetrically or asymmetrically. The symmetric division occurs to guarantee the self-renewal of the stem cell pool $Pax7^{+}/Myf5^{-}$; whereas the asymmetric division

generates both the stem ($Pax7^+/Myf5^-$) and committed active ($Pax7^+/Myf5^+$) MuSCs. The correct balance between the two MuSC division modalities is fundamental to preserving the regenerative potential of the muscle: any imbalance reduces the pool of quiescent cells (Figure 1A(c)) as in age-related sarcopenia, or the pool of committed progenitors as in muscular dystrophies [36].

Once activated, the MuSCs give rise to a committed population of proliferating progenitor cells named *myoblasts* ($Pax7^+/Myf5^+/MyoD^+$), which complete the terminal differentiation programme, becoming *myocytes* ($MyoD^+/MyoG^+$) which are ready to fuse into *myotubes* ($MyoG^+/Mrf4^+$; Figure 1A(d)).

Piezo1 is expressed early in quiescent $Pax7^+$ MuSCs that are still attached to the muscle fibers [26–29]. The pharmacological activation of Piezo1 with Yoda1 does not affect the total number of $Pax7^+$ cells both in in vivo or in in vitro conditions [27–30]. However, a significant reduction in the number of $Pax7^+$ MuSCs has been reported after knocking down PIEZO1 gene-expression, suggesting that Piezo1 is required for preserving the pool of MuSCs [29,30].

Investigations on the role of Piezo1 following MuSC activation were initially being performed both on MuSCs in isolated muscle fibers [27,29,30] and in intact muscle [28]. Interestingly, in intact TA muscle, Ma and colleagues [28] analysed the morphological changes of MuSCs induced by activation of Piezo1 channels by Yoda1. They associated the functional MuSC activity to the number and length of cell protrusions able to sense the microenvironment and identified three different MuSC subtypes; "responsive" (small and rounded, with 0–1 axon-like cytoplasmic extensions, less than 40% of the total MuSCs), "sensory" (large, with cytoplasmic extensions, less than 5%), and "intermediate" (with morphological properties in between the above subtypes, about 50%). Notably, after the in vivo administration of Yoda1, the cell morphology shifted toward the "responsive" phenotype; in the presence of the Piezo1 agonist there was a prevalence of the circular phenotype of MuSCs, similar of the *committed* cells in the G_{Alert} functional phase (Figure 1A(b)). Interestingly, the shift was reported in the absence of any regenerative signal, suggesting that Piezo1 activity favours the regenerative potential of MuSCs. This hypothesis was supported by the experiments in which, after PIEZO1 deletion, a change in cell morphology versus a more quiescent "sensory" phenotype was observed [28].

In another study, Peng and co-workers [29] investigated the role of Piezo1 in isolated TA muscle fibers. They reported an immunofluorescence-detected decline in the PIEZO1 expression in the $Pax7^+/MyoD^+$ MuSC population and that Yoda1 treatment reduced the number of the $Pax7^+/MyoD^+$ without affecting the total number of $Pax7^+$ cells. On the contrary, the lack of PIEZO1 expression caused a reduction of the total number of $Pax7^+$ cells and a relative increase in those expressing $Pax7^+/MyoD^+$, demonstrating a tendency towards a faster cell activation in the absence of Piezo1 activity. These findings indicate that Piezo1 secures a long-term MuSC quiescence pool and suggest that Piezo1 activity is needed to preserve the regenerative capability of the skeletal muscle.

2.2. Piezo1 in Myoblast Fusion

It has been recently shown that the expression of Piezo1 tends to increase during in vitro myogenesis [29]. The presence of Piezo1 in myocytes was first reported by Tsuchiya et al. [26] in the C2C12 cell line and then confirmed by our group and others in myocytes derived from freshly isolated FDB fibers [27]. With this model of primary cells, the pharmacological stimulation of Piezo1 with Yoda1 increased the fusion index, suggesting the ability of Piezo1 to promote myoblast fusion ([27]; Figure 1A(c)). Such a role in cell fusion, which is a critical step for muscle development and regeneration, was further confirmed by the decline in the fusion index observed, both in vivo and in vitro, after silencing of PIEZO1 [29,30].

Our understanding of the entire machinery involved in this process is still largely incomplete, but the role of the mechanical tension is important [37]. During fusion, the cell membrane undergoes several changes that affect the plasmalemma tension, and Piezo1

is activated due to cytoskeletal tethers (*force from filament*) and membrane tension (*force from lipids) [38].*

Moreover, since Piezo1 activity is affected by the lipidic composition of the cell membrane [39], a correct cell surface flip-flop of phosphatidylserine was found to control the myoblast fusion by regulating Piezo1 activity via a *force from lipids* effect [26]. In line with this, the increased exposure of phosphatidylserine induced by TMEM16F scramblase stimulates the fusion of the C2C12 cells [40], whereas the prevalence of phosphatidylserine inner translocation mediated by P4-ATP-ase flippase avoids the excess of syncytia formation [26].

Piezo1 activity controls the Ca^{2+} influx across the cell membrane needed for the cortical actinomyosin assembly via the Rho/ROCK/actomyosin pathway, which is also crucial for myotube formation; the silencing of PIEZO1 leads to an excessive cell fusion and elongation defects [26]. Notably, the pharmacological activation with Yoda1 improves the orientation of the cells in favour of a correct fusion and myotube formation [27,30].

Intriguingly, the type of mechanical stress (acute or persistent), its magnitude, as well as the subcellular localization of applied forces [41] might activate specific intracellular signalling [42] and thus induce different physiological responses. For instance, in cardiomyocytes, Piezo1 activation by mechanical stimuli elicits an intracellular Ca^{2+} increase, promoting a Ca^{2+} influx, or a Ca^{2+} release from intracellular stores controlling ROS production [43]. Interestingly, in skeletal muscle, low levels of intracellular ROS favour myoblast proliferation/differentiation [44], stimulate CREB (cAMP response element-binding protein) mediated gene expression in myotubes as well as the downstream ERK1/2, promoting muscle regeneration [45]. On the other hand, Piezo1 activated by destructive mechanical forces might trigger inflammatory cascades resulting in immune cell infiltration, the activation of pro-inflammatory agents such as IL-6 and large ROS production that contribute to the development of degenerative diseases and pathological conditions [46]. The latter observations indicate that the negative modulation of Piezo1 could reduce the inflammation and represent a potentially helpful therapeutic tool.

In skeletal myotubes, Piezo1 is also important for the maintenance of basal $[Ca^{2+}]_i$, even in the absence of any induced mechanical stimulation. This mechanism appears to be important for the down-regulation of atrophy-related genes [47]. Intriguingly, since before synaptogenesis, spontaneous electrical and mechanical activity detected in differentiating myotubes can regulate the Ca^{2+} homeostasis [48,49], Piezo1 could contribute to the control of the level of $[Ca^{2+}]_i$ to sustain the trophism of the myotubes before the arrival of the nerve [27].

2.3. Piezo1 in Adult Skeletal Muscle Fibers

While the role of the Piezo1 activity during the early steps of myogenesis begins to be unveiled, there are still only a few studies carried out on adult muscle fibers. PIEZO1 expression was first reported using RT-PCR analysis in murine adult muscle fibers [26]. More recently, we reported the existence of Piezo1 clusters in isolated mouse FDB muscle fibers, characterized by a smaller size than in myotubes [27]. After that, Piezo1 was also found in mouse *Gastrocnemius* muscle fibers [47]. Notably, the expression of Piezo1 has been found to decline in disused atrophic muscle (Figure 1B) [47]. In addition, it has also been shown that the decline in the expression and the consequent reduction in Piezo1 activity lead to an up-regulation of atrophy-related genes [47]. The decrease in PIEZO1 expression in response to disuse was also confirmed by the analysis of human muscle biopsies derived from patients who had undergone cast fixation upon bone fracture [47]. All of these findings strongly support the hypothesis that Piezo1 is involved in the control of skeletal muscle trophism (Figure 1B).

In isolated mouse FDB muscle fibers, the chemical activation of Piezo1 with Yoda1 failed to elicit a detectable variation of the $[Ca^{2+}]_i$ [27]. However, the intramuscular injection of Yoda1 increased the $[Ca^{2+}]_i$ in intact mouse TA muscle, and down regulated the expression of the atrophy-related genes Kruppel-like factor 15 (KLF15) and IL-6 [47]. The apparent discrepancy in these findings may be due to the different cell models analysed

and, in particular, to a different sensitivity of Piezo1 to the chemical activation in isolated skeletal muscle fibers, in which the plasmalemma tension forces are likely different than in the intact whole muscle.

3. Possible Role of Piezo1 in the Cooperation between Vascular and Skeletal Muscle Cell Networks

One interesting aspect of Piezo 1 activity in skeletal muscle is related to the cooperation between vascular and skeletal muscle cells. Prolonged periods of muscle inactivity, like bed rest, space flight, neuromuscular diseases or aging, cause arterial structural remodeling and reduced blood flow to the muscle [50] (Figure 1C).

Successful angiogenesis and capillary maintenance critically depend on mechanical signals and endothelial cell shear stress, which can involve Piezo1 activation. Piezo1 expressed in endothelial cells acts as a sensor to control blood flow in skeletal muscles during exercise [51,52]. In saphenous arteries, the activation of endothelial Piezo1 triggers a Ca^{2+} influx likely responsible for NO production, which promotes vasodilatation [52] and therefore supply to muscle (Figure 1C). Interestingly, NO also stimulates the activation of MuSCs promoting muscle regeneration [53]. Moreover, the normal shear between the sarcolemma and basal lamina has been reported to facilitate a pulsatile release of NO from the myofibers and likely from MuSCs [53].

On the other hand, capillary rarefaction and impaired muscle oxygenation contribute to the progressive loss in the ability to exercise and resistance to fatigue [54–56]. MuSCs are localized close to vessels and their number is positively correlated to the fiber capillarization, suggesting a MuSC-vessel cross-talk [17,57]. The basal lamina, the pericytes, and the smooth muscles apparently prevent any direct contact between MuSCs and endothelial cells. However, there is evidence of gaps in the basal lamina, which allows the communication between these two cell types [58]. Moreover, the remodeling of the tissue during muscle regeneration increases the distance between pericytes and capillaries. This likely further favours the interaction between MuSCs and endothelial cells, promoting angiogenesis and myogenesis [59].

Even if premature, we could speculate a simultaneous synergism of Piezo1-mediated NO release from endothelial cells, adult muscle fibers and MuSCs that improves the muscle performance. If this turns out to be true, Piezo1 could control the local NO levels (and maybe other released factors) contributing to the cross-talk between skeletal muscle tissue and vessels. This hypothesis could well explain the positive correlation between myofiber size and its number of capillaries [60,61]

A MuSC-endothelial cell cross-talk is supported, via paracrine mechanisms, by the released factors: MuSCs release VEGFA (vascular endothelial growth factor A), promoting angiogenesis and capillarization of muscle tissue [57] and endothelial cells release IGF-1, HGF and bFGF stimulating the myogenic cell growth [58].

The mutual dependence between capillary bed and MuSCs indicates that the angiogenesis might affect myogenesis and *vice-versa* [59]. Therefore, a functional capillary supply would be not only essential to delivering oxygen and nutrients to muscle tissue and for removal of heat, metabolites, and waste products but also to positively modulate the growth and regenerative capacity of muscles [54]. In line with this, capillary rarefaction in prolonged inactivity has a negative effect on muscle remodeling and repair [57].

4. Translational Perspectives for Developing Piezo1-Based Therapeutic Strategies

4.1. Skeletal Muscle Pathologies and Aging

As discussed in this review, Piezo1 is a mechanical transducer that controls both maintenance and activation of the MuSC pool as well as differentiation of myotubes. From these findings, Piezo1 emerges as a potential new molecular target for developing new treatments of various muscle pathologies associated with impaired adult myogenesis [36].

The pharmacological activation of Piezo1 partially restores the defective morphology of the dystrophic MuSCs [28]. Moreover, the observations that the Yoda1 treatment likely

contributes to the Ca^{2+} influx promoting cell fusion [27,30] and differentiation [27,30] suggest that Piezo1 could also be an important tool for the treatment of cell-cell fusion deficits reported in some genetic myopathies [62].

The regenerative capability of skeletal muscle also decreases during aging [7,8]. Sarcopenia is a common aged-related chronic condition characterized by loss of muscle mass (hypotrophy), strength and/or physical function impairment, leading to an increased risk of disability and to a poor quality of life in the elderly [63]. During aging, the increase of fibroses, as well the stiffness of the extracellular matrix, affect the mechanical sensitivity of MuSCs and cause defects in the expression of myogenic growth factors and protein synthesis of the skeletal muscle fibers [64].

The recent discovery that an impaired Piezo1 activity in MuSCs increases ROS production and accumulation of p53 tumor suppressor protein stimulating a massive induction of cell senescence phenomena [29] strongly suggest the crucial role of Piezo1 in the physiopathology of skeletal muscle aging [65]. The repetitive passive stretching of the sarcopenic muscle fibers recovers the hypotrophy and restores the expression of MRFs in MuSCs [5]. Appropriate physical exercises combined with a pharmacological activation of Piezo1 could represent a promising approach to counteract more efficiently the sarcopenic status and the decline of muscle trophism in the elderly.

4.2. Skeletal Muscle Atrophy

The presence of Piezo1 has been reported in adult skeletal muscle fibers, even though the downstream pathways are unknown, and deserves to be investigated in future studies. Some lessons could be taken from mature cardiomyocytes, where Piezo1 channels are important mechanosensors in mature cardiomyocytes, and they are localized near the T-tubules and intercalated discs. In cardiac cells, the Piezo1 activity does not contribute much to the basal Ca^{2+} level, but upon mechanical or chemical stimulation, it elicits Ca^{2+}-mediated calpain and calcineurin activation, responsible for the cardiac hypertrophy [66].

Calpain and calcineurin are also differently involved in skeletal muscle remodeling in response to exercise and inactivity-induced muscle atrophy [67,68]. In addition, in skeletal muscle fibers after immobilization or denervation, a reduction in the $[Ca^{2+}]_i$ associated with a down regulation of PIEZO1 expression and an up regulation of atrophy-related genes *Klf15* and *Il6* expression has been reported [47] (Figure 1B). The intramuscular administration of Yoda1 suppresses the expression of atrophy-related genes and restores the $[Ca^{2+}]_i$ [47], suggesting that the modulation of Piezo1 activity could be used to prevent skeletal muscle atrophy.

4.3. Skeletal Muscle Adaptation to Microgravity

Microgravity induces substantial cellular adaptations that affect cellular morphology, proliferation and adhesion [69]. Cell mechanical properties, including elasticity, viscoelasticity [70], and cytoskeletal organization (namely mechano-responsive structures) are the most affected cell compartments in real or simulated microgravity [71]. Microgravity disrupts the intracellular tension balance and causes irregular cytoskeleton formation, with substantial implications in the regulation of cell growth, locomotion and survival [72]. For example, extracellular matrix proteins, cytoskeletal components and intermediate filaments are significantly affected in human endothelial cells when cultured in a random positioning machine simulating microgravity conditions [73]. Since the mechanics of the microenvironment can modulate Piezo1 signalling [74], it is likely that similar adaptations can occur at the skeletal muscle level, in its adult cell compartments and/or in stem cell niches. On this basis, microgravity and consequent mechanical unloading could affect MuSC membrane stiffness, leading to perturbations in Piezo1 activation, with a consequent impairment in the myogenesis signalling cascade [75]. This would, at least in part, explain why some markers of myogenesis (MyoG, Mylpf, and Myh3) appear downregulated in mouse skeletal C2C12 myoblasts when cultured in simulated microgravity conditions [76].

The possibility to mechanically or chemically tune the Piezo1 activity could be used to counteract the negative effects of microgravity during prolonged space flights and in the long-lasting stay in extra-terrestrial habitats.

4.4. Dietary Strategies to Control Piezo1 Activity?

Due to the potential implication of Piezo1 in cardiovascular and inflammatory conditions [43,46,77], increasing attention has been directed in the last years to characterize new potential treatments capable of pharmacologically modulating Piezo1 function, or acting on the elastic properties of the plasma membrane, such as its lipid/cholesterol components, which regulate Piezo1 function in a dynamic manner [39]. Some in vitro studies underline statins, methyl-β-cyclodextrin, or dynasore (a GTPase inhibitor) and dietary fatty acid supplementation, in modulating Piezo 1 activation/inhibition by acting on the membrane cholesterol content and fatty acid metabolism [33,34,78,79]. In this context, in an elegant study, Romero and colleagues [34] have demonstrated that the cellular intrinsic lipid profile and changes in fatty acid metabolism are capable of remodeling the cellular response to mechanical stimuli. Fatty acid diet-supplementation can abrogate the phenotype of "gain-of-function Piezo1 mutations", which is linked to stomatocytosis, a human hereditary disease. Interestingly, as shown by these authors, non-saturated fatty acids may have an opposite effect on Piezo1 channels. In particular, the action of docosahexaenoic acid (DHA), contrary to that of eicosapentaenoic acid (EPA), is associated with the reduced inactivation of Piezo1, which might be translated as a promising effect to increase the channel activity in skeletal muscle (Figure 2). Likewise, ceramide, produced by sphingomyelin phosphodiesterase 3 [80] (Figure 2), is a powerful tool to remove inactivation of Piezo1. While the former can be widely used in patients with sarcopenia, the latter requires more exploration to be used as a therapeutic tool.

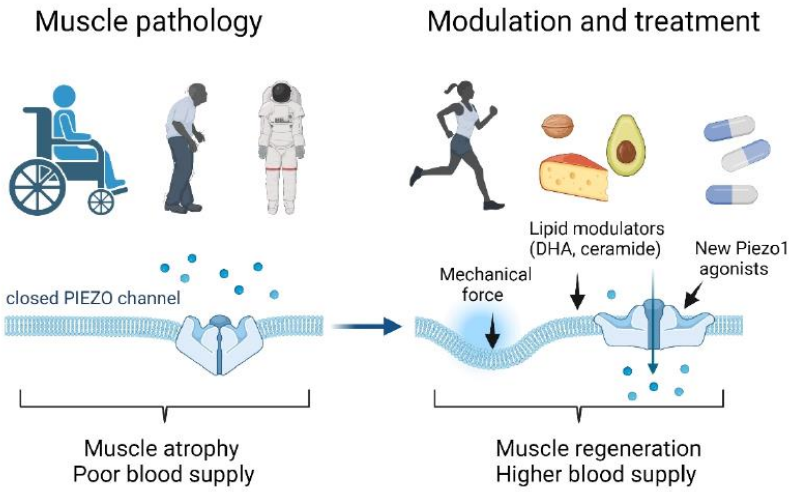

Figure 2. Potential Piezo1-based therapeutic strategies to counteract skeletal muscle impairments. Muscle disuse, aging and unloading might reduce Piezo1 activity, contributing to muscle atrophy and poor blood supply. Potentiation of Piezo 1 activity by physical exercise, diet and chemical/pharmacological activation might enhance the regenerative potential and, possibly, skeletal muscle vascularization and provide a higher blood supply. DHA and ceramide are lipids which are able to enhance the activity of Piezo1 channels, reducing their limiting inactivation state. These indirect and more direct Piezo1-based therapeutic strategies based on novel mechanisms of Piezo1 activation could thus represent promising new countermeasures versus atrophy and diseases related to muscle weaknesses (Figure created with Biorender.com, accessed on 2 May 2022).

5. Conclusions

There is growing evidence that Piezo1 controls trophism and the regenerative capability of skeletal muscle cells by transducing mechanical stimuli. According to this view, Piezo1 can be considered a physiological key player in skeletal muscle remodeling, tissue repair and perhaps in muscle vascularization. Physical exercise is well documented to attenuate some disuse-induced deficiency in skeletal muscle function, and this may be at least partially mediated through Piezo1 activation. Nonetheless, exercise alone does not fully protect the skeletal muscle system from prolonged periods of disuse, and there is an urgent need to develop a means of fully counteracting the effects of disuse. Pharmacological enhancement of Piezo1 activity by combining physical exercise with the diet then emerges as a potentially new powerful strategy for protecting skeletal muscle from the consequences of aging and skeletal muscle pathologies (Figure 2).

Author Contributions: Conceptualization, A.B. (Annalisa Bernareggi), A.B. (Alessandra Bosutti), M.S., P.L. and R.G.; methodology, A.B. (Alessandra Bosutti), A.B. (Annalisa Bernareggi), M.S. and P.L.; writing—original draft preparation, A.B. (Annalisa Bernareggi), A.B. (Alessandra Bosutti), G.M., T.M. and M.S.; writing—review and editing, A.B. (Annalisa Bernareggi), T.M., R.G. and P.L. visualization, G.M. and P.L.; supervision, A.B. (Annalisa Bernareggi); All authors have read and agreed to the published version of the manuscript.

Funding: This research received no external funding.

Institutional Review Board Statement: The study did not require ethical approval.

Informed Consent Statement: Not applicable.

Data Availability Statement: Not applicable (no data reported in this review).

Acknowledgments: We are grateful to Andrew Constanti (UCL, School of Pharmacy, London, UK) for critically reading the manuscript, and Adriana Della Pietra (University of Easter Finland, Kuopio, Finland) for her help in drawing the Figures. We acknowledge the support of the Italian Space Agency (ASI) with the grant "MIAG project ASI n.2021-13-U.0" (grant to Alessandra Bosutti and Paola Lorenzon).

Conflicts of Interest: The authors declare that they have no conflict of interest.

Abbreviations

MuSCs	Muscle Satellite Cells
MA channels	Mechanically-activated ion channels
MyoG	Myogenin
NO	Nitric Oxide
IGF	Insulin Growth Factor
MRF	Myogenic Regulatory factor
TA	Tibialis Anterior
FDB	Flexor Digitorum Brevis

References

1. Kefauver, J.M.; Ward, A.B.; Patapoutian, A. Discoveries in structure and physiology of mechanically activated ion channels. *Nature* **2020**, *587*, 567–576. [CrossRef] [PubMed]
2. Guharay, F.; Sachs, F. Stretch-activated single ion channel currents in tissue-cultured embryonic chick skeletal muscle. *J. Physiol.* **1984**, *352*, 685–701. [CrossRef] [PubMed]
3. Franco, A.; Lansman, J.B., Jr. Calcium entry through stretch-inactivated ion channels in mdx myotubes. *Nature* **1990**, *344*, 670–673. [CrossRef] [PubMed]
4. Huang, H.; Bae, C.; Sachs, F.; Suchyna, T.M. Caveolae regulation of mechanosensitive channel function in myotubes. *PLoS ONE* **2013**, *8*, e72894. [CrossRef] [PubMed]
5. Wang, Y.; Song, J.; Liu, X.; Liu, J.; Zhang, Q.; Yan, X.; Yuan, X.; Ren, D. Multiple Effects of Mechanical Stretch on Myogenic Progenitor Cells. *Stem Cells Dev.* **2020**, *29*, 336–352. [CrossRef]
6. Mauro, A. Satellite cell of skeletal muscle fibers. *J. Biophys. Biochem. Cytol.* **1961**, *9*, 493–495. [CrossRef]

7. Collins, C.A.; Zammit, P.S.; Ruiz, A.P.; Morgan, J.E.; Partridge, T.A. A population of myogenic stem cells that survives skeletal muscle aging. *Stem Cells* **2007**, *25*, 885–894. [CrossRef]
8. Chen, W.; Datzkiw, D.; Rudnicki, M.A. Satellite cells in ageing: Use it or lose it. *Open Biol.* **2020**, *10*, 200048. [CrossRef]
9. Blau, H.M.; Webster, C.; Pavlath, G.K. Defective myoblasts identified in Duchenne muscular dystrophy. *Proc. Natl. Acad. Sci. USA* **1983**, *80*, 4856–4860. [CrossRef]
10. Chang, N.C.; Chevalier, F.P.; Rudnicki, M.A. Satellite Cells in Muscular Dystrophy—Lost in Polarity. *Trends Mol. Med.* **2016**, *22*, 479–496. [CrossRef]
11. Tatsumi, R.; Sheehan, S.M.; Iwasaki, H.; Hattori, A.; Allen, R.E. Mechanical stretch induces activation of skeletal muscle satellite cells in vitro. *Exp. Cell Res.* **2001**, *267*, 107–114. [CrossRef] [PubMed]
12. Hara, M.; Tabata, K.; Suzuki, T.; Do, M.K.; Mizunoya, W.; Nakamura, M.; Nishimura, S.; Tabata, S.; Ikeuchi, Y.; Sunagawa, K.; et al. Calcium influx through a possible coupling of cation channels impacts skeletal muscle satellite cell activation in response to mechanical stretch. *Am. J. Physiol. Cell Physiol.* **2012**, *302*, C1741–C1750. [CrossRef] [PubMed]
13. Yin, H.; Price, F.; Rudnicki, M.A. Satellite cells and the muscle stem cell niche. *Physiol. Rev.* **2013**, *93*, 23–67. [CrossRef] [PubMed]
14. Babcock, L.W.; Knoblauch, M.; Clarke, M.S. The role of myostatin and activin receptor IIB in the regulation of unloading-induced myofiber type-specific skeletal muscle atrophy. *J. Appl. Physiol.* **2015**, *119*, 633–642. [CrossRef]
15. Arentson-Lantz, E.J.; English, K.L.; Paddon-Jones, D.; Fry, C.S. Fourteen days of bed rest induces a decline in satellite cell content and robust atrophy of skeletal muscle fibers in middle-aged adults. *J. Appl. Physiol.* **2016**, *120*, 965–975. [CrossRef]
16. Mirzoev, T.M.; Tyganov, S.A.; Petrova, I.O.; Shenkman, B.S. Acute recovery from disuse atrophy: The role of stretch-activated ion channels in the activation of anabolic signaling in skeletal muscle. *Am. J. Physiol.-Endocrinol. Metab.* **2019**, *316*, E86–E95. [CrossRef]
17. Verma, M.; Asakura, Y.; Murakonda, B.S.R.; Pengo, T.; Latroche, C.; Chazaud, B.; McLoon, L.K.; Asakura, A. Muscle Satellite Cell Cross-Talk with a Vascular Niche Maintains Quiescence via VEGF and Notch Signaling. *Cell Stem Cell* **2018**, *23*, 530–543. [CrossRef]
18. Coste, B.; Mathur, J.; Schmidt, M.; Earley, T.J.; Ranade, S.; Petrus, M.J.; Dubin, A.E.; Patapoutian, A. Piezo1 and Piezo2 are essential components of distinct mechanically activated cation channels. *Science* **2010**, *330*, 55–60. [CrossRef]
19. Mikhailov, N.; Leskinen, J.; Fagerlund, I.; Poguzhelskaya, E.; Giniatullina, R.; Gafurov, O.; Malm, T.; Karjalainen, T.; Gröhn, O.; Giniatullin, R. Mechanosensitive meningeal nociception via Piezo channels: Implications for pulsatile pain in migraine? *Neuropharmacology* **2019**, *149*, 113–123. [CrossRef]
20. Mikhailov, N.; Plotnikova, L.; Singh, P.; Giniatullin, R.; Hämäläinen, R.H. Functional Characterization of Mechanosensitive Piezo1 Channels in Trigeminal and Somatic Nerves in a Neuron-on-Chip Model. *Int. J. Mol. Sci.* **2022**, *23*, 1370. [CrossRef]
21. Syeda, R.; Xu, J.; Dubin, A.E.; Coste, B.; Mathur, J.; Huynh, T.; Matzen, J.; Lao, J.; Tully, D.C.; Engels, I.H.; et al. Chemical activation of the mechanotransduction channel Piezo1. *Elife* **2015**, *22*, e07369. [CrossRef] [PubMed]
22. Lacroix, J.J.; Botello-Smith, W.M.; Luo, Y. Probing the gating mechanism of the mechanosensitive channel Piezo1 with the small molecule Yoda. *Nat. Commun.* **2018**, *9*, 2029. [CrossRef] [PubMed]
23. Wang, Y.; Chi, S.; Guo, H.; Li, G.; Wang, L.; Zhao, Q.; Rao, Y.; Zu, L.; He, W.; Xiao, B. A lever-like transduction pathway for long-distance chemical- and mechano-gating of the mechanosensitive Piezo1 channel. *Nat. Commun.* **2018**, *9*, 1300. [CrossRef] [PubMed]
24. Evans, E.L.; Cuthbertson, K.; Endesh, N.; Rode, B.; Blythe, N.M.; Hyman, A.J.; Hall, S.J.; Gaunt, H.J.; Ludlow, M.J.; Foster, R.; et al. Yoda1 analogue (Dooku1) which antagonizes Yoda1-evoked activation of Piezo1 and aortic relaxation. *Br. J. Pharmacol.* **2018**, *175*, 1744–1759. [CrossRef] [PubMed]
25. Beech, D.J. Endothelial Piezo1 channels as sensors of exercise. *J. Physiol.* **2018**, *596*, 979–984. [CrossRef] [PubMed]
26. Tsuchiya, M.; Hara, Y.; Okuda, M.; Itoh, K.; Nishioka, R.; Shiomi, A.; Nagao, K.; Mori, M.; Mori, Y.; Ikenouchi, J.; et al. Cell surface flip-flop of phosphatidylserine is critical for PIEZO1-mediated myotube formation. *Nat. Commun.* **2018**, *9*, 2049. [CrossRef]
27. Bosutti, A.; Giniatullin, A.; Odnoshivkina, Y.; Giudice, L.; Malm, T.; Sciancalepore, M.; Giniatullin, R.; D'Andrea, P.; Lorenzon, P.; Bernareggi, A. "Time window" effect of Yoda1-evoked Piezo1 channel activity during mouse skeletal muscle differentiation. *Acta Physiol.* **2021**, *233*, e13702. [CrossRef]
28. Ma, N.; Chen, D.; Lee, J.H.; Kuri, P.; Hernandez, E.B.; Kocan, J.; Mahmood, H.; Tichy, E.D.; Rompolas, P.; Mourkioti, F. Piezo1 regulates the regenerative capacity of skeletal muscles via orchestration of stem cell morphological states. *Sci. Adv.* **2022**, *8*, eabn0485. [CrossRef]
29. Peng, Y.; Du, J.; Günther, S.; Guo, X.; Wang, S.; Schneider, A.; Zhu, L.; Braun, T. Mechano-signaling via Piezo1 prevents activation and p53-mediated senescence of muscle stem cells. *Redox Biol.* **2022**, *52*, 102309. [CrossRef]
30. Ortuste Quiroga, H.P.; Ganassi, M.; Yokoyama, S.; Nakamura, K.; Yamashita, T.; Raimbach, D.; Hagiwara, A.; Harrington, O.; Breach-Teji, J.; Asakura, A.; et al. Fine-Tuning of Piezo1 Expression and Activity Ensures Efficient Myoblast Fusion during Skeletal Myogenesis. *Cells* **2022**, *11*, 393. [CrossRef]
31. Wang, M.J.; Zhu, Y.C.; Shi, J. A crucial physiological role of Piezo1 channel in differentiation rather than proliferation during myogenesis. *Acta Physiol.* **2021**, *233*, 4. [CrossRef] [PubMed]
32. Jagasia, R.; Wagner, K.R. Piezo1: Opening the way to preventing muscle atrophy. *J. Clin. Investig.* **2022**, *132*, e159668. [CrossRef] [PubMed]

33. Ridone, P.; Pandzic, E.; Vassalli, M.; Cox, C.D.; Macmillan, A.; Gottlieb, P.A.; Martinac, B. Disruption of membrane cholesterol organization impairs the activity of PIEZO1 channel clusters. *J. Gen. Physiol.* **2020**, *152*, e201912515. [CrossRef] [PubMed]
34. Romero, L.O.; Massey, A.E.; Mata-Daboin, A.D.; Sierra-Valdez, F.J.; Chauhan, S.C.; Cordero-Morales, J.F.; Vásquez, V. Dietary fatty acids fine-tune Piezo1 mechanical response. *Nat. Commun.* **2019**, *10*, 1200. [CrossRef] [PubMed]
35. Rodgers, J.T.; King, K.Y.; Brett, J.O.; Cromie, M.J.; Charville, G.W.; Maguire, K.K.; Brunson, C.; Mastey, N.; Liu, L.; Tsai, C.R.; et al. mTORC1 controls the adaptive transition of quiescent stem cells from G0 to G(Alert). *Nature* **2014**, *510*, 393–396. [CrossRef]
36. Feige, P.; Brun, C.E.; Ritso, M.; Rudnicki, M.A. Orienting Muscle Stem Cells for Regeneration in Homeostasis, Aging, and Disease. *Cell Stem Cell* **2018**, *23*, 653–664. [CrossRef]
37. Kim, J.H.; Jin, P.; Duan, R.; Chen, E.H. Mechanisms of myoblast fusion during muscle development. *Curr. Opin. Genet. Dev.* **2015**, *32*, 162–170. [CrossRef]
38. Guo, Y.R.; MacKinnon, R. Structure-based membrane dome mechanism for Piezo mechanosensitivity. *Elife* **2017**, *6*, e33660. [CrossRef]
39. Yang, X.; Lin, C.; Chen, X.; Li, S.; Li, X.; Xiao, B. Structure deformation and curvature sensing of PIEZO1 in lipid membranes. *Nature* **2022**, *604*, 377–383. [CrossRef]
40. Zhao, P.; Torcaso, A.; Mariano, A.; Xu, L.; Mohsin, S.; Zhao, L.; Han, R. Anoctamin 6 regulates C2C12 myoblast proliferation. *PLoS ONE* **2014**, *9*, e92749. [CrossRef]
41. Gudipaty, S.A.; Lindblom, J.; Loftus, P.D.; Redd, M.J.; Edes, K.; Davey, C.F.; Krishnegowda, V.; Rosenblatt, J. Mechanical stretch triggers rapid epithelial cell division through Piezo1. *Nature* **2017**, *543*, 118–121. [CrossRef] [PubMed]
42. Ingber, D.E. Tensegrity: The architectural basis of cellular mechanotransduction. *Annu. Rev. Physiol.* **1997**, *59*, 575–599. [CrossRef] [PubMed]
43. Jiang, F.; Yin, K.; Wu, K.; Zhang, M.; Wang, S.; Cheng, H.; Zhou, Z.; Xiao, B. The mechanosensitive Piezo1 channel mediates heart mechano-chemo transduction. *Nat. Commun.* **2021**, *12*, 869. [CrossRef] [PubMed]
44. Sciancalepore, M.; Luin, E.; Parato, G.; Ren, E.; Giniatullin, R.; Fabbretti, E.; Lorenzon, P. Reactive oxygen species contribute to the promotion of the ATP-mediated proliferation of mouse skeletal myoblasts. *Free Radic. Biol. Med.* **2012**, *53*, 1392–1398. [CrossRef] [PubMed]
45. Espinosa, A.; Leiva, A.; Pena, M.; Muller, M.; Debandi, A.; Hidalgo, C. Myotube depolarization generates reactive oxygen species through NAD(P)H oxidase; ROS-elicited Ca2+ stimulates ERK, CREB, early genes. *J. Cell. Physiol.* **2006**, *209*, 379–388. [CrossRef]
46. Liu, H.; Hu, J.; Zheng, Q.; Feng, X.; Zhan, F.; Wang, X.; Xu, G.; Hua, F. Piezo1 Channels as Force Sensors in Mechanical Force-Related Chronic Inflammation. *Front. Immunol.* **2022**, *13*, 816149. [CrossRef]
47. Hirata, Y.; Nomura, K.; Kato, D.; Tachibana, Y.; Niikura, T.; Uchiyama, K.; Hosooka, T.; Fukui, T.; Oe, K.; Kuroda, R.; et al. A Piezo1/KLF15/IL-6 axis mediates immobilization-induced muscle atrophy. *J. Clin. Investig.* **2022**, *132*, 1–13. [CrossRef]
48. Bandi, E.; Bernareggi, A.; Grandolfo, M.; Mozzetta, C.; Augusti-Tocco, G.; Ruzzier, F.; Lorenzon, P. Autocrine activation of nicotinic acetylcholine receptors contributes to Ca2+ spikes in mouse myotubes during myogenesis. *J. Physiol.* **2005**, *568*, 171–180. [CrossRef]
49. Sciancalepore, M.; Afzalov, R.; Buzzin, V.; Jurdana, M.; Lorenzon, P.; Ruzzier, F. Intrinsic ionic conductances mediate the spontaneous electrical activity of cultured mouse myotubes. *Biochim. Biophys. Acta-Biomembr.* **2005**, *1720*, 117–124. [CrossRef]
50. Thijssen, D.H.; Green, D.J.; Hopman, M.T. Blood vessel remodeling and physical inactivity in humans. *J. Appl. Physiol.* **2011**, *111*, 1836–1845. [CrossRef]
51. Rode, B.; Shi, J.; Endesh, N.; Drinkhill, M.J.; Webster, P.J.; Lotteau, S.J.; Bailey, M.A.; Yuldasheva, N.Y.; Ludlow, M.J.; Cubbon, R.M.; et al. Piezo1 channels sense whole body physical activity to reset cardiovascular homeostasis and enhance performance. *Nat. Commun.* **2017**, *8*, 350. [CrossRef] [PubMed]
52. Bartoli, F.; Debant, M.; Chuntharpursat-Bon, E.; Evans, E.L.; Musialowski, K.E.; Parsonage, G.; Morley, L.C.; Futers, T.S.; Sukumar, P.; Bowen, T.S.; et al. Endothelial Piezo1 sustains muscle capillary density and contributes to physical activity. *J. Clin. Investig.* **2022**, *132*, e141775. [CrossRef] [PubMed]
53. Anderson, J.E. A role for nitric oxide in muscle repair: Nitric oxide-mediated activation of muscle satellite cells. *Mol. Biol. Cell* **2000**, *11*, 1859–1874. [CrossRef] [PubMed]
54. Bosutti, A.; Salanova, M.; Blottner, D.; Buehlmeier, J.; Mulder, E.; Rittweger, J.; Yap, M.H.; Ganse, B.; Degens, H. Whey protein with potassium bicarbonate supplement attenuates the reduction in muscle oxidative capacity during 19 days of bed rest. *J. Appl. Physiol.* **2016**, *121*, 838–848. [CrossRef]
55. Blottner, D.; Hastermann, M.; Weber, R.; Lenz, R.; Gambara, G.; Limper, U.; Rittweger, J.; Bosutti, A.; Degens, H.; Salanova, M. Reactive Jumps Preserve Skeletal Muscle Structure, Phenotype, and Myofiber Oxidative Capacity in Bed Rest. *Front. Physiol.* **2020**, *10*, 1527. [CrossRef] [PubMed]
56. Tickle, P.G.P.; Hendrickse, W.; Degens, H.; Egginton, S. Impaired skeletal muscle performance as a consequence of random functional capillary rarefaction can be restored with overload-dependent angiogenesis. *J. Physiol.* **2020**, *598*, 1187–1203. [CrossRef]
57. Collins, B.C.; Kardon, G. Won't You Be My Neighbor? Muscle Stem Cells Recruit Endothelial Cells to Their Niche. *Cell Stem Cell* **2018**, *23*, 455–456. [CrossRef]
58. Latroche, C.; Gitiaux, C.; Chrétien, F.; Desguerre, I.; Mounie, R.; Chazaud, B. Skeletal muscle microvasculature: A highly dynamic lifeline. *Physiology* **2015**, *30*, 417–427. [CrossRef]

59. Christov, C.; Chrétien, F.; Abou-Khalil, R.; Bassez, G.; Vallet, G.; Authier, F.J.; Bassaglia, Y.; Shinin, V.; Tajbakhsh, S.; Chazaud, B.; et al. Muscle satellite cells and endothelial cells: Close neighbors and privileged partners. *Mol. Biol. Cell* **2007**, *18*, 1397–1409. [CrossRef]
60. Wüst, R.C.I.; Morse, C.I.; Haan, A.; Rittweger, J.; Jones, D.A.; Degens, H. Skeletal muscle properties and fatigue resistance in relation to smoking history. *Eur. J. Appl. Physiol.* **2008**, *104*, 103–110. [CrossRef]
61. Bosutti, A.; Egginton, S.; Barnouin, Y.; Ganse, B.; Rittweger, J.R.; Degens, H. Local capillary supply in muscle is not determined by local xidative capacity. *J. Exp. Biol.* **2015**, *218*, 3377–3380. [CrossRef] [PubMed]
62. Di Gioia, S.A.; Connors, S.; Matsunami, N.; Cannavino, J.; Rose, M.F.; Gilette, N.M.; Artoni, P.; de Macena Sobreira, N.L.; Chan, W.M.; Webb, B.D.; et al. A defect in myoblast fusion underlies Carey-Fineman-Ziter syndrome. *Nat. Commun.* **2017**, *8*, 16077. [CrossRef] [PubMed]
63. Cruz-Jentoft, A.J.; Sayer, A.A. Sarcopenia. *Lancet* **2019**, *393*, 2636–2646. [CrossRef]
64. Lacraz, G.; Rouleau, A.J.; Couture, V.; Söllrald, T.; Drouin, G.; Veillette, N.; Grandbois, M.; Grenier, G. Increased Stiffness in Aged Skeletal Muscle Impairs Muscle Progenitor Cell Proliferative Activity. *PLoS ONE* **2015**, *10*, e0136217. [CrossRef] [PubMed]
65. Boers, H.E.; Haroon, M.; Le Grand, F.; Bakker, A.D.; Klein-Nulend, J.; Jaspers, R.T. Mechanosensitivity of aged muscle stem cells. *J. Orthop. Res.* **2018**, *36*, 632–641. [CrossRef] [PubMed]
66. Zhang, Y.; Su, S.A.; Li, W.; Ma, Y.; Shen, J.; Wang, Y.; Shen, Y.; Chen, J.; Ji, Y.; Xie, Y.; et al. Piezo1-Mediated Mechanotransduction Promotes Cardiac Hypertrophy by Impairing Calcium Homeostasis to Activate Calpain/Calcineurin Signaling. *Hypertension* **2021**, *78*, 647–660. [CrossRef]
67. Hyatt, H.W.; Powers, S.K. The Role of Calpains in Skeletal Muscle Remodeling with Exercise and Inactivity-induced Atrophy. *Int. J. Sports Med.* **2020**, *41*, 994–1008. [CrossRef]
68. Sakuma, K.; Yamaguchi, A. The functional role of calcineurin in hypertrophy, regeneration, and disorders of skeletal muscle. *J. Biomed. Biotechnol.* **2010**, *2010*, 721219. [CrossRef]
69. Bradbury, P.; Wu, H.; Choi, J.U.; Rowan, A.E.; Zhang, H.; Poole, K.; Lauko, J.; Chou, J. Modeling the Impact of Microgravity at the Cellular Level: Implications for Human Disease. *Front. Cell. Dev. Biol.* **2020**, *8*, 96. [CrossRef]
70. Janmaleki, M.; Pachenari, M.; Seyedpour, S.M.; Shahghadami, R.; Sanati-Nezhad, A. Impact of Simulated Microgravity on Cytoskeleton and Viscoelastic Properties of Endothelial Cell. *Sci. Rep.* **2016**, *6*, 32418. [CrossRef]
71. Basirun, C.; Ferlazzo, M.L.; Howell, N.R.; Liu, G.J.; Middleton, R.J.; Martinac, B.; Narayanan, S.A.; Poole, K.; Gentile, C.; Chou, J. Microgravity × Radiation: A Space Mechanobiology Approach Toward Cardiovascular Function and Disease. *Front. Cell Dev. Biol.* **2021**, *9*, 750775. [CrossRef] [PubMed]
72. Topal, U.; Zamur, C. Microgravity, Stem Cells, and Cancer: A New Hope for Cancer Treatment. *Stem Cells Int.* **2021**, *2021*, 5566872. [CrossRef] [PubMed]
73. Infanger, M.; Kossmehl, P.; Shakibaei, M.; Baatout, S.; Witzing, A.; Grosse, J.; Bauer, J.; Cogoli, A.; Faramarzi, S.; Derradji, H.; et al. Induction of three-dimensional assembly and increase in apoptosis of human endothelial cells by simulated microgravity: Impact of vascular endothelial growth factor. *Apoptosis* **2006**, *11*, 749–764. [CrossRef] [PubMed]
74. Bavi, N.; Richardson, J.; Heu, C.; Martinac, B.; Poole, K. PIEZO1-Mediated Currents Are Modulated by Substrate Mechanics. *ACS Nano* **2019**, *13*, 13545–13559. [CrossRef] [PubMed]
75. ElGindi, M.; Sapudom, J.; Ibrahim, I.H.; Al-Sayegh, M.; Chen, W.; Garcia-Sabaté, A.; Teo, J.C.M. May the Force Be with You (Or Not): The Immune System under Microgravity. *Cells* **2021**, *10*, 1941. [CrossRef] [PubMed]
76. Cazzaniga, A.; Ille, F.; Wuest, S.; Haack, C.; Koller, A.; Giger-Lange, C.; Zocchi, M.; Egli, M.; Castiglioni, S.; Maier, J.A. Scalable Microgravity Simulator Used for Long-Term Musculoskeletal Cells and Tissue Engineering. *Int. J. Mol. Sci.* **2020**, *21*, 8908. [CrossRef] [PubMed]
77. Davies, J.E.; Lopresto, D.; Apta, B.H.R.; Lin, Z.; Ma, W.; Harper, M.T. Using Yoda-1 to mimic laminar flow in vitro: A tool to simplify drug testing. *Biochem. Pharmacol.* **2019**, *168*, 473–480. [CrossRef]
78. Caputo, A.; Caci, E.; Ferrera, L.; Pedemonte, N.; Barsanti, C.; Sondo, E.; Pfeffer, U.; Ravazzolo, R.; Zegarra-Moran, O.; Galietta, L.J. TMEM16A, a membrane protein associated with calcium-dependent chloride channel activity. *Science* **2008**, *322*, 590–594. [CrossRef]
79. Llanos, P.; Contreras-Ferrat, A.; Georgiev, T.; Osorio-Fuentealba, C.; Espinosa, A.; Hidalgo, J.; Hidalgo, C.; Jaimovich, E. The cholesterol-lowering agent methyl-β-cyclodextrin promotes glucose uptake via GLUT4 in adult muscle fibers and reduces insulin resistance in obese mice. *Am. J. Physiol. Endocrinol. Metab.* **2015**, *308*, E294–E305. [CrossRef]
80. Shi, J.; Hyman, A.J.; De Vecchis, D.; Chong, J.; Lichtenstein, L.; Futers, T.S.; Rouahi, M.; Salvayre, A.N.; Auge, N.; Kalli, A.C.; et al. Sphingomyelinase Disables Inactivation in Endogenous PIEZO1 Channels. *Cell Rep.* **2020**, *33*, 108225. [CrossRef]

4. DISCUSSION

There is a growing need to understand skeletal muscle cell biology in order to counteract damages caused by congenital defects, neuromuscular disorders and age/injury-atrophy related phenotypes. Skeletal muscle shows a potential intrinsic plasticity in response to both intracellular and extracellular stimuli and the knowledge of the involved molecular mechanisms is potentially useful and required to develop new clinical treatments to counteract skeletal muscle impairments. Because innervation and the nerve-driven muscle activity are fundamental for structural support and functional integrity of the skeletal muscle, the skeletal muscle trophism requires stable and functional nerve-muscle interactions via NMJ. In the case of impaired nerve-muscle communication, EPS is used as clinical treatment to mimic the nerve activity and to ameliorate abnormal or damaged muscle tissue conditions. Indeed, EPS prevents the denervation age/disuse related effects, representing an efficient tool to simulate the electro-mechanical muscle behavior, contributing to the maintenance of structure and functions of the skeletal muscle.

Ca^{2+} release from intracellular stores controls an impressive number of both normal and pathological skeletal muscle intracellular signaling: it is involved not only in the EC coupling machinery during contraction, but also in the so called ET coupling mechanisms, by which the IP_3Rs activation generates long-lasting $[Ca^{2+}]_i$ transients. IP_3R1, which is the most abundant and best studied among the three isoforms of IP_3Rs, is highly expressed in skeletal muscle postsynaptic area near the nAChRs and surrounding skeletal muscle fiber nuclei. The nerve activity-mediated IP_3R-induced Ca^{2+} release beneath the endplate suggests a role for the IP_3-sensitive Ca^{2+} pool not only in gene expression regulation, but also in the mechanism stabilizing the NMJ apparatus.
By using FDB denervated cultures as a cell model to reproduce *in vitro* the denervation effects at the endplate level[139], we observed a direct proportionality between the subsynaptic IP_3R1-stained volume and the endplate size. Moreover, we demonstrated a significant reduction of the IP_3R1-stained volume associated with the endplate fragmentation after *in vitro* denervation. Interestingly, the effect of denervation on IP_3R1s resulted even stronger than the effects on the nAChRs.

Motoneurons control the stability and the number of junctional nAChRs through evoked muscle activity and trophic factors[36–38,119,140]. In our hands, during *in vitro* denervation, the levels of subsynaptic IP_3R1 volumes did not significantly change in the presence of agrin but a positive electrical activity-dependent regulation of the endplate IP_3R1 distribution was observed. Thus, our results indicate a prevalence of the electrical muscle activity in the control of the subsynaptic IP_3R1 expression level. Several studies reported that EPS is able to reversibly increase the stability of AChRs at surgically denervated synapses[78,112,141–144] suggesting that the muscle activity is able to prevent the denervation-induced phenotype and endplate instability.

The positive electrical activity-dependent regulation of the IP_3R1 is an intriguing hypotheses which merits further investigations. If this hypothesis was confirmed, EPS protocols could be optimized to promote IP_3R activation[145] in order to specifically trigger the Ca^{2+}-dependent signaling pathways responsible for NMJ stability. Nerve-muscle co-cultures could provide a useful *in vitro* model to optimize the EPS protocols signaling pathways activated by electrical stimulations.

In skeletal muscle cells, Homer proteins colocalize with IP_3Rs and not with RyRs[63], therefore IP_3R-Homer interaction was suggested to be responsible for generating regulated IP_3-sensitive Ca^{2+} signals. Interestingly, Homer 2 isoform expression and localization at NMJ is nerve and muscle activity dependent. Homer 2 is involved in muscle differentiation, trophism, and plasticity[73,76,121,122,146,147] regulating key transcriptional programs, presumed to be altered in atrophic conditions. Genes involved in controlling ubiquitination and ensuing proteolysis, such as *MuRF1* and *Atrogin-1*, appeared upregulated in Homer $2^{-/-}$ rat SOL, as occurs in conditions of atrophy, suggesting a role for Homer 2 as co-regulator of the skeletal muscle normo-trophic *status.*

According to previous results[50,76], we observed smaller fibers and an apparent thickening of the extracellular matrix in Homer $2^{-/-}$ mice SOL muscles; hypotrophy instead of atrophy characterized Homer $2^{-/-}$ mice, suggesting that in innervated animals, Homer 2 works synergistically with additional independent factors in the maintenance of physiological SOL muscle structure.

Even if downstream effects in the nAChR signaling pathway cannot be fully excluded, we also observed that nAChRs isoform, localization and activity were not affected by the

absence of the Homer 2 protein. A pretzel-like morphology of endplates was appreciable in Homer $2^{-/-}$ as well as in WT FDB skeletal muscle fibers. However, in Homer $2^{-/-}$ FDB skeletal muscle fibers, the NMJ resulted reduced in size. Thus, further experiments are required to better characterize the function of Homer 2 in the NMJ stability and in controlling skeletal muscle trophism via possible nAChR-regulated intracellular signaling pathways.

Skeletal muscle disuse results in a progressive and significant loss of muscle mass and bone tissues, whereas physical exercise and EPS are able to counteract such effects[148–156]. The skeletal muscle is a secretory organ, which releases myokines during adequate contractions. Even if the mechanism is still unknown, myokines operate in autocrine, paracrine and/or endocrine manner.

IL-6, is mainly known for its role in the immune response and acute phase reactions; however, it is also considered as an energy sensor as its production is regulated by substrate availability as well as by muscle contraction. The amount of the released IL-6 is related to the intensity and duration of the exercise and also to the percentage of the muscle mass involved[127]. Independently from the mechanism of release, a beneficial role of IL-6 acting in autocrine/paracrine way on skeletal muscle regeneration was observed[130,157].

In our laboratory, we developed an *in vitro* exercise model offering the advantage to detect myokine release from cultured contracting muscle cells, avoiding other possible myokine sources, like immune system or other endocrine cells. As well as the exercise, *in vitro* EPS induce visible muscle cell contraction[95,101,102], time locked Ca^{2+} increase and myokine release. During contraction *in vivo*, as well as during EPS delivered *in vitro*, the mechanical strain causes the activation and enrollment of mechanosensitive channels (MA), which could potentially control a several number of intracellular signaling pathways, including myokine production.

We reported the presence of Piezo 1 expression in adult cultured myotubes and the positive modulation of IL-6 release induced by chemical activation of Piezo 1 channels.

Our data indicate that the pharmacological activation of Piezo 1 is even more efficient than the EPS, suggesting that specific Piezo 1 agonists might represent a potential pharmacological tool to promote IL-6 release in a pathophysiological scenario[158]. New

parameters for EPS, (i.e. pulse duration, amplitude, frequency and pulse intervals) could be potentially optimized to enhance the myokine release.

In conclusion, our results confirm that the electrical stimulation is a powerful tool to modulate different important aspects of the skeletal muscle physiology and that the knowledge of the mechanisms responsible for the muscle plasticity combined with the optimization of the electrostimulation protocols represent a promising strategy to ameliorate the benefits of the therapeutic electrostimulation in patients. The use of innovative “noisy” electrical stimulations with a pattern that is not spatially fixed and not temporally synchronous would also help to get better results reducing muscle fatigue and patient discomforts.

5. BIBLIOGRAPHY

1. Nations Unies, ed. *World Population Ageing, 2015: Highlights*. United Nations; 2015.

2. Frontera WR, Ochala J. Skeletal Muscle: A Brief Review of Structure and Function. *Calcif Tissue Int*. 2015;96(3):183-195. doi:10.1007/s00223-014-9915-y

3. Wolfe RR. The underappreciated role of muscle in health and disease. *Am J Clin Nutr*. 2006;84(3):475-482. doi:10.1093/ajcn/84.3.475

4. Kirk-Sanchez N, McGough E. Physical exercise and cognitive performance in the elderly: current perspectives. *Clin Interv Aging*. Published online December 2013:51. doi:10.2147/CIA.S39506

5. Ensari I, Sandroff BM, Motl RW. Effects of Single Bouts of Walking Exercise and Yoga on Acute Mood Symptoms in People with Multiple Sclerosis. *Int J MS Care*. 2016;18(1):1-8. doi:10.7224/1537-2073.2014-104

6. Basso JC, Suzuki WA. The Effects of Acute Exercise on Mood, Cognition, Neurophysiology, and Neurochemical Pathways: A Review. :26.

7. Roig M, Reid WD. Electrical stimulation and peripheral muscle function in COPD: a systematic review. *Respir Med*. 2009;103(4):485-495. doi:10.1016/j.rmed.2008.11.008

8. Gibson JN, Smith K, Rennie MJ. Prevention of disuse muscle atrophy by means of electrical stimulation: maintenance of protein synthesis. *Lancet Lond Engl*. 1988;2(8614):767-770. doi:10.1016/s0140-6736(88)92417-8

9. Mukund K, Subramaniam S. Skeletal muscle: A review of molecular structure and function, in health and disease. *Wiley Interdiscip Rev Syst Biol Med*. 2020;12(1):e1462. doi:10.1002/wsbm.1462

10. Block BA, Imagawa T, Campbell KP, Franzini-Armstrong C. Structural evidence for direct interaction between the molecular components of the transverse tubule/sarcoplasmic reticulum junction in skeletal muscle. *J Cell Biol*. 1988;107(6 Pt 2):2587-2600. doi:10.1083/jcb.107.6.2587

11. Mauro A. SATELLITE CELL OF SKELETAL MUSCLE FIBERS. *J Biophys Biochem Cytol*. 1961;9(2):493-495. doi:10.1083/jcb.9.2.493

12. Reznik M. THYMIDINE-3H UPTAKE BY SATELLITE CELLS OF REGENERATING SKELETAL MUSCLE. *J Cell Biol*. 1969;40(2):568-571. doi:10.1083/jcb.40.2.568

13. Moss FP, Leblond CP. NATURE OF DIVIDING NUCLEI IN SKELETAL MUSCLE OF GROWING RATS. *J Cell Biol*. 1970;44(2):459-461. doi:10.1083/jcb.44.2.459

14. Fukada S ichiro, Ma Y, Ohtani T, Watanabe Y, Murakami S, Yamaguchi M. Isolation, characterization, and molecular regulation of muscle stem cells. *Front Physiol*. 2013;4:317. doi:10.3389/fphys.2013.00317

15. Schultz E, McCormick KM. Skeletal muscle satellite cells. *Rev Physiol Biochem Pharmacol*. 1994;123:213-257. doi:10.1007/BFb0030904

16. Han MS, White A, Perry RJ, et al. Regulation of adipose tissue inflammation by interleukin 6. *Proc Natl Acad Sci*. 2020;117(6):2751-2760. doi:10.1073/pnas.1920004117

17. Megeney LA, Kablar B, Garrett K, Anderson JE, Rudnicki MA. MyoD is required for myogenic stem cell function in adult skeletal muscle. *Genes Dev*. 1996;10(10):1173-1183. doi:10.1101/gad.10.10.1173

18. Schiaffino S, Reggiani C. Fiber types in mammalian skeletal muscles. *Physiol Rev*. 2011;91(4):1447-1531. doi:10.1152/physrev.00031.2010

19. Bassel-Duby R, Olson EN. Signaling pathways in skeletal muscle remodeling. *Annu Rev Biochem*. 2006;75:19-37. doi:10.1146/annurev.biochem.75.103004.142622

20. Plotkin DL, Roberts MD, Haun CT, Schoenfeld BJ. Muscle Fiber Type Transitions with Exercise Training: Shifting Perspectives. *Sports Basel Switz*. 2021;9(9):127. doi:10.3390/sports9090127

21. Scott W, Stevens J, Binder-Macleod SA. Human skeletal muscle fiber type classifications. *Phys Ther*. 2001;81(11):1810-1816.

22. Trappe S, Creer A, Slivka D, Minchev K, Trappe T. Single muscle fiber function with concurrent exercise or nutrition countermeasures during 60 days of bed rest in women. *J Appl Physiol Bethesda Md 1985*. 2007;103(4):1242-1250. doi:10.1152/japplphysiol.00560.2007

23. Grimby G, Broberg C, Krotkiewska I, Krotkiewski M. Muscle fiber composition in patients with traumatic cord lesion. *Scand J Rehabil Med*. 1976;8(1):37-42.

24. Burnham R, Martin T, Stein R, Bell G, MacLean I, Steadward R. Skeletal muscle fibre type transformation following spinal cord injury. *Spinal Cord*. 1997;35(2):86-91. doi:10.1038/sj.sc.3100364

25. Gallagher P, Trappe S, Harber M, et al. Effects of 84-days of bedrest and resistance training on single muscle fibre myosin heavy chain distribution in human vastus lateralis and soleus muscles. *Acta Physiol Scand*. 2005;185(1):61-69. doi:10.1111/j.1365-201X.2005.01457.x

26. Ditor DS, Hamilton S, Tarnopolsky MA, et al. Na+,K+-ATPase concentration and fiber type distribution after spinal cord injury. *Muscle Nerve*. 2004;29(1):38-45. doi:10.1002/mus.10534

27. Talbot J, Maves L. Skeletal muscle fiber type: using insights from muscle developmental biology to dissect targets for susceptibility and resistance to muscle disease. *Wiley Interdiscip Rev Dev Biol*. 2016;5(4):518-534. doi:10.1002/wdev.230

28. Wood SJ, Slater CR. Safety factor at the neuromuscular junction. *Prog Neurobiol*. 2001;64(4):393-429. doi:10.1016/s0301-0082(00)00055-1

29. Quantal Nature of Synaptic Transmission | Physiological Reviews. Accessed August 31, 2022. https://journals.physiology.org/doi/abs/10.1152/physrev.1966.46.1.51

30. Kuffler SW, Yoshikami D. The number of transmitter molecules in a quantum: an estimate from iontophoretic application of acetylcholine at the neuromuscular synapse. *J Physiol*. 1975;251(2):465-482.

31. Aminoff MJ. Myology, Basic and Clincal, 3rd Edition, edited by Andrew G. Engel and Clara Franzini-Armstrong, 2 vols., 1960 pp., ill., New York, McGraw-Hill, 2004, $395. *Muscle Nerve*. 2005;31(4):531-531. doi:10.1002/mus.20246

32. Wood SJ, Slater CR. The contribution of postsynaptic folds to the safety factor for neuromuscular transmission in rat fast- and slow-twitch muscles. *J Physiol*. 1997;500 (Pt 1):165-176. doi:10.1113/jphysiol.1997.sp022007

33. Mishina M, Takai T, Imoto K, et al. Molecular distinction between fetal and adult forms of muscle acetylcholine receptor. *Nature*. 1986;321(6068):406-411. doi:10.1038/321406a0

34. Wu H, Xiong WC, Mei L. To build a synapse: signaling pathways in neuromuscular junction assembly. *Dev Camb Engl*. 2010;137(7):1017-1033. doi:10.1242/dev.038711

35. Sanes JR, Lichtman JW. Development of the vertebrate neuromuscular junction. *Annu Rev Neurosci*. 1999;22:389-442. doi:10.1146/annurev.neuro.22.1.389

36. Duclert A, Changeux JP. Acetylcholine receptor gene expression at the developing neuromuscular junction. *Physiol Rev*. 1995;75(2):339-368. doi:10.1152/physrev.1995.75.2.339

37. Missias AC, Chu GC, Klocke BJ, Sanes JR, Merlie JP. Maturation of the acetylcholine receptor in skeletal muscle: regulation of the AChR gamma-to-epsilon switch. *Dev Biol*. 1996;179(1):223-238. doi:10.1006/dbio.1996.0253

38. Sanes JR, Lichtman JW. Induction, assembly, maturation and maintenance of a postsynaptic apparatus. *Nat Rev Neurosci*. 2001;2(11):791-805. doi:10.1038/35097557

39. [PDF] Chapter 22 – Neuromuscular Physiology and Pharmacology Neuromuscular Transmission | Semantic Scholar. Accessed September 20, 2022. https://www.semanticscholar.org/paper/Chapter-22-%E2%80%93-Neuromuscular-Physiology-and-Martyn/33a27062336f1b58ffd1f5aad7696c0a4cd1f298

40. Wallace B. Agrin-induced specializations contain cytoplasmic, membrane, and extracellular matrix-associated components of the postsynaptic apparatus. *J Neurosci*. 1989;9(4):1294-1302. doi:10.1523/JNEUROSCI.09-04-01294.1989

41. Meier T, Hauser DM, Chiquet M, Landmann L, Ruegg MA, Brenner HR. Neural agrin induces ectopic postsynaptic specializations in innervated muscle fibers. *J Neurosci Off J Soc Neurosci*. 1997;17(17):6534-6544.

42. Glass DJ, Bowen DC, Stitt TN, et al. Agrin acts via a MuSK receptor complex. *Cell*. 1996;85(4):513-523. doi:10.1016/s0092-8674(00)81252-0

43. Kim N, Stiegler AL, Cameron TO, et al. Lrp4 is a receptor for Agrin and forms a complex with MuSK. *Cell*. 2008;135(2):334-342. doi:10.1016/j.cell.2008.10.002

44. Zhang B, Luo S, Wang Q, Suzuki T, Xiong WC, Mei L. LRP4 serves as a coreceptor of agrin. *Neuron*. 2008;60(2):285-297. doi:10.1016/j.neuron.2008.10.006

45. Borges LS, Richman DP. Muscle-Specific Kinase Myasthenia Gravis. *Front Immunol*. 2020;0. doi:10.3389/fimmu.2020.00707

46. Gautam M, Noakes PG, Mudd J, et al. Failure of postsynaptic specialization to develop at neuromuscular junctions of rapsyn-deficient mice. *Nature*. 1995;377(6546):232-236. doi:10.1038/377232a0

47. Ferns M. An Inside Job: Molecular Determinants for Postsynaptic Localization of Nicotinic Acetylcholine Receptors. *Mol Basel Switz*. 2021;26(11):3065. doi:10.3390/molecules26113065

48. Martinez-Pena y Valenzuela I, Akaaboune M. The Metabolic Stability of the Nicotinic Acetylcholine Receptor at the Neuromuscular Junction. *Cells*. 2021;10(2):358. doi:10.3390/cells10020358

49. Strack S, Khan MM, Wild F, Rall A, Rudolf R. Turnover of acetylcholine receptors at the endplate revisited: novel insights into nerve-dependent behavior. *J Muscle Res Cell Motil*. 2015;36(6):517-524. doi:10.1007/s10974-015-9418-0

50. Midrio M. The denervated muscle: facts and hypotheses. A historical review. *Eur J Appl Physiol*. 2006;98(1):1-21. doi:10.1007/s00421-006-0256-z

51. Wu P, Chawla A, Spinner RJ, et al. Key changes in denervated muscles and their impact on regeneration and reinnervation. *Neural Regen Res*. 2014;9(20):1796-1809. doi:10.4103/1673-5374.143424

52. Melton LJ, Khosla S, Crowson CS, O'Connor MK, O'Fallon WM, Riggs BL. Epidemiology of sarcopenia. *J Am Geriatr Soc*. 2000;48(6):625-630.

53. Holloszy JO. The biology of aging. *Mayo Clin Proc*. 2000;75 Suppl:S3-8; discussion S8-9.

54. Bao Z, Cui C, Chow SKH, Qin L, Wong RMY, Cheung WH. AChRs Degeneration at NMJ in Aging-Associated Sarcopenia–A Systematic Review. *Front Aging Neurosci*. 2020;12:597811. doi:10.3389/fnagi.2020.597811

55. Suzuki T, Maruyama A, Sugiura T, Machida S, Miyata H. Age-related changes in two- and three-dimensional morphology of type-identified endplates in the rat diaphragm. *J Physiol Sci JPS*. 2009;59(1):57-62. doi:10.1007/s12576-008-0005-7

56. Volpe P, Martini A, Nori A. The Sarcoplasmic Reticulum of Skeletal Muscle: A Look from Inside. *Excit-Contract Coupling Skelet Card Smooth Muscle*. Published online 1992:263-275. doi:10.1007/978-1-4615-3362-7_19

57. Porter KR, Palade GE. Studies on the endoplasmic reticulum. III. Its form and distribution in striated muscle cells. *J Biophys Biochem Cytol*. 1957;3(2):269-300. doi:10.1083/jcb.3.2.269

58. Campbell AK. Calcium as an Intracellular Regulator. *Calcium Hum Biol*. Published online 1988:261-316. doi:10.1007/978-1-4471-1437-6_11

59. S Fleischer and, Inui M. Biochemistry and Biophysics of Excitation-Contraction Coupling. https://doi.org/10.1146/annurev.bb.18.060189.002001. doi:10.1146/annurev.bb.18.060189.002001

60. Volpe P, Salviati G, Di Virgilio F, Pozzan T. Inositol 1,4,5-trisphosphate induces calcium release from sarcoplasmic reticulum of skeletal muscle. *Nature*. 1985;316(6026):347-349. doi:10.1038/316347a0

61. Vergara J, Tsien RY, Delay M. Inositol 1,4,5-trisphosphate: a possible chemical link in excitation-contraction coupling in muscle. *Proc Natl Acad Sci U S A*. 1985;82(18):6352-6356. doi:10.1073/pnas.82.18.6352

62. Moschella MC, Watras J, Jayaraman T, Marks AR. Inositol 1,4,5-trisphosphate receptor in skeletal muscle: differential expression in myofibres. *J Muscle Res Cell Motil*. 1995;16(4):390-400. doi:10.1007/BF00114504

63. Salanova M, Priori G, Barone V, et al. Homer proteins and InsP(3) receptors co-localise in the longitudinal sarcoplasmic reticulum of skeletal muscle fibres. *Cell Calcium*. 2002;32(4):193-200. doi:10.1016/s0143416002001549

64. Casas M, Figueroa R, Jorquera G, Escobar M, Molgó J, Jaimovich E. IP3-dependent, post-tetanic calcium transients induced by electrostimulation of adult skeletal muscle fibers. *J Gen Physiol*. 2010;136(4):455-467. doi:10.1085/jgp.200910397

65. Zhu H, Bhattacharyya BJ, Lin H, Gomez CM. Skeletal Muscle IP3R1 Receptors Amplify Physiological and Pathological Synaptic Calcium Signals. *J Neurosci*. 2011;31(43):15269-15283. doi:10.1523/JNEUROSCI.3766-11.2011

66. Powell JA, Molgó J, Adams DS, et al. IP3 receptors and associated Ca2+ signals localize to satellite cells and to components of the neuromuscular junction in skeletal muscle. *J Neurosci Off J Soc Neurosci*. 2003;23(23):8185-8192.

67. Dauber W, Voigt T, Heini A. Junctions between subsynaptic folds and rough sarcoplasmic reticulum of muscle fibres. *J Muscle Res Cell Motil*. 1999;20(7):697-701. doi:10.1023/a:1005521529855

68. Dauber W, Meister A. Ultrastructure of junctional folds of motor end plates in extensor digitorum longus muscles of mice. *J Ultrastruct Mol Struct Res*. 1986;97(1-3):158-164. doi:10.1016/s0889-1605(86)80015-5

69. Dauber W, Voigt T, Härtel X, Mayer J. The T-tubular network and its triads in the sole plate sarcoplasm of the motor end-plate of mammals. *J Muscle Res Cell Motil*. 2000;21(5):443-449. doi:10.1023/a:1005614917564

70. Dezaki K, Tsuneki H, Kimura I. [Slow Ca2+ (RAMIC) mobilization operated by postsynaptic neuronal nicotinic receptor regulates synaptic function at the mouse neuromuscular junction]. *Nihon Yakurigaku Zasshi Folia Pharmacol Jpn*. 1997;110 Suppl 1:114P-119P. doi:10.1254/fpj.110.supplement_114

71. Megeath LJ, Fallon JR. Intracellular calcium regulates agrin-induced acetylcholine receptor clustering. *J Neurosci Off J Soc Neurosci*. 1998;18(2):672-678.

72. Zayas R, Groshong JS, Gomez CM. Inositol-1,4,5-triphosphate receptors mediate activity-induced synaptic Ca2+ signals in muscle fibers and Ca2+ overload in slow-channel syndrome. *Cell Calcium*. 2007;41(4):343-352. doi:10.1016/j.ceca.2006.07.007

73. Yuan JP, Kiselyov K, Shin DM, et al. Homer binds TRPC family channels and is required for gating of TRPC1 by IP3 receptors. *Cell*. 2003;114(6):777-789. doi:10.1016/s0092-8674(03)00716-5

74. Sala C, Roussignol G, Meldolesi J, Fagni L. Key role of the postsynaptic density scaffold proteins Shank and Homer in the functional architecture of Ca2+ homeostasis at dendritic

spines in hippocampal neurons. *J Neurosci Off J Soc Neurosci*. 2005;25(18):4587-4592. doi:10.1523/JNEUROSCI.4822-04.2005

75. Fagni L, Worley PF, Ango F. Homer as both a scaffold and transduction molecule. *Sci STKE Signal Transduct Knowl Environ*. 2002;2002(137):re8. doi:10.1126/stke.2002.137.re8

76. Salanova M, Volpe P, Blottner D. Homer protein family regulation in skeletal muscle and neuromuscular adaptation. *IUBMB Life*. 2013;65(9):769-776. doi:10.1002/iub.1198

77. Evans S, Goldman D, Heinemann S, Patrick J. Muscle acetylcholine receptor biosynthesis. Regulation by transcript availability. *J Biol Chem*. 1987;262(10):4911-4916.

78. Brenner HR, Rudin W. On the effect of muscle activity on the end-plate membrane in denervated mouse muscle. *J Physiol*. 1989;410:501-512. doi:10.1113/jphysiol.1989.sp017546

79. Doucet BM, Lam A, Griffin L. neuromuscular Electrical Stimulation for Skeletal Muscle Function. :15.

80. Baker JS, McCormick MC, Robergs RA. Interaction among Skeletal Muscle Metabolic Energy Systems during Intense Exercise. *J Nutr Metab*. 2010;2010:905612. doi:10.1155/2010/905612

81. Nikolić N, Görgens SW, Thoresen GH, Aas V, Eckel J, Eckardt K. Electrical pulse stimulation of cultured skeletal muscle cells as a model for *in vitro* exercise - possibilities and limitations. *Acta Physiol*. 2017;220(3):310-331. doi:10.1111/apha.12830

82. Tarum J, Folkesson M, Atherton PJ, Kadi F. Electrical pulse stimulation: an in vitro exercise model for the induction of human skeletal muscle cell hypertrophy. A proof-of-concept study. *Exp Physiol*. 2017;102(11):1405-1413. doi:10.1113/EP086581

83. SHAINBERG A, BURSTEIN M. Decrease of acetylcholine receptor synthesis in muscle cultures by electrical stimulation | Nature. Accessed February 2, 2022. https://www.nature.com/articles/264368a0

84. Nedachi T, Fujita H, Kanzaki M. Contractile C2C12 myotube model for studying exercise-inducible responses in skeletal muscle. *Am J Physiol Endocrinol Metab*. 2008;295(5):E1191-1204. doi:10.1152/ajpendo.90280.2008

85. Jaatinen L, Young E, Hyttinen J, Vörös J, Zambelli T, Demkó L. Quantifying the effect of electric current on cell adhesion studied by single-cell force spectroscopy. *Biointerphases*. 2016;11(1):011004. doi:10.1116/1.4940214

86. Ahadian S, Ostrovidov S, Hosseini V, et al. Electrical stimulation as a biomimicry tool for regulating muscle cell behavior. *Organogenesis*. 2013;9(2):87-92. doi:10.4161/org.25121

87. H Hoppeler, SR Kayar. Capillarity and Oxidative Capacity of Muscles. *Physiology*. Published online June 1, 1988. doi:10.1152/physiologyonline.1988.3.3.113

88. Booth FW, Thomason DB. Molecular and cellular adaptation of muscle in response to exercise: perspectives of various models. *Physiol Rev*. 1991;71(2):541-585. doi:10.1152/physrev.1991.71.2.541

89. S E. Invited review: activity-induced angiogenesis. *Pflugers Arch*. 2009;457(5). doi:10.1007/s00424-008-0563-9

90. Rowe GC, El-Khoury R, Patten IS, Rustin P, Arany Z. PGC-1α is Dispensable for Exercise-Induced Mitochondrial Biogenesis in Skeletal Muscle. *PLOS ONE*. 2012;7(7):e41817. doi:10.1371/journal.pone.0041817

91. Rowe GC, Safdar A, Arany Z. Running forward: new frontiers in endurance exercise biology. *Circulation*. 2014;129(7):798-810. doi:10.1161/CIRCULATIONAHA.113.001590

92. Lüthi JM, Howald H, Claassen H, Rösler K, Vock P, Hoppeler H. Structural changes in skeletal muscle tissue with heavy-resistance exercise. *Int J Sports Med*. 1986;7(3):123-127. doi:10.1055/s-2008-1025748

93. Phillips SM, Glover EI, Rennie MJ. Alterations of protein turnover underlying disuse atrophy in human skeletal muscle. *J Appl Physiol Bethesda Md 1985*. 2009;107(3):645-654. doi:10.1152/japplphysiol.00452.2009

94. Egan B, Zierath JR. Exercise metabolism and the molecular regulation of skeletal muscle adaptation. *Cell Metab*. 2013;17(2):162-184. doi:10.1016/j.cmet.2012.12.012

95. Nikolić N, Bakke SS, Kase ET, et al. Electrical Pulse Stimulation of Cultured Human Skeletal Muscle Cells as an In Vitro Model of Exercise. *PLOS ONE*. 2012;7(3):e33203. doi:10.1371/journal.pone.0033203

96. Lambernd S, Taube A, Schober A, et al. Contractile activity of human skeletal muscle cells prevents insulin resistance by inhibiting pro-inflammatory signalling pathways. *Diabetologia*. 2012;55(4):1128-1139. doi:10.1007/s00125-012-2454-z

97. Pettersen E, Anderson J, Ortiz-Catalan M. Electrical stimulation to promote osseointegration of bone anchoring implants: a topical review. *J Neuroengineering Rehabil*. 2022;19(1):31. doi:10.1186/s12984-022-01005-7

98. Kim IS, Song JK, Zhang YL, et al. Biphasic electric current stimulates proliferation and induces VEGF production in osteoblasts. *Biochim Biophys Acta*. 2006;1763(9):907-916. doi:10.1016/j.bbamcr.2006.06.007

99. Lagerquist O, Collins DF. Influence of stimulus pulse width on M-waves, H-reflexes, and torque during tetanic low-intensity neuromuscular stimulation. *Muscle Nerve*. 2010;42(6):886-893. doi:10.1002/mus.21762

100. Gregory CM, Bickel CS. Recruitment patterns in human skeletal muscle during electrical stimulation. *Phys Ther*. 2005;85(4):358-364.

101. Sciancalepore M, Coslovich T, Lorenzon P, Ziraldo G, Taccola G. Extracellular stimulation with human “noisy” electromyographic patterns facilitates myotube activity. *J Muscle Res Cell Motil*. 2015;36(4):349-357. doi:10.1007/s10974-015-9424-2

102. Bosutti A, Bernareggi A, Massaria G, et al. A “noisy” electrical stimulation protocol favors muscle regeneration in vitro through release of endogenous ATP. *Exp Cell Res*. 2019;381(1). doi:10.1016/j.yexcr.2019.05.012

103. Severinsen MCK, Pedersen BK. Muscle–Organ Crosstalk: The Emerging Roles of Myokines. *Endocr Rev*. 2020;41(4):594-609. doi:10.1210/endrev/bnaa016

104. Febbraio MA, Pedersen BK. Contraction-induced myokine production and release: is skeletal muscle an endocrine organ? *Exerc Sport Sci Rev*. 2005;33(3):114-119. doi:10.1097/00003677-200507000-00003

105. Nielsen AR, Mounier R, Plomgaard P, et al. Expression of interleukin-15 in human skeletal muscle effect of exercise and muscle fibre type composition. *J Physiol*. 2007;584(Pt 1):305-312. doi:10.1113/jphysiol.2007.139618

106. Lee JH, Jun HS. Role of Myokines in Regulating Skeletal Muscle Mass and Function. *Front Physiol*. 2019;0. doi:10.3389/fphys.2019.00042

107. Laurens C, Bergouignan A, Moro C. Exercise-Released Myokines in the Control of Energy Metabolism. *Front Physiol*. 2020;0. doi:10.3389/fphys.2020.00091

108. Hirata Y, Nomura K, Kato D, et al. A Piezo1/KLF15/IL-6 axis mediates immobilization-induced muscle atrophy. *J Clin Invest*. 2022;132(10):1-13. doi:10.1172/JCI154611

109. Steensberg A, van Hall G, Osada T, Sacchetti M, Saltin B, Klarlund Pedersen B. Production of interleukin-6 in contracting human skeletal muscles can account for the exercise-induced increase in plasma interleukin-6. *J Physiol*. 2000;529 Pt 1:237-242. doi:10.1111/j.1469-7793.2000.00237.x

110. Toft AD, Falahati A, Steensberg A. Source and kinetics of interleukin-6 in humans during exercise demonstrated by a minimally invasive model. *Eur J Appl Physiol*. 2011;111(7):1351-1359. doi:10.1007/s00421-010-1755-5

111. Pedersen BK, Steensberg A, Fischer C, et al. Searching for the exercise factor: is IL-6 a candidate? *J Muscle Res Cell Motil*. 2003;24(2):113. doi:10.1023/A:1026070911202

112. Akaaboune M, Culican SM, Turney SG, Lichtman JW. Rapid and reversible effects of activity on acetylcholine receptor density at the neuromuscular junction in vivo. *Science*. 1999;286(5439):503-507. doi:10.1126/science.286.5439.503

113. Bruneau E, Sutter D, Hume RI, Akaaboune M. Identification of nicotinic acetylcholine receptor recycling and its role in maintaining receptor density at the neuromuscular junction in vivo. *J Neurosci Off J Soc Neurosci*. 2005;25(43):9949-9959. doi:10.1523/JNEUROSCI.3169-05.2005

114. Bruneau EG, Akaaboune M. The dynamics of recycled acetylcholine receptors at the neuromuscular junction in vivo. *Dev Camb Engl*. 2006;133(22):4485-4493. doi:10.1242/dev.02619

115. Jaimovich E, Reyes R, Liberona JL, Powell JA. IP3 receptors, IP3 transients, and nucleus-associated Ca2+ signals in cultured skeletal muscle. *Am J Physiol-Cell Physiol*. Published online May 1, 2000. doi:10.1152/ajpcell.2000.278.5.C998

116. Powell JA, Carrasco MA, Adams DS, et al. IP3 receptor function and localization in myotubes: an unexplored Ca2+ signaling pathway in skeletal muscle. *J Cell Sci*. 2001;114(20):3673-3683. doi:10.1242/jcs.114.20.3673

117. Carrasco MA, Riveros N, Ríos J, et al. Depolarization-induced slow calcium transients activate early genes in skeletal muscle cells. *Am J Physiol Cell Physiol*. 2003;284(6):C1438-1447. doi:10.1152/ajpcell.00117.2002

118. Juretić N, Urzúa U, Munroe DJ, Jaimovich E, Riveros N. Differential gene expression in skeletal muscle cells after membrane depolarization. *J Cell Physiol*. 2007;210(3):819-830. doi:10.1002/jcp.20902

119. Li L, Xiong WC, Mei L. Neuromuscular Junction Formation, Aging, and Disorders. *Annu Rev Physiol*. 2018;80:159-188. doi:10.1146/annurev-physiol-022516-034255

120. Lømo T. What controls the position, number, size, and distribution of neuromuscular junctions on rat muscle fibers? *J Neurocytol*. 2003;32(5-8):835-848. doi:10.1023/B:NEUR.0000020627.18156.b1

121. Bortoloso E, Megighian A, Furlan S, Gorza L, Volpe P. Homer 2 antagonizes protein degradation in slow-twitch skeletal muscles. *Am J Physiol Cell Physiol*. 2013;304(1):C68-77. doi:10.1152/ajpcell.00108.2012

122. Salanova M, Bortoloso E, Schiffl G, et al. Expression and regulation of Homer in human skeletal muscle during neuromuscular junction adaptation to disuse and exercise. *FASEB J*. 2011;25(12):4312-4325. doi:10.1096/fj.11-186049

123. Severinsen MCK, Pedersen BK. Muscle-Organ Crosstalk: The Emerging Roles of Myokines. *Endocr Rev*. 2020;41(4):bnaa016. doi:10.1210/endrev/bnaa016

124. Hirano T. Interleukin 6 and its receptor: ten years later. *Int Rev Immunol*. 1998;16(3-4):249-284. doi:10.3109/08830189809042997

125. Bustamante M, Fernández-Verdejo R, Jaimovich E, Buvinic S. Electrical stimulation induces IL-6 in skeletal muscle through extracellular ATP by activating Ca2+ signals and an IL-6 autocrine loop. *Am J Physiol - Endocrinol Metab*. 2014;306(8):E869-E882. doi:10.1152/ajpendo.00450.2013

126. Muñoz-Cánoves P, Scheele C, Pedersen BK, Serrano AL. Interleukin-6 myokine signaling in skeletal muscle: a double-edged sword? *FEBS J*. 2013;280(17):4131-4148. doi:10.1111/febs.12338

127. Knuttgen HG. Strength training and aerobic exercise: comparison and contrast. *J Strength Cond Res*. 2007;21(3):973-978. doi:10.1519/R-505011.1

128. Batista ML, Rosa JC, Lopes RD, et al. Exercise training changes IL-10/TNF-alpha ratio in the skeletal muscle of post-MI rats. *Cytokine*. 2010;49(1):102-108. doi:10.1016/j.cyto.2009.10.007

129. Petersen AMW, Pedersen BK. The anti-inflammatory effect of exercise. *J Appl Physiol Bethesda Md 1985*. 2005;98(4):1154-1162. doi:10.1152/japplphysiol.00164.2004

130. Belizário JE, Fontes-Oliveira CC, Borges JP, Kashiabara JA, Vannier E. Skeletal muscle wasting and renewal: a pivotal role of myokine IL-6. *SpringerPlus*. 2016;5(1):619. doi:10.1186/s40064-016-2197-2

131. Baeza-Raja B, Muñoz-Cánoves P. p38 MAPK-induced nuclear factor-kappaB activity is required for skeletal muscle differentiation: role of interleukin-6. *Mol Biol Cell*. 2004;15(4):2013-2026. doi:10.1091/mbc.e03-08-0585

132. Haddad F, Zaldivar F, Cooper DM, Adams GR. IL-6-induced skeletal muscle atrophy. *J Appl Physiol Bethesda Md 1985*. 2005;98(3):911-917. doi:10.1152/japplphysiol.01026.2004

133. Buvinic S, Almarza G, Bustamante M, et al. ATP released by electrical stimuli elicits calcium transients and gene expression in skeletal muscle. *J Biol Chem*. 2009;284(50):34490-34505. doi:10.1074/jbc.M109.057315

134. Coste B, Mathur J, Schmidt M, et al. Piezo1 and Piezo2 are essential components of distinct mechanically activated cation channels. *Science*. 2010;330(6000):55-60. doi:10.1126/science.1193270

135. Shinge SAU, Zhang D, Achu Muluh T, Nie Y, Yu F. Mechanosensitive Piezo1 Channel Evoked-Mechanical Signals in Atherosclerosis. *J Inflamm Res*. 2021;14:3621-3636. doi:10.2147/JIR.S319789

136. Tsuchiya M, Hara Y, Okuda M, et al. Cell surface flip-flop of phosphatidylserine is critical for PIEZO1-mediated myotube formation. *Nat Commun*. 2018;9(1):1-15. doi:10.1038/s41467-018-04436-w

137. Bosutti A, Giniatullin A, Odnoshivkina Y, et al. "Time window" effect of Yoda1-evoked Piezo1 channel activity during mouse skeletal muscle differentiation. *Acta Physiol Oxf Engl*. 2021;233(4):e13702. doi:10.1111/apha.13702

138. Squecco R, Kern H, Biral D, Rossini K, Francini F. Mechano-sensitivity of normal and long term denervated soleus muscle of the rat. *Neurol Res*. 2008;30(2):155-159. doi:10.1179/174313208X281028

139. Grohovaz F, Lorenzon P, Ruzzier F, Zorec R. Properties of acetylcholine receptors in adult rat skeletal muscle fibers in culture. *J Membr Biol*. 1993;136(1):31-42. doi:10.1007/BF00241487

140. Shi L, Fu AKY, Ip NY. Molecular mechanisms underlying maturation and maintenance of the vertebrate neuromuscular junction. *Trends Neurosci*. 2012;35(7):441-453. doi:10.1016/j.tins.2012.04.005

141. Rotzler S, Brenner HR. Metabolic stabilization of acetylcholine receptors in vertebrate neuromuscular junction by muscle activity. *J Cell Biol*. 1990;111(2):655-661. doi:10.1083/jcb.111.2.655

142. Shyng SL, Salpeter MM. Degradation rate of acetylcholine receptors inserted into denervated vertebrate neuromuscular junctions. *J Cell Biol*. 1989;108(2):647-651. doi:10.1083/jcb.108.2.647

143. Rotzler S, Schramek H, Brenner HR. Metabolic stabilization of endplate acetylcholine receptors regulated by Ca2+ influx associated with muscle activity. *Nature*. 1991;349(6307):337-339. doi:10.1038/349337a0

144. Andreose JS, Xu R, Lømo T, Salpeter MM, Fumagalli G. Degradation of two AChR populations at rat neuromuscular junctions: regulation in vivo by electrical stimulation. *J Neurosci Off J Soc Neurosci*. 1993;13(8):3433-3438.

145. Jorquera G, Altamirano F, Contreras-Ferrat A, et al. Cav1.1 controls frequency-dependent events regulating adult skeletal muscle plasticity. *J Cell Sci*. 2013;126(Pt 5):1189-1198. doi:10.1242/jcs.116855

146. Stiber JA, Tabatabaei N, Hawkins AF, et al. Homer modulates NFAT-dependent signaling during muscle differentiation. *Dev Biol*. 2005;287(2):213-224. doi:10.1016/j.ydbio.2005.06.030

147. Bortoloso E, Pilati N, Megighian A, Tibaldo E, Sandonà D, Volpe P. Transition of Homer isoforms during skeletal muscle regeneration. *Am J Physiol Cell Physiol*. 2006;290(3):C711-718. doi:10.1152/ajpcell.00217.2005

148. Brotto M, Bonewald L. Bone and muscle: Interactions beyond mechanical. *Bone*. 2015;80:109-114. doi:10.1016/j.bone.2015.02.010

149. Daly RM, Saxon L, Turner CH, Robling AG, Bass SL. The relationship between muscle size and bone geometry during growth and in response to exercise. *Bone*. 2004;34(2):281-287. doi:10.1016/j.bone.2003.11.009

150. Duncan CS, Blimkie CJR, Cowell CT, Burke ST, Briody JN, Howman-Giles R. Bone mineral density in adolescent female athletes: relationship to exercise type and muscle strength. *Med Sci Sports Exerc*. 2002;34(2):286-294. doi:10.1097/00005768-200202000-00017

151. Laurent MR, Dubois V, Claessens F, et al. Muscle-bone interactions: From experimental models to the clinic? A critical update. *Mol Cell Endocrinol*. 2016;432:14-36. doi:10.1016/j.mce.2015.10.017

152. McKeehen JN, Novotny SA, Baltgalvis KA, Call JA, Nuckley DJ, Lowe DA. Adaptations of mouse skeletal muscle to low-intensity vibration training. *Med Sci Sports Exerc*. 2013;45(6):1051-1059. doi:10.1249/MSS.0b013e3182811947

153. Oxlund BS, Ørtoft G, Andreassen TT, Oxlund H. Low-intensity, high-frequency vibration appears to prevent the decrease in strength of the femur and tibia associated with ovariectomy of adult rats. *Bone*. 2003;32(1):69-77. doi:10.1016/s8756-3282(02)00916-x

154. Perrini S, Laviola L, Carreira MC, Cignarelli A, Natalicchio A, Giorgino F. The GH/IGF1 axis and signaling pathways in the muscle and bone: mechanisms underlying age-related skeletal muscle wasting and osteoporosis. *J Endocrinol*. 2010;205(3):201-210. doi:10.1677/JOE-09-0431

155. Reyes ML, Hernández M, Holmgren LJ, Sanhueza E, Escobar RG. High-frequency, low-intensity vibrations increase bone mass and muscle strength in upper limbs, improving autonomy in disabled children. *J Bone Miner Res Off J Am Soc Bone Miner Res*. 2011;26(8):1759-1766. doi:10.1002/jbmr.402

156. Thompson WR, Rubin CT, Rubin J. Mechanical regulation of signaling pathways in bone. *Gene*. 2012;503(2):179-193. doi:10.1016/j.gene.2012.04.076

157. Serrano AL, Baeza-Raja B, Perdiguero E, Jardí M, Muñoz-Cánoves P. Interleukin-6 Is an Essential Regulator of Satellite Cell-Mediated Skeletal Muscle Hypertrophy. *Cell Metab*. 2008;7(1):33-44. doi:10.1016/j.cmet.2007.11.011

158. Bernareggi A, Bosutti A, Massaria G, et al. The State of the Art of Piezo1 Channels in Skeletal Muscle Regeneration. *Int J Mol Sci*. 2022;23(12):6616. doi:10.3390/ijms23126616

Ringraziamenti

Desidero ringraziare con particolare stima la prof.ssa Paola Lorenzon. Per la sua figura di Group Leader, per la grande professionalità, disponibilità, competenza, dedizione e responsabilità dimostratami, doti che hanno contribuito a farmi crescere sia professionalmente che umanamente.

Desidero ringraziare di cuore la prof.ssa Marina Sciancalepore, una figura cardine durante il mio intero percorso accademico; portatrice di utili consigli tecnici da grande scienziata e di consigli di vita da Amica.

Ringrazio tutte le figure professionali che mi hanno accompagnato in questi anni, rivolgendo un particolare ringraziamento alle prof.ssa Annalisa Bernareggi, prof.ssa Federica Tramer e dott.ssa Alessandra Bosutti, dalle quali ho appreso nuove tecniche, consigli e metodiche di lavoro.

I miei ringraziamenti più preziosi li rivolgo alla mia famiglia, in particolare ai miei genitori, Cinzia e Paolo, due persone che hanno scelto sempre i figli prima di loro stessi. Dico loro semplicemente Grazie… per avermi dato sempre più del necessario ed esserci stati sempre, per avermi trasmesso dei principi forti e dei valori sani su cui poter costruire la propria vita, per avermi insegnato a lottare per ciò in cui si crede e si desidera, per essere stati esempi da seguire, per avermi trasmesso l'importanza ed il senso della famiglia, ma soprattutto per essere stati semplicemente "Mamma e Papà". Un grazie di cuore lo rivolgo a mio fratello Andrea, una pilastro fondamentale della mia vita, persona testarda ma di gran cuore, che ammiro e stimo moltissimo. Grazie per essere sempre stato mio compagno di giochi, per essermi stato d'ispirazione nei momenti in cui ne avevo bisogno, e per aver contribuito a rendermi l'uomo che sono oggi. Un ringraziamento a lui ed alla sua compagna Alexia, per avermi fatto provare una delle emozioni più grandi ed importanti della mia vita, diventare zio di mio nipote Tommaso, al quale cercherò di trasmettere i consigli migliori che possa dare e tutto l'affetto che merita. Grazie a nonna Grazia per avermi donato sempre tanto tempo e pazienza e per avermi trasmesso la grande forza d'animo che la contraddistingue. Grazie a zia Silvi che ha sempre saputo donarmi un semplice sorriso con garbo e pacatezza. Un grazie lo rivolgo ad Alexia, Susanna ed Armando, per avermi donato tanta allegria, positività e spensieratezza con grandi sorrisi e forti abbracci.

Un ringraziamento di vero cuore lo rivolgo ad Angelo, Anna e Francesca, la mia seconda famiglia. Grazie per avermi accolto come un figlio ed un fratello, rafforzando principi, concetti e legami familiari, per avermi sempre donato e dimostrato tanto affetto, fiducia, lealtà, supporto e vicinanza in tutti questi anni.

Il ringraziamento più grande e speciale però lo rivolgo alla mia compagna di vita Graziana, la mia vera ed unica forza, alla quale dedico questo mio traguardo. Grazie per avermi spronato a migliorare ogni giorno, per aver creduto sempre in me, per esserci sempre in ogni situazione, per sostenermi, capirmi e per riuscire a tirare fuori il meglio di me. L'intesa, la serenità, la semplicità, l'autenticità, l'entusiasmo e la condivisone dei nostri gesti racchiudono, per me, il segreto della felicità, e la vera gioia di vivere. Sei la persona più importante della mia vita.